Technische Universität München

Fakultät für Medizin

III. Medizinische Klinik und Poliklinik

Forward genetic screening identifies actionable drivers of B-cell lymphomagenesis

Markus Kilian Schick

Vollständiger Abdruck der von der Fakultät für Medizin der Technischen Universität München zur Erlangung des akademischen Grades eines

Doktors der Naturwissenschaften (Dr. rer. nat.)

genehmigten Dissertation.

Vorsitzender:	Prof. Dr. Radu Roland Rad
Prüfende der Dissertation:	1. apl. Prof. Dr. Ulrich Keller
	2. Prof. Dr. Michael Groll
	3. Prof. Dr. Florian Heidel

Die Dissertation wurde am 31.08.2020 bei der Technischen Universität München eingereicht und durch die Fakultät für Medizin am 16.02.2021 angenommen.

Parts of this work have been published in the following peer-reviewed articles or are part of a submitted publication:

Schick M, Maurer S, Zhang L, Isaakidis K, Schneider L, Schunck K, Rohleder E, Maurer C, Hofstetter J, Baluapuri A, Zhang L, Scherger AK, Slotta-Huspenina J, Weber J, Engleitner T, Maresch R, Slawska J, Isaakaidis K, Lewis R, Istvanffy R, Habringer S, Steiger K, Baiker A, Oostendorp R, Miething C, Lenhof HP, Bassermann F, Chapuy B, Wolf E, Rad R, Müller S, and Keller U. Actionable genetic alterations of the SUMO isopeptidase SENP6 drive lymphomagenesis and genetic instability in diffuse large B-cell lymphoma. Manuscript submitted.

Biederstädt A*, Hassan Z*, Schneeweis C*, **Schick M***, SchneiderL, Muckenhuber A, Hong Y, Siegers G, Nilsson L, Wirth M, Dantes Z, Steiger K, Schunck K, Langston S, Lenhof HP, Coluccio A, Orben F, Slawska J, Scherger AK, Saur D, Müller S, Rad R, Weichert W, Nilsson J, Reichert M ,Schneider G , Keller U. SUMO pathway inhibition targets an aggressive pancreatic cancer subtype. **Gut.** 2020. doi:10.1136/gutjnl-2018-317856. *contributed equally

Weber J*, de la Rosa J*, Grove CS*, **Schick M**, Rad L, Baranov O, Strong A, Pfaus A, Friedrich MJ, Engleitner T, Lersch R, Öllinger R, Grau M, Menendez IG, Martella M, Kohlhofer U, Banerjee R, Turchaninova MA, Scherger A, Hoffman GJ, Hess J, Kuhn LB, Ammon T, Kim J, Schneider G, Unger K, Zimber-Strobl U, Heikenwälder M, Schmidt-Supprian M, Yang F, Saur D, Liu P, Steiger K, Chudakov DM, Lenz G, Quintanilla-Martinez L, Keller U, Vassiliou GS, Cadiñanos J, Bradley A, Rad R. PiggyBac transposon tools for recessive screening identify B-cell lymphoma drivers in mice. **Nat Commun. 2019** Mar 29;10(1):1415. *contributed equally

Schick M*, Habringer S*, Nilsson JA, Keller U. Pathogenesis and therapeutic targeting of aberrant MYC expression in haematological cancers. **Br J Haematol**. 2017 Dec;179(5):724-738. *contributed equally

Contents

ABBREVIATIONS

ABC DLBCL	activated B-cell like diffuse large B-cell lymphoma
ACK	ammonium chloride–potassium bicarbonate
ADP	adenosine diphosphate
ANOVA	analysis of variance
APS	ammonium persulfate
ATP	adenosine triphosphate
BCL	B-cell lymphoma
BCR	B-cell receptor
bHLH	basic helix-loop-helix
BL	Burkitt's lymphoma
BM	bone marrow
B-NHL	B-cell non-Hodgkin lymphoma
bp	base pair
BSA	bovine serum albumin
CAG	chicken β-actin promoter coupled to the CMV enhancer
cDNA	complementary DNA
ChIP	chromatin immunoprecipitation
CLL	chronic lymphocytic leukemia
Ct	threshold cycle
CTL	control
Cy	cyanine dye
DDR	DNA damage response
DEG	differentially expressed genes
DEL	double-expressor lymphoma
dest.	Destillata
DHL	double-hit lymphoma
DLBCL	diffuse large B-cell lymphoma
DMEM	Dulbecco´s Modified Eagle Medium
DMSO	dimethyl sulfoxide
DNA	desoxyribonucleic acid
dNTP	2'-Desoxyribonucleosid-5'-triphosphat
DRB	doxorubicin
DTT	dithiothreitol
DZ	dark zone
E13.5	embryonic day 13.5
Eμ	enhancer of immunoglobulin M (μ) gene

E.coli	escherichia coli
EBV	Epstein-Barr virus
EDTA	ethylenediaminetetraacetic acid
EGTA	ethylene glycol-bis(2-aminoethylether)-N,N,N′,N′-tetraacetic acid
env	envelope
et al.	et alii
EtBr	ethidium bromide
FACS	fluorescence activated cell scanning/sorting
FCS	fetal calf serum
FDR	false discovery rate
FITC	fluorescein isothiocyanate
FL	follicular lymphoma
FL-HSPC	fetal liver hematopoietic stem/progenitor cell
FSC	forward scatter
Fwd	forward
g	gravity (9,81 m/s2), gram
gag	group-specific antigen
GAPDH	glyceraldehyde 3-phosphate dehydrogenase
GC	germinal center
GCB DLBCL	germinal center B-cell like diffuse large B-cell lymphoma
gDNA	genomic DNA
GEO	Gene Expression Omnibus Database
GFP	green fluorescent protein
Gy	gray (1 Gy=1 J/kg)
H.E.	hematoxylin-eosin
HBSS	Hank’s Balanced Salt Solution
HCl	hydrochloric acid
HEPES	4-(2-hydroxyethyl)-1-piperazineethanesulfonic acid
Hoxb8-FL	Hoxb8-FLT3 cells
HRP	horseradish peroxidase
HSC	hematopoietic stem cells
HSPC	hematopoietic stem and progenitor cells
IHC	immunohistochemistry
IG	immunoglobulin locus
IgH	immunoglobulin heavy locus
i.p.	intraperitoneal injection
IRES	internal ribosomal entry site

i.v.	intravenous injection
kb	kilobases, 1000 base pairs
kDa	kilodalton
KO	knock out
L	ladder
LN	lymph node
LZ	light zone
MCL	mantle cell lymphoma
$MgCl_2$	magnesium chloride
mRNA	messenger RNA
MSCV	murine stem cell virus
MYC	myelocytomatosis oncogene
MZ	marginal zone
n	number
NaB	disodium tetraborate
NaCl	sodium chloride
NaF	sodium fluoride
$NaVO_4$	sodium orthovanadate
NEAA	non-essential amino acids
NES	normalized enrichment scores
ORF	open reading frame
o.n.	overnight
OS	overall survival
p	phosphorylated
PARP	poly (ADP-ribose) polymerase
PB	piggyBac
PBS	phosphate buffered saline
PBST	PBS + 1% Tween
PCR	polymerase chain reaction
PDAC	pancreatic ductal adenocarcinoma
PE	phycoerythrin
Pen/Strep	penicillin/streptomycin
pH	pondus Hydrogenii
PI	propidium iodide
PMSF	phenylmethylsulphonyl fluoride
pre-B	precursor B-cell
pro-B	progenitor B-cell

PVDF	polyvinylidene fluoride
qRT-PCR	quantitative real time PCR
R26	Rosa26 locus
rev	reverse
RNA	ribonucleic acid
RNAseq	RNA sequencing
rpm	rounds per minute
RPMI	Roswell Park Memorial Institute medium
RNF	ring finger protein
RT	reverse Transcriptase, room temperature
SA	splice acceptor
SCT	stem cell transplantation
SD	splice donor
SDS-PAGE	sodium dodecyl sulfate polyacrylamide gel electrophoresis
SEM	standard error of the mean
SENP	sentrin/SUMO-specific protease
seq	sequencing
SHM	somatic hypermutation
SPF	specific-pathogen-free
SSC	side scatter
STOP	stop sequence
StUbL	SUMO-targeted ubiquitin ligase
SUMO	small ubiquitin-like modifier
SUMOi	SUMO inhibition
pA	polyadenylation signal
TEMED	N,N,N',N'-Tetramethylendiamine
TG	transgene
TR	inverted terminal repeats
Tris	2-Amino-2-(hydroxymethyl)-propane-1,3-diol
Trp53	transformation related protein 53
Tween 20	poly(oxyethylen)n-sorbitan-monolaurate
TUM	Technical University Munich
U	unit
UTR	untranslated region
UV	ultra violet
V	volt, variable
VDJ	variable (V), diversity (D), and joining (J) gene segments

Vol	volume
w/	with
WBC	white blood cell
w/o	without
WT	wildtype
x	times

1 SUMMARY

Diffuse-large B-cell lymphoma (DLBCL) is a genetically heterogeneous malignancy with poor clinical outcome in about one third of patients. Poor clinical outcome has been associated with complex genetic alterations frequently activating the oncoprotein MYC.

Here we describe a genome-wide cancer gene discovery screen in a murine model of MYC-driven B-cell lymphomagenesis and define a large set of lymphoma associated cancer genes. We identify dysregulated SUMOylation as one of the top altered pathways in this screen and show that the SUMO isopeptidase SENP6 is a tumor suppressor of B-cell lymphomagenesis. SUMOylation is a post-translational modification of proteins regulating their localization, half-life and function. Activated SUMOylation is frequently found in cancer but its origin remains elusive. Notably, *SENP6* is recurrently deleted in human B-cell lymphomas and SENP6 deficiency results in unrestricted SUMOylation. Mechanistically, SENP6 loss triggers extraction of DNA repair- and genome maintenance-associated protein complexes from chromatin and thereby impairs DNA repair in response to DNA damage stress, ultimately promoting genomic instability. In line with this hypothesis, SENP6 deficiency drives synthetic lethality to PARP inhibitors and our data reveal the potential therapeutic application of PARP inhibitors in B-cell lymphoma (BCL). Beyond this specific vulnerability, we prove efficacy of SUMO inhibition as a therapeutic strategy in preclinical models of BCL and pancreatic adenocarcinoma (PDAC), a human cancer with well-established role of MYC and dismal prognosis.

Together, we provide first-time experimental evidence that aberrant SUMOylation accelerates cancer pathogenesis. Specifically, we link deficiency of the SUMO isopeptidase SENP6 to impaired DNA damage response and genomic instability *in vivo* and explore synthetic lethality to PARP inhibition as therapeutic option in a subgroup of BCL. Moreover, we exploit inhibition of activated SUMOylation as a potential therapeutic strategy in aggressive human cancers with MYC involvement.

2 INTRODUCTION

2.1 The oncoprotein MYC in tissue homeostasis and cancer

c-MYC (MYC, encoded by *MYC*) is a transcription factor containing a basic helix-loop-helix (bHLH) and a leucine zipper domain for DNA-binding and heterodimer formation with MAX, respectively. The MYC family of transcription factors includes MYC, L-MYC and N-MYC with similar structure and function (reviewed in (Eilers and Eisenman, 2008; Meyer and Penn, 2008). MYC received its name from oncogenic retroviruses integrating a virally encoded oncogene (*v-myc*) into chicken DNA, thereby causing leukemia and sarcoma-like cancers (myelocytomatosis) (Sheiness and Bishop, 1979). This discovery eventually led to the identification of the human homologue *MYC* and its involvement in many human cancers (Figure 1). Of note, over 50% of all human cancers show elevated MYC levels (Boxer and Dang, 2001). In many of these cancers like PDAC or DLBCL, dysregulation of MYC is associated with adverse prognosis (Biederstadt et al., 2020; Chapuy et al., 2018; Reddy et al., 2017).

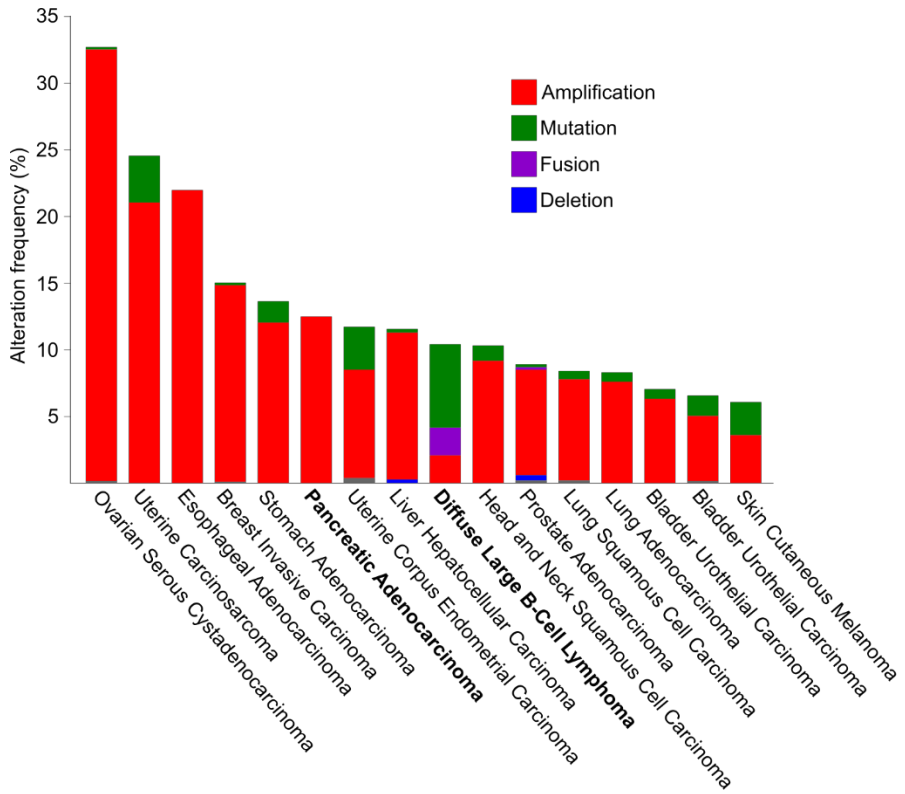

Figure 1. Genetic alterations affecting *MYC* in human cancers. Frequencies of genetic *MYC* alterations in human cancers. The analysis is based on TCGA data and was derived from https://www.cbioportal.org/. All cancers with alteration frequencies exceeding 5% are shown. Diffuse large B-cell lymphoma and pancreatic adenocarcinoma, which were investigated in this thesis are highlighted in bold.

In physiologic processes, MYC expression and stability is tightly regulated to limit its activity to the accurate biological context (Eilers and Eisenman, 2008; Meyer and Penn, 2008). MYC deficiency by means of gene knock-out is lethal early during embryogenesis, emphasizing its fundamental role in organogenesis and developmental biology (Davis et al., 1993). In cancer,

oncogenic activation of signal transduction results in a growth promoting change in transcription (Figure 2). When MYC levels are elevated by events leading to increased expression or stability, the growth promoting transcriptome is further enhanced (Lin et al., 2012; Nie et al., 2012). By binding to E-boxes that are present throughout the genome but only accessible to MYC in open chromatin, MYC can recruit histone acetyltransferases (HATs) to other chromatin

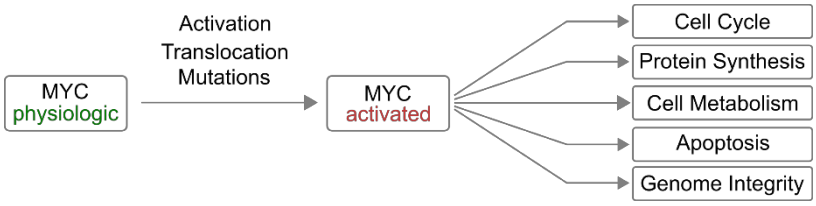

Figure 2. MYC-driven pathomechanisms in cancer cells. MYC can be activated by translocation or amplification of the *MYC* gene, activated mRNA expression or by mutations stabilizing the MYC protein. Activated MYC expression affects a broad spectrum of cellular mechanisms.

remodelling complexes to stimulate transcriptional elongation (Wolf et al., 2015). Some E-boxes and genes are high affinity targets whereas other genes are low affinity targets and thus require high MYC levels for binding and activation. MYC can also repress genes via interaction with factors such as MIZ-1 or by inducing MNT, which works as an anti-amplifier, or by simply inducing all genes in open chromatin so that the remainder appears suppressed if not properly normalized (Hurlin et al., 2003; Loven et al., 2012; Nilsson et al., 2004; Peukert et al., 1997; Wolf et al., 2015).

In cancers where MYC is the 'driving' oncogene itself, the grossly elevated MYC levels (Sabo et al., 2014) can therefore lead to enhanced transcription of apoptosis pathways, including the activation of the ARF-P53 apoptotic pathway. Loss of this failsafe mechanism results in rapid onset of aggressive cancers as shown e.g. in mouse models of BCL (Eischen et al., 1999) (reviewed in (Nilsson and Cleveland, 2003)). MYC's prominent role as a pivotal oncoprotein makes it an attractive target for pharmacological inhibition. Indeed, a mouse model expressing a switchable dominant negative form of MYC, called OmoMYC has demonstrated that MYC can be inactivated in cancer cells without causing detrimental tissue dyshomeostasis (Soucek et al., 2008). However, the lack of hydrophobic pockets, unorganized tertiary structure and protein-protein interactions has made development of highly selective inhibitory molecules extremely difficult and MYC is therefore often referred to as "undruggable" (McKeown and Bradner, 2014). These challenges led to the idea of targeting cellular processes selectively perturbed in cancer cells with high MYC levels, thereby conferring so called "synthetic lethality" (Guarente, 1993; Kaelin, 2005). This approach is highly attractive due to sparing of non-cancer cells and thus reducing toxicity. However, this approach requires detailed understanding of the mechanisms driving tumor biology downstream of activated MYC signalling.

2.2 Pathogenesis of B-cell non-Hodgkin lymphomas

2.2.1 The role of MYC in BCLs

Burkitt lymphoma (BL) is the human disease in which MYC was initially discovered and found to play an essential role in initiation and progression. In the early 1980ies, translocations of the *MYC* gene on the long arm of chromosome 8 to the *IGH* locus (t(14;18)(q24;q32)), the κ light chain locus (t(2;8)(p11;q24)) and the λ light chain locus (t(8;22)(q24;q11)) were found to be pathognomonic for BL (Dalla-Favera et al., 1982; Taub et al., 1982). The fact that BL is presumably the fastest growing human cancer, with doubling times often less than 1-2 days, emphasizes the dramatic effect of aberrant MYC expression. Epstein Barr virus (EBV) infection plays a role in endemic BL and EBV nuclear antigen 2 (EBNA-2) is itself known to activate MYC and thereby increase B-cell proliferation (Kaiser et al., 1999). The exact pathogenesis of BL is not known but likely involves an intricate balance between the growth-promoting and anti-apoptotic effects of EBV and the B-cell receptor (BCR) and how these effects are being amplified by MYC. Endemic BL also involves immune escape (Durand-Panteix et al., 2012). Despite the highly aggressive nature of BL, both endemic and sporadic BL have an excellent prognosis if treated appropriately with aggressive immuno-chemotherapy (Hoelzer et al., 2014).

In diffuse large B-cell lymphoma (DLBCL), *MYC* translocations are present in 5-10% of the cases and are associated with adverse prognosis and increased risk for relapse both systemically and within the central nervous system (Savage et al., 2009). Concomitant translocations involving *BCL2* and/or *BCL6* (double- [DHL] or triple-hit lymphoma) are common in this subset of DLBCLs, contributing to adverse prognosis (Hu et al., 2013). Expression of MYC and BCL2 evaluated by immunohistochemistry (so called “double-expressor” lymphomas [DEL]) also defines a subgroup with worse prognosis (Johnson et al., 2012). Due to this prognostic significance, the new 2016 WHO classification of haematological malignancies introduced a new provisional lymphoma entity named “high grade B-cell lymphoma with *MYC* and *BCL2* and/or *BCL6* translocations” (Swerdlow et al., 2016). Currently, there is no consensus if intensified chemotherapeutic regimens or high-dose chemotherapy with hematopoietic stem cell transplantation (SCT) improves prognosis in DHL/DEL. Therefore, inclusion of this patient population into clinical trials testing intensified regimens or targeted substances is warranted. Recent work demonstrated that MYC augments BCR signalling events and that MYC overexpression confers resistance to the Bruton’ tyrosine kinase inhibitor ibrutinib in a MYC-induced lymphoma model. This implicates that targeting BCR signalling in MYC-driven lymphomas might be more challenging than anticipated and that regimens rationally combining BCR inhibition with inhibition of potential resistance mechanisms might be beneficial (Moyo et al., 2017).

Mantle cell lymphoma (MCL) is characterized by increased proliferation and cell cycle progression mediated by the t(11;14)(q13;q32) translocation leading to overexpression of CyclinD1. Further genetic perturbations altering proliferation, the DNA damage response (DDR), or apoptosis are frequently acquired leading to lymphoma progression. Case studies suggest a role of translocations involving *MYC* that are associated with adverse prognosis and aggressive behaviour (Au et al., 2000; Nagy et al., 2003). Apart from the known collaboration between CyclinD1 and MYC (Bodrug et al., 1994), recent data suggest that in a subset of patients mutated NOTCH1 leads to MYC overexpression (Kridel et al., 2012).

Disease	Type of MYC involvement	Incidence	Clinical frequency
DLBCL	Translocation	5-15%	32%
	Overexpression	29%	
FL	Translocation	2-10%	25%
CLL	Translocation	Rare cases	8%
	Overexpression via *NOTCH1*	10%	
MCL	Overexpression via *NOTCH1*	12%	7%

Table 1. Summary of MYC involvement in the most common types of B-NHL.

MYC translocations can also be found in transformed or high-grade follicular lymphoma (FL) (Horn et al., 2011; Pasqualucci et al., 2014), indicating a more aggressive phenotype with adverse prognosis, similar to aforementioned DHL (Koch et al., 2016). However, in a recent study including high- and low grade FL, *MYC* breaks were also found in 6.3% of low-grade FL, but the fraction of cells affected by this alteration was low compared to high-grade FL with *MYC* translocations (Leich et al., 2016). These data reflect the complexity in the continuum of transformation of FL into a more aggressive disease, where the role of MYC activation is not fully understood.

Chronic lymphocytic leukaemia (CLL) often displays an indolent course of disease without requiring treatment for years. Apart from well-established prognostic factors like del(17p), CD38 expression, ZAP70 expression and IGHV mutation status, *MYC* translocations have also been implicated to be present and associated with a more aggressive phenotype (Huh et al., 2008). Whole genome sequencing of 538 CLL patients also identified MYC as a central player in this disease (Landau et al., 2015). NOTCH1, which can be mutated in CLL, has recently been shown to regulate MYC expression in CLL (Pozzo et al., 2017) and NOTCH1-MYC activation by the stromal niche induces metabolic changes associated with increased glucose dependence (Jitschin et al., 2015).

2.2.2 The cellular origin of BCLs

Typically, when B-cells experience malignant transformation, they conserve features of their cell of origin, most prominently the specific B-cell phenotype of the lymphoma originating cell (Kuppers, 2005). Most human B-cell lymphomas origin from mature B-cells (Figure 3). From here on, we will focus on DLBCL, the most common type of B-NHL.

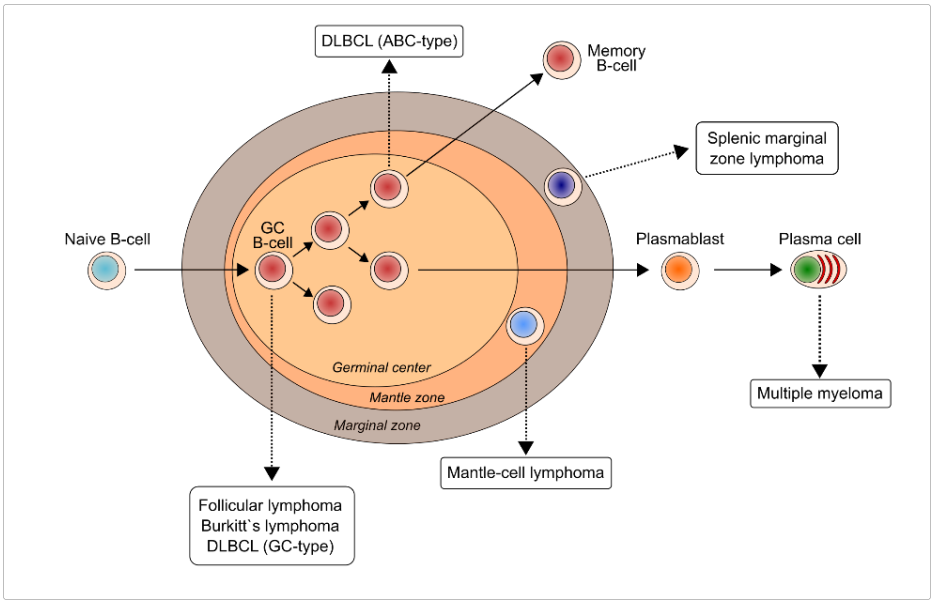

Figure 3. The origin of aggressive human BCLs. Graphical illustration of the origin of aggressive human BCLs in the germinal center. GCs are microanatomical transient structures initiated when B-cells are challenged by a T-cell presented foreign antigen surrounded by the mantle zone and the marginal zone. Each zone is characterized by specific B-cell phenotypes. [Figure adapted from (Kuppers, 2005)].

DLBCL origins from the malignant transformation of germinal center (GC) B-cells, which went through the GC reaction (Pasqualucci and Dalla-Favera, 2018). GCs are microanatomical transient structures initiated when B-cells are challenged by a T-cell presented foreign antigen. In GCs high-affinity antibody expressing B-cells develop and differentiate into secreted-antibody producing plasma cells and memory B-cells (De Silva and Klein, 2015). GCs are built up by two distinct areas – the dark zone (DZ) and the light zone (LZ). B-cells constantly cycle between the two zones. In the DZ, a process termed somatic hypermutation (SHM) introduces mutations in the variable region of immunoglobulin genes of B-cells. In the LZ, B-cells undergo affinity maturation or class switch recombination (De Silva and Klein, 2015). The application of genome-wide transcriptome analysis enabled the identification of distinct subgroups in the heterogeneous group of DLBCLs comprising the two main subgroups germinal center B-cell-like (GCB) DLBCL and activated B-cell like (ABC) DLBCL (Alizadeh et al., 2000; Rosenwald et al., 2002). Whereas GCB DLBCLs are characterized by a high similarity of the lymphoma cells to GC B-cells, ABC DLBCLs show high similarity to *in vitro* activated B-cells lacking most specific features of GC B-cells (Alizadeh et al., 2000; Rosenwald et al., 2002). Whereas GCB DLBCLs show a more favorable clinical course, ABC DLBCLs are the most aggressive form of this entity

(Rosenwald et al., 2002) and the distinction between the two subgroups has been incorporated into clinical practice. Of note, recent studies suggested a classification into five subtypes based on molecular features revealing an even larger complexity of DLBCL subtypes (Chapuy et al., 2018).

2.2.3 Genetics of B-cell non-Hodgkin lymphomas

The pathogenesis of DLBCL is characterized by the accumulation of genetic lesions implying altered expression of proto-oncogenes as well as tumor suppressor genes. In comparison to other hematological cancers, DLBCLs present a remarkable structural and functional complexity. Considering mutations and copy number alterations, every DLBCL biopsy harbors an average of 70 lesions in coding regions. Many of these genes are mutated in less than 10% of patients (Chapuy et al., 2018; Pasqualucci et al., 2011; Reddy et al., 2017). Beyond this, dysregulation by non-genetic mechanisms like differential gene expression or epigenetic modification is adding an additional layer of complexity and the average number of 70 alterations may represent an underestimate of the biologically significant mutation load of DLBCL (Pasqualucci and Dalla-Favera, 2018).

Like for the vast majority of human cancers, several mechanisms contribute to the genetic complexity of DLBCL including somatically acquired point mutations and copy number changes of genes (Pasqualucci and Dalla-Favera, 2018). Importantly, the genome of DLBCL is particularly affected by two mechanisms of DNA damage essentially taking place in GCs to remodel the immunoglobulin (*IG)* locus: First, errors occurring during VDJ recombination can lead to chromosomal translocations. Other than in acute leukemia, where translocations often cause fusion proteins, translocations in DLBCL mostly juxtapose regulatory sequences in the proximity of proto-oncogenes activating the expression of their encoded proteins (e.g. *MYC-IGH* translocation) (Pasqualucci and Dalla-Favera, 2018). Second, aberrant SHM is causing perturbations in gene expression as well as functional changes of various oncogenes and tumor suppressor genes (e.g. *MYC* and *PIM1*) (Pasqualucci and Dalla-Favera, 2018).

These mechanisms altogether lead to a high structural and functional complexity, which is currently understudied and reveals an urgent need for functional dissection of the molecular DLBCL landscape.

2.2.4 The *Eμ-myc* mouse model of MYC-driven B-cell lymphomagenesis

The huge structural and molecular complexity of DLBCL underscores the need for models to investigate the pathobiology of specific driver genes. Among DLBCL patients, MYC expression defines a subgroup with poor prognosis (Chapuy et al., 2018; Reddy et al., 2017). However, it

has been shown that activated MYC signaling alone is not sufficient to initiate tumorigenesis and that further genetic alterations are needed for cellular transformation (Dang, 2012).

The earliest mouse model of high incidence and spontaneous MYC-induced B-cell lymphomagenesis, the *Eμ-myc* model, was established in 1985. In this model MYC expression is driven by the immunoglobulin heavy chain (IgH) enhancer and thereby limited to B-cells (Harris et al., 1988). In this extensively used mouse model, almost all mice develop lymphomas within five months of age and present with enlarged lymph nodes, spleen and thymus. MYC-driven B-cell lymphomas in the *Eμ-myc* model origin from early B-cells and represent either pre-B, immature or mixed B-cell lymphomas (Bric et al., 2009; Harris et al., 1988).

Even though lymphomagenesis in the *Eμ-myc* model is initiated by a specific oncogene on a defined genetic background, gene expression profiling revealed a striking degree of heterogeneity between lymphomas (Mori et al., 2008) and several studies reveal that *Eμ-myc* lymphomas acquire secondary mutations leading to the activation or inactivation of co-drivers. These mutations frequently affect intrinsic tumor suppressor genes such as *Trp53* (in humans *P53*), which counteracts MYC-driven malignant transformation by promoting cell cycle arrest, senescence or apoptosis (Eischen et al., 1999; Riley et al., 2008). The tumor suppressor P53 is activated in response to cellular stresses, like oncogene-induced replicative stress, which is caused by mitogenic oncoproteins like MYC. Thereby, the ARF-P53 apoptotic axis functions as failsafe mechanism avoiding the expansion of uncontrollably proliferating cells (Bric et al., 2009; Riley et al., 2008). Further, activation of antiapoptotic BCL2-family members like *Bcl2* can accelerate MYC-driven lymphomagenesis (Strasser et al., 1990). However, other than known mutations like in *Trp53*, *Cdkn2a* and *Nras* further cooperating drivers however remain largely unknown (Lefebure et al., 2017).

Next to intercrossing with transgenic or knockout mice, *Eμ-myc* derived hematopoietic stem and progenitor cells (HSPCs) can be transduced with constructs for inactivation or depletion of target genes *in vitro*. Subsequently the HSPC pool can be transplanted into syngeneic recipient mice to investigate the effect of the introduced lesion on lymphomagenesis (Schmitt and Lowe, 2002). Of note, this approach was also used to show that shRNA mediated deletion of *Trp53* mimics the tumor promoting effects observed in intercrossing experiments (Hemann et al., 2003).

Due to its short latency, its high penetrance and the possibility of genetic modification in transduction-transplantation experiments, the *Eμ-myc* model has evolved as a versatile tool and attractive model for the investigation of MYC-driven B-cell transformation and lymphomagenesis.

2.3 Genetic *in vivo* screening for cancer gene discovery

Due to the large number of genes altered by genetic and non-genetic mechanisms, it remains challenging to pinpoint functionally relevant drivers of B-cell lymphomagenesis. Cancer gene discovery screenings in mice have emerged as powerful tools for the unbiased qualitative assessment of the cancer causing potential of genes. Due to the unbiased activation and inactivation of virtually all genes of the mouse genome and the clinically relevant endpoint tumorigenesis they can be used to complement large-scale sequencing studies (Rad et al., 2015; Weber et al., 2019).

Genome-wide screenings in mice can be performed by chemical- or radiation-induced mutagenesis or insertional mutagenesis using viruses. However, these approaches are hampered by limitations like high costs, the challenge of finding the induced insertions and the tissue tropism of viruses (Friedrich et al., 2017). The development of transposon mutagenesis screening systems overcame these limitations and can be used without tissue tropism and

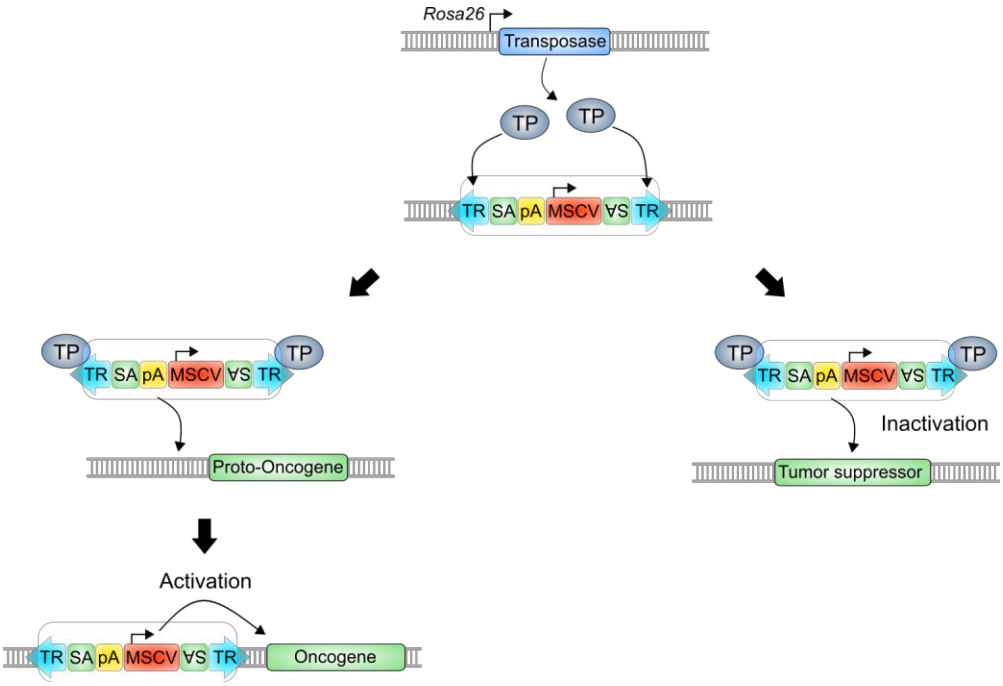

Figure 4. Transposon mobilization and insertion. The transposase recognizes the flanking terminal repeats (TR) and catalyzes the excision of the transposon. Next, the transposase catalyzes the insertion of the transposon at a new locus. For activation, a MSCV promotor located on the transposon drives the expression of proto-oncogenes if inserted upstream and sense-oriented of a gene. For inactivation, genes can either be directly disrupted by transposon integration or by transcript trapping if inserted into an intron. TP, transposase; TR, terminal repeats; SA, splice acceptor; MSCV, murine stem cell virus long terminal repeat; pA, polyadenylation signal. [Scheme adapted from (Friedrich et al., 2017)].

thereby with broad applicability. Moreover, transposon-induced mutations can be easily detected due to molecular fingerprints (Friedrich et al., 2017; Rad et al., 2010).

DNA transposons are mobile genetic elements, which can change their localization across a genome via a "cut and paste" mechanism. The transposition mechanism is catalyzed by the activity of a transposase (Figure 4) (Friedrich et al., 2017). Whereas still active and

available in invertebrates, transposons were inactivated in higher organisms millions of years ago until the two transposon systems *Sleeping Beauty (SB)* and *PiggyBac (PB)* were reconstructed for transposon-induced insertional mutagenesis in mice (Ivics et al., 1997; Rad et al., 2010). The transposon system carried by the *ATP2-H32* mouse line used in this study has been designed bifunctional and can be used for loss of function (identification of tumor suppressors) and gain of function (oncogene identification) studies in a single experimental approach (Figure 4). By combining with a mouse line expressing the tranposase either ubiquitous or in a tissue-specific manner, transposition can be tightly controlled (Rad et al., 2010; Rad et al., 2015). The transposase recognizes the inverted terminal repeats (TR) flanking the transposon and catalyzes the “cut and paste” process, which takes place in a random fashion at all TTAA sites across the mouse genome (Rad et al., 2010). If inserted upstream and sense-oriented of the transcription start site of a gene, the unidirectional MSCV promoter drives the expression of the gene. On the other hand, when inserted in an exonic region of a gene, gene expression is disrupted by either frameshift or premature termination. Moreover, bidirectional splice acceptors (SAs) and polyadenylation signals (pAs) facilitate gene trapping, when the transposon is inserted in an intronic region (Friedrich et al., 2017).

Based on the mechanism of transposon-mediated mutagenesis, the transposon insertion patterns in genes predict their putative function in tumorigenesis. In the case of candidate oncogenes, all transposon insertions are located upstream of the transcription start site and sense-oriented (Figure 5). For both mechanisms of inactivation, the orientation of the transposon does is not essential and the insertion pattern of candidate tumor suppressor genes is typically bidirectional and scattered across the gene (Figure 5) (de la Rosa et al., 2017; Rad et al., 2015; Weber et al., 2019).

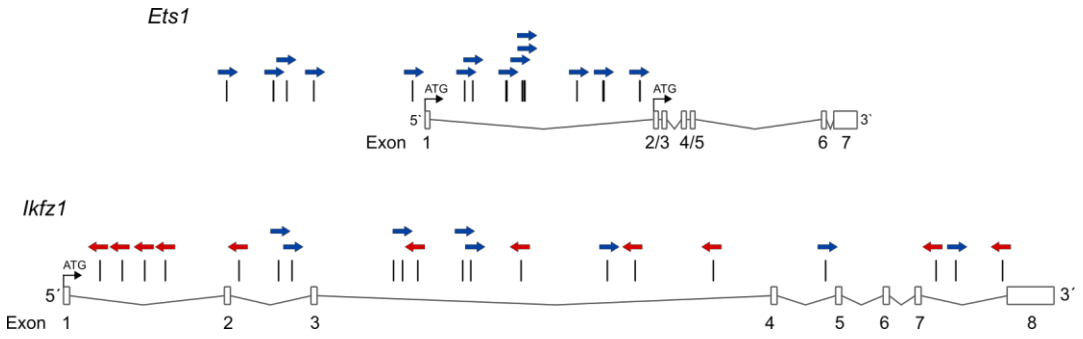

Figure 5. Transposon insertion patterns in well-known cancer genes. In the *PB* screening described in this study, transposon insertions in the well-known oncogene *Ets1* were found in several tumors. Each arrow represents the dominant transposon insertion from one tumor. All transposons were found sense-oriented and upstream of the transcriptions start site (ATG) or upstream of the alterative ATG located in exon two indicating a role as oncogene. The transposon insertion pattern in the well-known tumor suppressor gene *Ikfz1* was bidirectional and scattered across the gene indicating inactivation and a function as tumor suppressor.

2.4 The post-translational modification SUMO

Recently, we and others showed that MYC-driven cancers are highly dependent on the post-translational modification SUMO (Hoellein et al., 2014; Kessler et al., 2012) and all core components of the SUMO-conjugation machinery are activated in human cancers (Seeler and Dejean, 2017).

Covalent ligation of the small ubiquitin-like modifier (SUMO1, SUMO2 or SUMO3) moiety to a target protein (SUMOylation) is an important post-translational modification, which regulates the localization, stability and activity of target proteins. As such, SUMOylation serves as an essential regulatory mechanism for fundamental cellular processes such as cell cycle progression, DNA damage repair, nucleocytoplasmic transport, transcription, and chromatin remodeling (Flotho and Melchior, 2013; Seeler and Dejean, 2017).

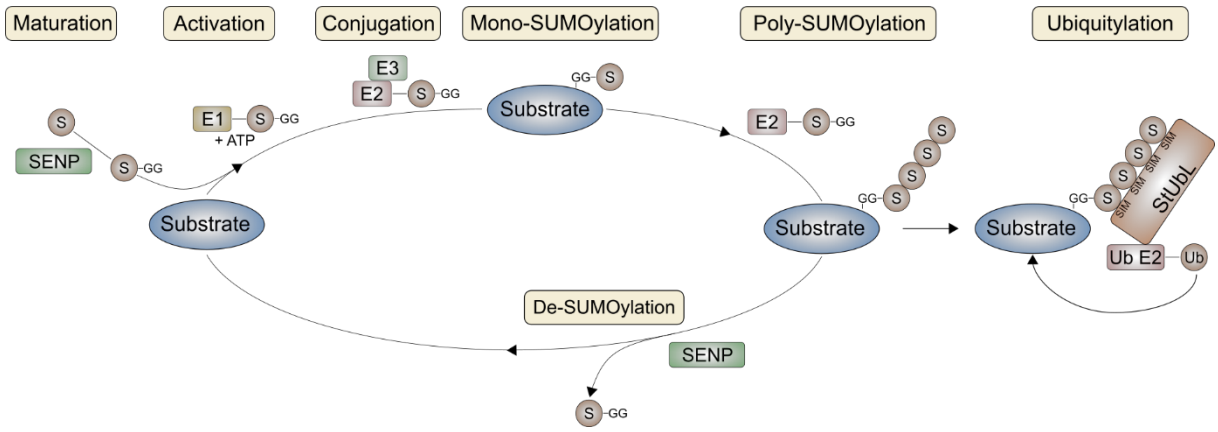

Figure 6. The SUMOylation pathway. All SUMO isoforms are expressed as precursors and need SENP-mediated maturation. Subsequently, SUMO is activated in an ATP-dependent reaction by the heterodimeric E1 enzyme SAE1/UBA2 and then transferred to the E2 enzyme UBC9 for conjugation to a substrate. Following mono-SUMOylation, substrates can be poly-SUMOylated. Poly-SUMOylated substrates can be recognized and ubiquitinated by StUbLs. SUMOylation is a fully reversible and dynamic reaction in which SENPs can cleave SUMOs from substrates. [Scheme adapted from (Seeler and Dejean, 2017)].

The human SUMO system comprises three related SUMO isoforms (SUMO1, SUMO2 and SUMO3), which are all expressed as precursors and need processing to exhibit a carboxy-terminal di-glycine motif (-GG). This motif is essential for subsequent SUMO conjugation (Nayak and Muller, 2014). The conjugation of SUMO is dependent on an enzymatic cascade. Following processing, the heterodimeric E1 activating enzyme (SAE1/UBA2) forms a SUMO-SAE1 thioester in an ATP-dependent reaction, which is then conveyed to the E2 conjugating enzyme UBC9. In the last conjugation step, SUMO is attached to a lysine residue of the substrate via an isopeptide bond (Figure 6) (Seeler and Dejean, 2017).

Whereas SUMO1 is typically conjugated as monoSUMO modification, SUMO2 and SUMO3 are prone to form SUMO2/3 chains (poly-SUMO) via internal lysine residues (Kunz et al., 2018; Ulrich, 2008; Vertegaal, 2010). SUMO chains provide a binding interface for a specific subtype

of ubiquitin ligases, known as SUMO targeted ubiquitin ligases (StUbL). RNF4, the best characterized StUbL in humans, catalyzes proteolytic- or non-proteolytic ubiquitination of poly-SUMOylated targets (Figure 6) (Vertegaal, 2010).

SUMOylation is a dynamic and fully reversible process. Deconjugation of SUMOs from substrates is primarily catalyzed by SUMO-specific isopeptidases of the SENP family, which comprises six members (SENP1, SENP2, SENP3, SENP5, SENP6 and SENP7) in human cells. Whereas SENP1, SENP2, SENP3 and SENP5 display activities on SUMO maturation and deconjugation, SENP6 and SENP7 specifically edit polymeric SUMO chains (poly-SUMOylation) (Kunz et al., 2018). The molecular structure of SENP6 and SENP7 clearly separates these two SENPs from SENP1, SENP2, SENP3 and SENP5. Of note, the catalytic domain of SENP6 and SENP7 possesses specific loops, which miss in the other SENPs. Particularly loop 1 is essential for the preference for editing SUMO chains (Kunz et al., 2018).

Whereas several studies show the association of activated SUMOylation and cancer, its origin and if deregulated SUMOylation directly contributes to cancer pathogenesis remains elusive.

2.5 The role of SUMO chains in the DDR

The SUMO system has been implicated as a key player in the DDR and the maintenance of genome integrity (Bergink and Jentsch, 2009). Particularly during replicative stress, balanced SUMOylation and the control of poly-SUMOylation is an important regulator of the DDR (Kunz et al., 2018). The DDR promotes checkpoint activation following DNA damage or enforced oncogene expression, which typically causes replicative stress. During replicative stress activated checkpoints limit tumorigenesis by allowing DNA repair in order to maintain genomic integrity (Halazonetis et al., 2008). Ectopic MYC expression alone is thereby insufficient to induce cellular transformation because it triggers checkpoint activation, cell-cycle arrest and apoptosis through intrinsic tumor suppressive pathways involved in the DDR (Dominguez-Sola and Gautier, 2014).

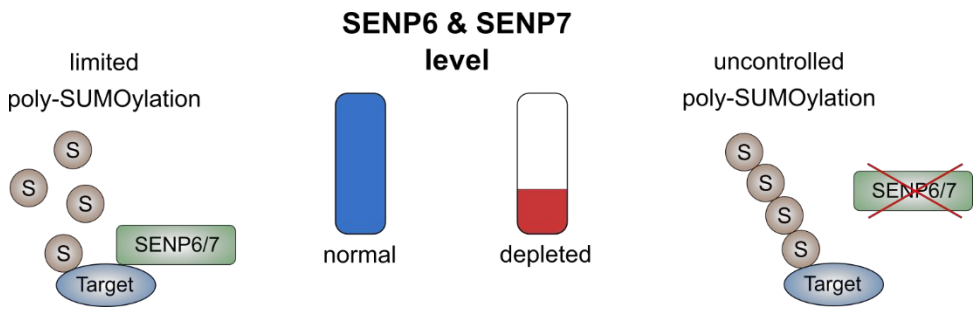

Figure 7. The control of the poly-SUMO equilibrium. The SUMO isopeptidases SENP6 and SENP7 antagonize the formation of poly-SUMO2/3 chains and are thereby critical determinants of the poly-SUMO equilibrium. S, SUMO. [Scheme adapted from (Wagner et al., 2019)].

The SUMO-specific isopeptidases SENP6 and SENP7 counterbalance poly-SUMOylation and are thereby important determinants of the SUMO state of their substrates (Figure 7) (Kunz et al., 2018). Poly-SUMOylation initiates the StUbL pathway in which poly-SUMOylation primes substrates for ubiquitination by the E3 ubiquitin ligase RNF4 or RNF111 (Keiten-Schmitz et al., 2019). RNF4 is the best characterized mammalian StUbL and is involved in several DDR pathways. In the Fanconi anemia pathway, polySUMO-dependent ubiquitination by RNF4 leads to the extraction of the FANCI-FANCD2 complex from DNA lesions. SENP6 limits poly-SUMOylation of FANCI and thereby antagonizes the StUbL pathway (Gibbs-Seymour et al., 2015).

However, the understanding of the processes controlled by poly-SUMOylation is still limited and recent proteomic screens have focused on the identification of substrates undergoing dynamic poly-SUMOylation controlled by SENP6 (Liebelt et al., 2019; Wagner et al., 2019). The set of candidate SENP6 substrates suggests a broad and highly interconnected spectrum of targets proteins involved in DNA repair, the DDR as well as chromatin organization (Keiten-Schmitz et al., 2019). Moreover, the studies describe a critical role for SENP6-controlled poly-SUMOylation for the chromatin-localization of substrates in a RNF4-dependent as well as a RNF4-independent manner. These mechanisms were exemplified for the constitutive centromere associated network (CCAN), the cohesin complex and the hPSO4/PRP19 complex, which drives ATR-CHK1 activation (Liebelt et al., 2019; Wagner et al., 2019).

Considering the important function of poly-SUMOylation in the DDR and genome maintenance, deregulation of poly-SUMOylation might have implications in human cancers.

2.6 Aim of the study

DLBCL is the most common aggressive BCL and comprises a clinical and molecular heterogeneous disease entity with a complex genetic background. Due to the large number of genes altered by genetic and non-genetic mechanisms, it remains challenging to pinpoint functionally relevant drivers of B-cell lymphomagenesis. Accordingly, several large phase 3 trials have failed to advance the therapeutic standard beyond classical immuno-chemotherapy (R-CHOP) towards mechanism-based novel therapies.

To address this challenge, I aimed to perform a genome-scale cancer gene discovery screen in a murine model of MYC-driven B-cell lymphomagenesis to identify heretofore unsuspected genes as drivers of lymphoma pathogenesis and biomarkers to inform cancer treatment. Starting from this approach, I wanted to investigate the mechanism shaping tumor biology downstream of selected alterations to develop biomarker-driven and mechanism-based treatments for BCL patients with adverse prognosis.

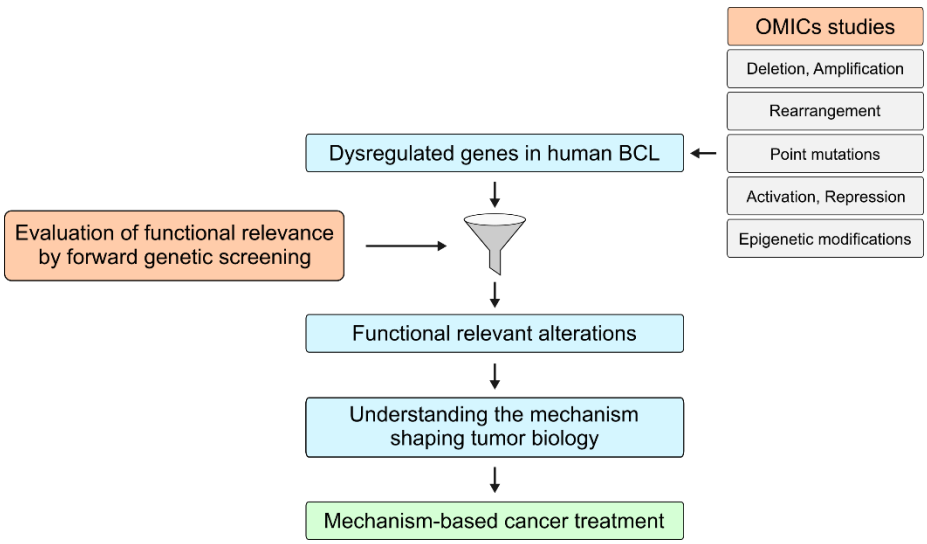

Figure 8. Forward genetic screening allows the unbiased functional evaluation of genetic alterations identified by large-scale OMICs studies. Different levels of knowledge gain starting out from sequencing data sets aiming to develop mechanism-based cancer treatment strategies.

3 RESULTS

3.1 Identification of novel cancer genes in BCL

3.1.1 *PB* mutagenesis promotes MYC-driven B-cell lymphomagenesis

Over 70% of all human cancers show elevated MYC levels and B-cell specific MYC expression in mice initiates BCL with full penetrance. However, to fully transform B-cells, activation of co-oncogenes or inactivation of tumor suppressor genes is required (Bisso et al., 2019; Harris et al., 1988).

To identify cooperating alterations promoting MYC-driven B-cell lymphomagenesis, we performed a genome-wide forward-genetic *in vivo* screen using the *PB* transposon mutagenesis system (Rad et al., 2010). To achieve mutagenesis on a MYC-activated background, *Eμ-myc (M)* mice were crossed to mice expressing the *piggyBac* transposase *(R)* and to transgenic mice carrying the *ATP-H32* transposon *(A)* (Figure 9a). Thereby the transposon can be

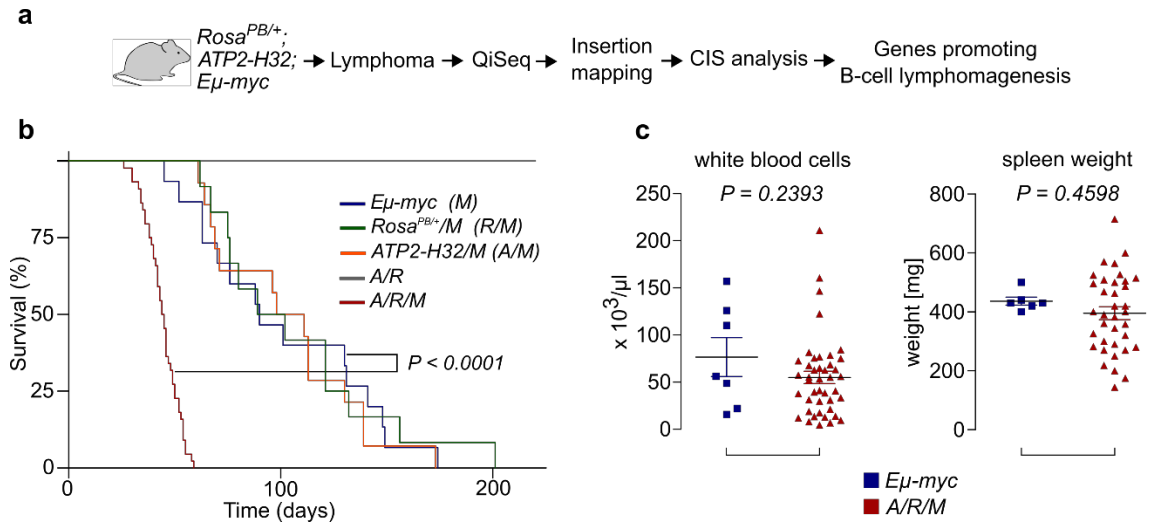

Figure 9. *piggyBac* mutagenesis promotes MYC-driven B-cell lymphomagenesis. (a) Outline of experimental setup for the identification of novel tumor suppressor genes and oncogenes promoting B-cell lymphomagenesis. **(b)** Kaplan-Meier survival curves are shown for the indicated cohorts. In total 90 mice were aged up to 220 days to investigate the effects of *piggyBac* transposon mutagenesis on lymphomagenesis on a MYC-activated background. *Eμ-myc (M)*, n = 15; *Rosa*$^{PB/+}$*/M (R/M)*, n = 12; *ATP2-H32/M (A/M)*, n = 14; *A/R*, n = 5; *A/R/M*, n = 44. The mean survival times (days) were 44.5 for the *A/R/M* cohort and 90 for the *M* cohort. *P<0.0001*; log-rank (Mantel-Cox) test. **(c)** Analysis of white blood cell counts (WBC) and spleen weight of *A/R/M* mice (n=36 for spleen weight, n=43 for WBC) in comparison to *Eμ-myc* control mice (n=6 for spleen weight, n=7 for WBC).

mobilized by the transposase and reinserted across the entire genome without any preference for specific loci (Rad et al., 2010). We generated and analyzed a total of forty-eight *ATP2-H32;Rosa26*$^{PB/+}$*;Eμ-myc (A/R/M)* triple transgenic mice (Figure 9a). *PB* transposon mutagenesis led to accelerated lymphomagenesis and significantly reduced survival (median survival of 44.5 days and 90 days in *A/R/M* mice and *M* mice, respectively) (Figure 9b). Moreover, *A/R/M*

lymphomas were comparable aggressive to *Eμ-myc* control lymphomas indicated by similar white blood cell count (WBC) and spleen weight (SW) (Figure 9c). We next performed extensive phenotype analysis of lymphomas from *A/R/M* mice by multi-color flow cytometry and immunohistochemistry. We thereby found lymphoma characteristics comparable to those observed in *Eμ-myc* control mice (Bric et al., 2009), suggesting that transposon mutagenesis had direct effect on lymphomagenesis rather than on the cell of tumor origin (Figure 10a and b).

In summary, *PB* mutagenesis significantly accelerated lymphoma onset and we concluded that alterations upon *PB* mutagenesis promoted B-cell lymphomagenesis. Moreover, the alterations might cooperate with MYC.

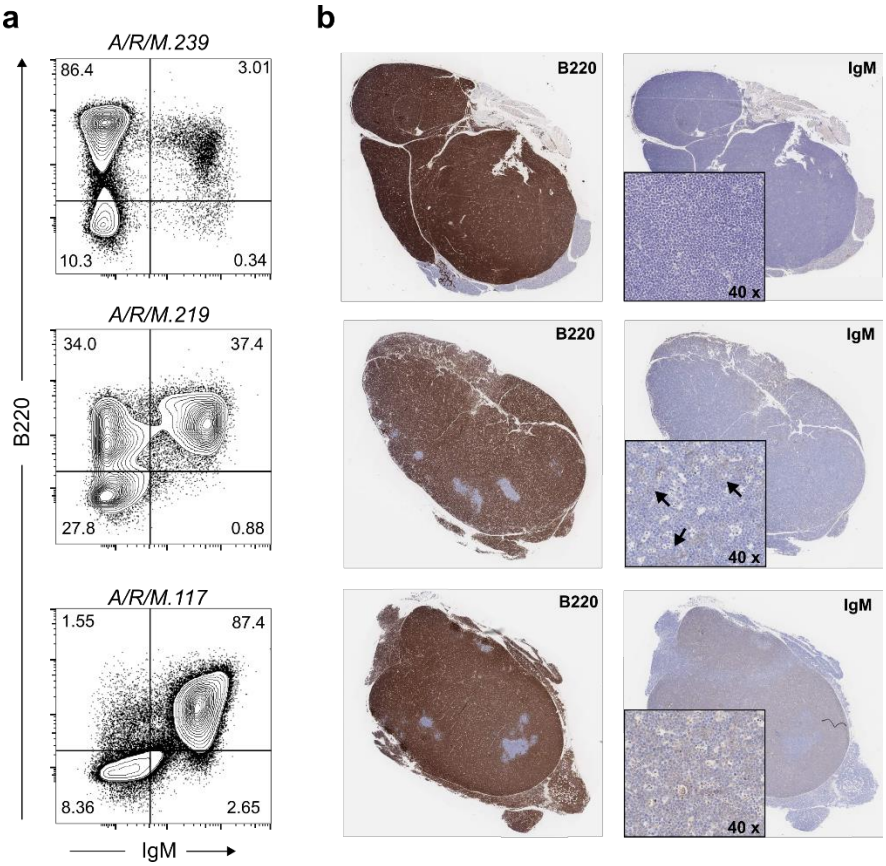

Figure 10. Analysis of B-cell phenotype of *A/R/M* lymphomas. (a) Single cell suspensions of tumors arising in triple transgenic *A/R/M* or *Eμ-myc* control mice were stained with specific antibodies against the B-cell markers B220 and IgM. Shown is one representative example of either B220+/IgM-, mixed or B220+/IgM+ lymphomas. Shown is only the population of CD45+ viable cells. **(b)** Histological and immunohistochemical analysis of three representative *A/R/M* lymphomas with the indicated antibodies.

3.1.2 Identification of novel BCL cancer genes and cross-species validation

To identify alterations promoting B-cell lymphomagenesis, we recovered transposon insertion sites from the murine lymphomas and performed quantitative insertion-site sequencing (QiSeq) and subsequent bioinformatics analysis like described earlier (Weber et al., 2019) (Figure 9a).

We analyzed 48 lymphomas and identified 126,770 non-redundant transposon insertion sites in total. Next, we identified genomic regions harboring more transposon insertions than expected by chance by applying Gaussian Kernel convolution analysis (Weber et al., 2019) and identified 958 common insertion sites (CISs) in *Eμ-myc* lymphomas (see section 7.1). We then analyzed the distribution of the top 100 KERNEL CIS genes across the 48 analyzed *A/R/M* lymphomas. Some cancers contributed to a small number of CIS genes, whereas several cancers contributed to a broad spectrum of CIS genes, suggesting different levels of clonality and potential cooperation and co-occurrence of CIS genes (Figure 11a).

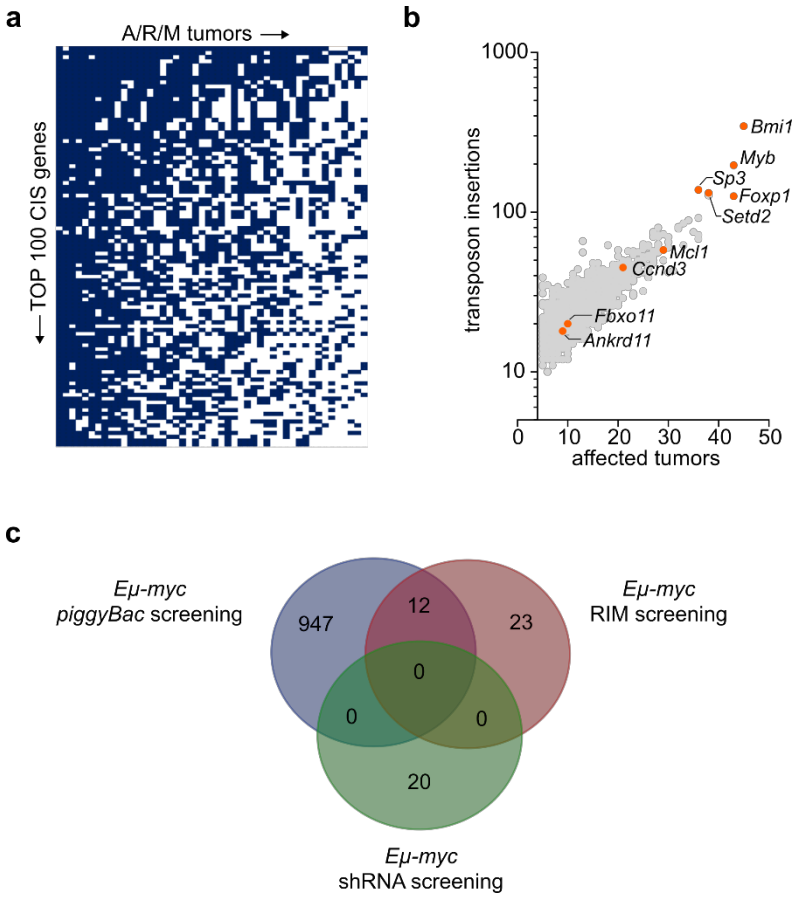

Figure 11. Transposon mutagenesis identified well-known cancer genes. (a) Distribution of the top 100 CIS genes across the analyzed 48 tumors. The blue boxes represent individual tumors with insertions contributing to CIS genes. **(b)** Graph showing the number of transposon insertions per CIS against the number of affected tumors. Examples listed in the Cancer Gene Census database are highlighted in orange. **(c)** The CIS genes identified in our screen were compared to the hits from a retroviral insertional mutagenesis screening (Mikkers et al., 2002) and a shRNA screening (Bric et al., 2009).

Concerning specific CIS genes, various well-known MYC-cooperating genes like *Bmi1*, *Myb* or *Mcl1* (Campbell et al., 2010; Jacobs et al., 1999) scored among the top hits (Figure 11b), suggesting that the identified alterations might cooperate with MYC to promote B-cell lymphomagenesis. Moreover, we compared the CIS genes identified in our screen to the genes identified in two screenings performed in the *Eμ-myc* model earlier (Bric et al., 2009; Mikkers et al., 2002). Only twelve overlapping genes were identified indicating no redundancy of the screenings (Figure 11c).

To test the biological and clinical relevance of *Eμ-myc* CIS genes, we analyzed their enrichment in genes with well-established functions in human cancers. We found that the identified set of 958 CIS genes was significantly enriched ($P = 0.65 \times 10^{-68}$) in the genes listed in the Cancer Gene Census (Sondka et al., 2018) (Figure 12a, upper panel). Moreover, several well-known tumor suppressor genes and oncogenes like *Mcl1*, *Sp3* or *Bmi1* were identified among the top hits of the screen (Figure 11b). Importantly, due to the chosen experimental lymphoma model, we investigated the enrichment of CIS genes in sets of established driver genes of human B-cell lymphomagenesis. Therefore, we analyzed datasets of recurrent mutations in DLBCL, an aggressive human B-cell lymphoma with established biological role of MYC. CIS genes were significantly enriched in the set of 150 DLBCL driver genes (Reddy et al., 2017) ($P = 0.95 \times 10^{-52}$) as well as in the set of 98 DLBCL driver genes (Chapuy et al., 2018) ($P = 0.24 \times 10^{-20}$) recently identified in the two largest available DLBCL sequencing studies (Figure 12a, lower panel).

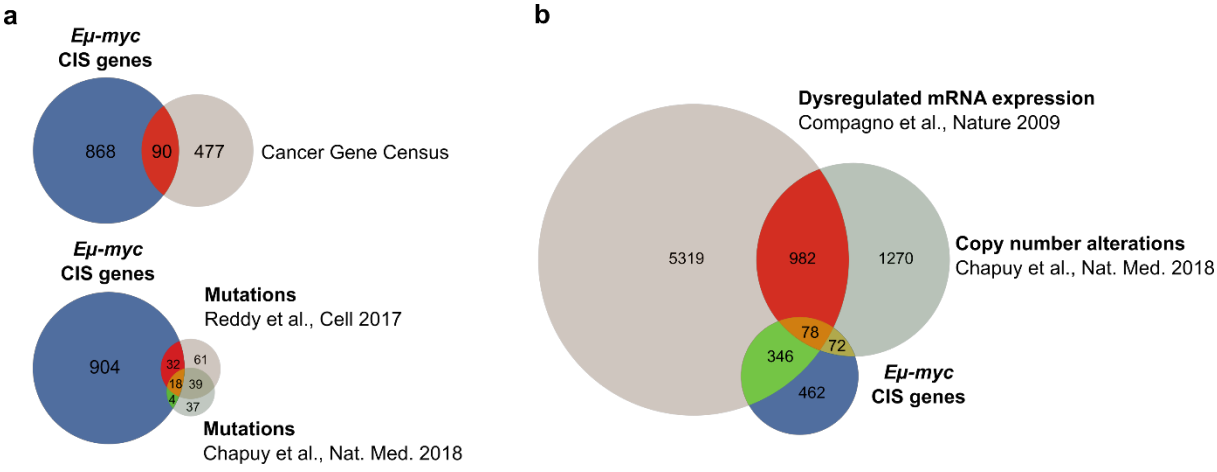

Figure 12. Cross-species validation of CIS genes identified in the *Eμ-myc piggyBac* screening. (a) Venn diagram showing the overlap between common insertion site (CIS) genes in triple-transgenic *A/R/M* lymphomas and genes listed in the Cancer Gene Census (upper panel) or B-cell lymphoma (DLBCL) driver genes (lower panel) described in the two largest available DLBCL sequencing studies (Chapuy et al., 2018; Reddy et al., 2017). **(b)** Venn diagram showing the overlap between CIS genes derived from the *Eμ-myc* transposon mutagenesis screen and genes with differential mRNA expression (*FDR P-value* < *0.05*) in DLBCL patients when compared to healthy GC B-cells (Compagno et al., 2009) or genes affected by copy number alterations in DLBCL patients (Chapuy et al., 2018).

Only a small fraction of driver genes in human cancers is altered by mutations or focal copy number alterations. The vast majority of altered genes is transcriptionally dysregulated. To test, if the genes identified in the *Eμ-myc PB* screen might be affected by non-genetic mechanisms, we interrogated a dataset comparing human DLBCL samples to control GC B-cells. Notably, 44% of all identified genes were dysregulated in human DLBCL on transcript level (Figure 12b). Moreover, 8% of the identified CIS genes was exclusively affected by copy number alterations (Figure 12b). In summary, 52% of *Eμ-myc* CIS genes were dysregulated in this analysis, indicating potential relevance in human BCL.

Thus, the *Eμ-myc PB* screen defined a catalogue of putative oncogenes and tumor suppressor genes promoting B-cell lymphomagenesis in murine and possibly human lymphoma.

3.2 Novel models for the investigation of B-cell lymphomagenesis

3.2.1 Generation of Hoxb8-FL progenitor cell lines

Whereas testing the potential of an alteration in tumorigenesis is depending on *in vivo* models, the mechanistic investigation of MYC-driven B-cell transformation in the *Eμ-myc* model is often limited by the availability of pre-malignant B-cells. The biology of these cells is characterized by MYC activation, however the cells are not yet transformed and need additional genetic alterations to ultimately transform. The spontaneous nature of *Eμ-myc* lymphomas and the time spectrum of lymphoma onset (50 to 250 days) does not allow the preparation of large amounts of premalignant cells e.g. by pooling of mice, which is needed for approaches like proteome analysis.

To allow the *in vitro* generation of premalignant *Eμ-myc* B-cells in literally unlimited numbers, we aimed to establish an immortalization protocol based on conditional expression of the transcription factor Hoxb8 (Redecke et al., 2013). This protocol implies the retroviral transduction of mouse bone marrow cells with an estrogen-regulated Hoxb8 expression construct (Figure 13). In combination with the Flt3 ligand it allows the conditional immortalization of early hematopoietic progenitor cells (Hoxb8-FL cells). Notably, after expansion and potential gene editing *in vitro*, Hoxb8-FL cells can be differentiated into B-cells *in vitro* when co-cultured on an irradiated OP9 layer in the presence of Flt3 ligand (Figure 13a) (Redecke et al., 2013). We applied this protocol to generate *Eμ-myc* and *control (Rosa26*^{Cas9}) Hoxb8-FL cells. Both cell lines exponentially grew in culture (Figure 13b). To test the potential of the cell lines to differentiate into B-cells *in vitro,* we co-cultured both generated Hoxb8-FL cell lines on OP9 cells in the presence of Flt3 ligand. After 12 days of co-culture a large fraction of cells was positive for the B-cell markers B220 and CD19 indicating successful differentiation to B-cells and moreover, cells were proliferating rapidly in the co-cultures (Figure 13c and d).

In summary, we successfully established *control* and *Eμ-myc* Hoxb8-FL cell lines, which can be expanded and modified *in vitro* and subsequently differentiated to B-cells.

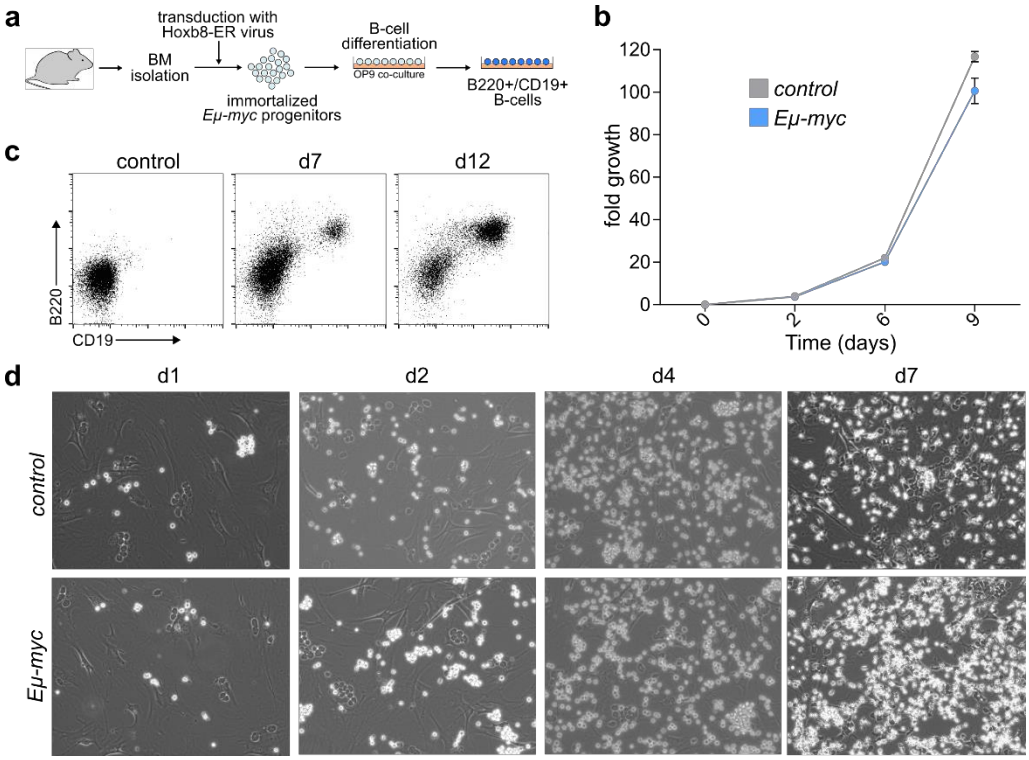

Figure 13. Generation of *Eμ-myc* and *control* Hoxb8-FL cell lines. (a) Experimental workflow for the generation of Hoxb8-immortalized progenitor cell lines and subsequent B-cell differentiation. **(b)** Growth analysis of *control (Rosa26^{Cas9})* and *Eμ-myc* Hoxb8-FL cells. **(c)** Flow cytometry analysis of *Eμ-myc* Hoxb8-FL cells after 7 and 12 days of co-culture in comparison to not co-cultured controls. **(d)** Co-culture of *control* and *Eμ-myc* Hoxb8-FL cells on OP9 cells at the indicated time points.

3.2.2 Testing the potential of *Eμ-myc* Hoxb8-FL cells to model MYC biology

To test the potential of the generated Hoxb8-FL cell lines to model pre-malignant B-cells and MYC biology *in vitro*, we first differentiated the *Eμ-myc* and *control (Rosa26^{Cas9})* Hoxb8-FL cells to B-cells (Figure 14a). We then performed CD19+ purification and subsequent qPCR analysis. *MYC* expression was substantially higher in *Eμ-myc* B-cells when compared to *control* B-cells.

To test if the generated cell lines could also be used to model MYC-driven B-cell lymphomagenesis *in vivo* and to thereby reduce the number of experimental animals, we performed retroviral transduction of *Eμ-myc* Hoxb8-FL progenitor cells with a Bcl-2 overexpressing vector and an empty vector. Transduction efficacy was typically between 20 and 40% as assessed by the co-expressed GFP marker. After pre-differentiation, we transplanted the cells into sub-lethally irradiated syngeneic recipient mice and monitored for lymphoma onset. Notably, all mice transplanted with Bcl-2 overexpressing *Eμ-myc* Hoxb8-FL cells developed lym-

phomas whereas empty vector transduced *Eμ-myc* Hoxb8-FL cells did not induce any lymphoma (Figure 14c). Spleen weight and white blood cell count of these mice were significantly higher when compared to control mice (Figure 14d and e) indicating the presence and infiltration of lymphoma cells. However, to which extent the *Eμ-myc* Hoxb8-FL model can be used for the validation of genetic alterations which are not as powerful as Bcl-2 overexpression needs to be tested in further experiments.

Together, we conclude that *Eμ-myc* Hoxb8-FL progenitor cells allow the generation of pre-malignant *Eμ-myc* B-cells in large numbers *in vitro*. Moreover, the generated cell lines allow the genetic modification of progenitor cells *in vitro* and can subsequently be transplanted into recipient mice to investigate MYC-driven B-cell lymphomagenesis *in vivo.*

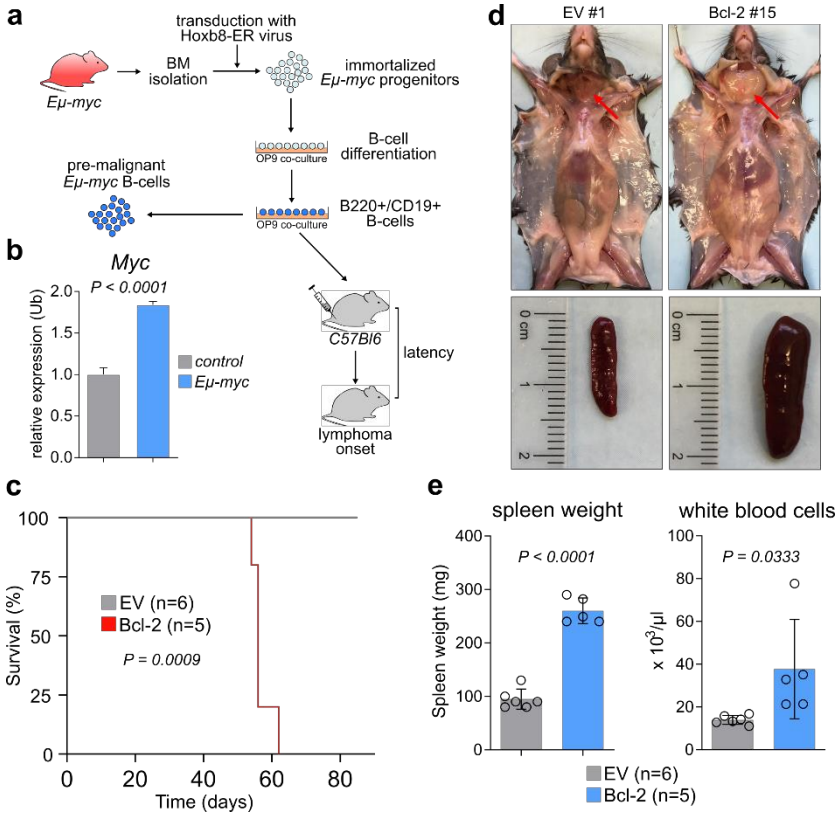

Figure 14. Generation of *Eμ-myc* Hoxb8-FL cell lines for investigating MYC biology *in vitro* and *in vivo*. (a) Experimental outline for the immortalization of hematopoietic progenitor cells and subsequent B-cell differentiation or transplantation. **(b)** *MYC* expression in CD19+ B-cells derived from *control* and *Eμ-myc* Hoxb8-FL progenitors after 12 days of differentiation. *MYC* expression was normalized to *Ubiquitin*. *P-value* determined with unpaired t-test. **(c)** Kaplan-Meier curves for survival of mice transplanted with *Eμ-myc*-FL progenitors transduced with either empty vector (EV) or Bcl-2 expressing vector. EV, n = 6; Bcl-2, n = 5; P = 0.0009, log-rank (Mantel-Cox) test. **(d)** Representative EV mouse and mouse transplanted with Bcl-2 overexpressing *Eμ-myc* Hoxb8-FL cells. **(e)** Analysis of spleen weight and white blood cell count of transplanted mice. *P-value* determined by unpaired t test.

3.2.3 A CRISPR/Cas9-based *in vivo* platform for functional validation

The validation of cancer genes identified in our transposon mutagenesis screen *in vitro* is limited due to the aggressive nature of cancer cell lines and the broad mutational background of these cell lines, which have been established many years ago.

To overcome these limitations and to perform validations in an *in vivo* system with minimal mutational background, we applied a transduction-transplantation system based on hematopoietic stem and progenitor cells (HSPCs) derived from E13.5 fetal livers. To this end, we combined the *Eμ-myc* mouse model with a Cas9 expressing mouse line and generated HSPCs (Figure 15a). To validate our model, we lentivirally transduced the cells with a sgRNA targeting the well-known tumor suppressor *Trp53* coupled to a GFP reporter to monitor transduction ef-

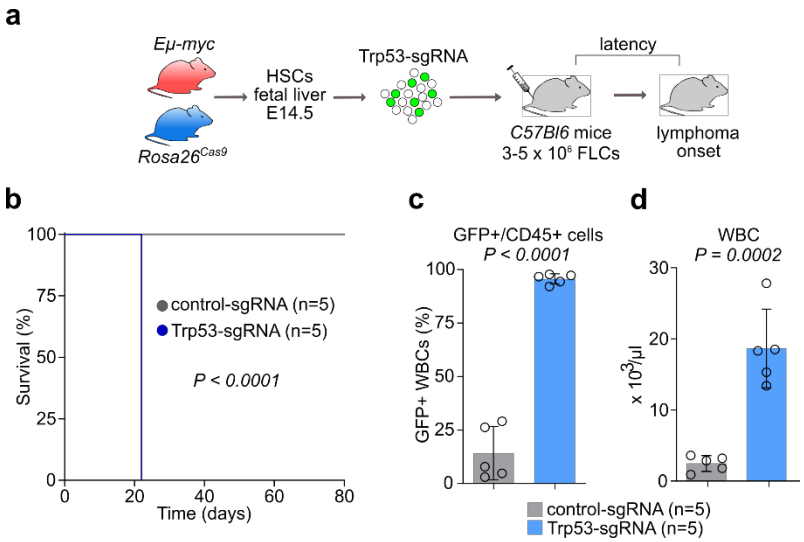

Figure 15. Establishment of a CRISPR/Cas9 based platform for the *in vivo* validation of BCL tumor suppressor genes. (a) Outline of the experimental workflow for the *in vivo* validation of tumor suppressor genes in a transduction-transplantation model. **(b)** Kaplan-Meier curves of overall survival in mice transplanted with *Eμ-myc;Rosa26*^{Cas9} HSPCs transduced with sgRNAs targeting *Trp53*. Trp53, n = 5; control n = 5; P < 0.0001, log-rank (Mantel-Cox) test. **(c)** Flow cytometry based quantification of GFP+/CD45+ cells from mice transplanted with control-sgRNA and Trp53-sgRNA. *P-value* was determined by unpaired t test. **(d)** White blood cell counts from mice transplanted with control-sgRNA and Trp53-sgRNA. *P-value* was determined by unpaired t test.

ficiency, which was usually between 20 and 30%. We then transplanted the cells into sublethally irradiated *C57Bl6* recipient mice (Figure 15a). Recipient mice were monitored for engraftment 20 d after transplantation and afterwards for lymphoma. We detected significantly accelerated lymphomagenesis and the sgRNA targeting *Trp53* induced lymphomas in all transplanted mice whereas the non-targeting control did not produce any lymphoma with comparable latency (Figure 15b). We detected strong expansion of CD45+/GFP+ and hence Trp53-depleted cells (Figure 15c), indicating positive selection of the sgRNA targeting *Trp53.* Moreover, animals transplanted with Trp53-sgRNA had significantly higher WBCs when compared to animals transplanted with control sgRNA (Figure 15d).

Thus, we successfully established a versatile platform for CRISPR/Cas9 based testing of candidate tumor suppressor genes *in vivo*.

3.3 *In vivo* validation of candidate tumor suppressor genes

3.3.1 *Snrnp70* and *Slf2* are putative tumor suppressor genes

From the KERNEL analysis of the entire library we identified 958 CIS genes, which were present in lymphomas (see section 7.1). To filter for highly relevant CIS genes, we used a scoring system implying prognostic impact, expression and TCGA data. Based on literature research we removed known driver genes and chose *Snrnp70* and *Slf2* for validation.

SNRNP70 is a component of the spliceosomal U1 snRNP, which is essential for the assembly of the spliceosome (Pomeranz Krummel et al., 2009). A role of SNRNP70 in cancer is not described. To investigate the biological function of Snrnp70 in lymphoma pathogenesis, we analyzed the transposon insertion pattern. Transposon insertions were bidirectional and scattered across the *Snrnp70* gene indicating tumor suppressor function (Figure 16a). Of note, 29 out of 48 *A/R/M* lymphomas harbored *Snrnp70* insertions (Figure 16b). To validate the inactivation of *Snrnp70*, we performed immunoblot analysis and compared *A/R/M* lymphomas

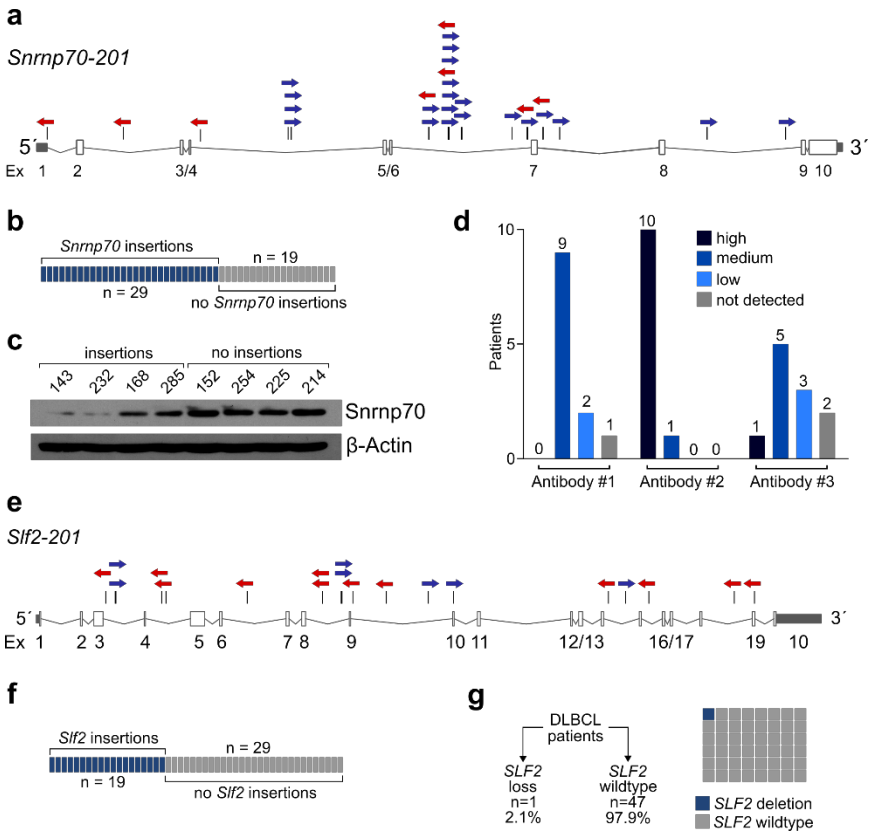

Figure 16. *Snrnp70* and *Slf2* are putative tumor suppressor genes in mice and dysregulated in human BCL. **(a)** Transposon insertion pattern in *Snrnp70* indicating tumor suppressor function. Only the dominant insertion per tumor is shown. **(b)** Number of tumors affected by *Snrnp70* transposon insertions**. (c)** Immunoblot analysis of Snrnp70 expression in A/R/M lymphomas with transposon insertions in comparison to *A/R/M* lymphomas without transposon insertions. **(d)** SNRNP70 expression in human DLBCL as detected by immunohistochemistry with three different antibodies (data from the Human Protein Atlas (Uhlen et al., 2015)). **(e)** Transposon insertion pattern in *Slf2* indicating tumor suppressor function. Only the dominant insertion per tumor is shown. **(f)** Number of tumors affected by *Slf2* transposon insertions. **(g)** Analysis of *SLF2* copy number status in a dataset comprising 48 human DLBCL patients (TCGA DLBCL cohort).

with transposon insertions in *Snrnp70* to *A/R/M* lymphomas without *Snrnp70* insertions. Snrnp70 expression was reduced in lymphomas harboring transposon insertions in *Snrnp70* revealing effective inactivation (Figure 16c). To test potential translational relevance in human BCLs, we interrogated datasets of DLBCL, a BCL with well-described biological role of MYC. Surprisingly, *SNRNP70* was identified as part of a long amplification in DLBCL patient samples, which is associated with an increase in *SNRNP70* mRNA expression rather indicating putative function as oncogene (Chapuy et al., 2018). We then analyzed SNRNP70 protein expression as detected by immunohistochemistry with three different antibodies (data from the Human Protein Atlas (Uhlen et al., 2015)). Importantly, and not presumed from the genome and transcriptome data, SNRNP70 protein expression was low or not detected in a subset of DLBCL patients, revealing loss of function (Figure 16d). From this we concluded that low SNRNP70 expression might also functionally contribute to human BCL pathogenesis.

SLF2 plays a role in the DDR and controls genome stability (Raschle et al., 2015). A role of SLF2 in cancer biology has not been described. To probe the biological role of *Slf2* in lymphomagenesis, we analyzed the transposon insertion pattern. Transposon insertions were bidirectional and scattered across the gene, indicating tumor suppressor function (Figure 16e). *Slf2* insertions were found in 19 out of 48 *A/R/M* lymphomas (Figure 16f) and moreover, genomic deletions of *SLF2* were found with low frequencies in human DLBCL patients samples indicating potential relevance in human BCL (Figure 16g).

In summary, *Snrnp70* and *Slf2* are candidate tumor suppressor genes in murine BCL and have potential relevance in human BCL. Moreover, the findings underscore the value of functional *in vivo* screenings to support the interpretation of OMICs studies based on large patient cohorts.

3.3.2 *Slf2* and *Snrnp70* restrict MYC-driven B-cell lymphomagenesis

To test the tumor suppressor gene function *in vivo,* we applied the CRISPR/Cas9 platform for *in vivo* validation of candidate genes. We lentivirally transduced HSPCs with sgRNAs coupled to a GFP reporter to monitor transduction efficiency, which was usually between 20 and 30%. We then transplanted the cells into sub-lethally irradiated recipient mice (Figure 17a). 20 days after transplantation we controlled engraftment by FACS analysis of blood samples of recipient mice. Besides engraftment, we detected a striking positive selection of sgRNAs targeting *Snrnp70* and *Slf2*, but not for the control sgRNA (Figure 17b) and both sgRNAs accelerated lymphomagenesis (Figure 17c). In all mice we verified the BCL phenotype by immunohisto-

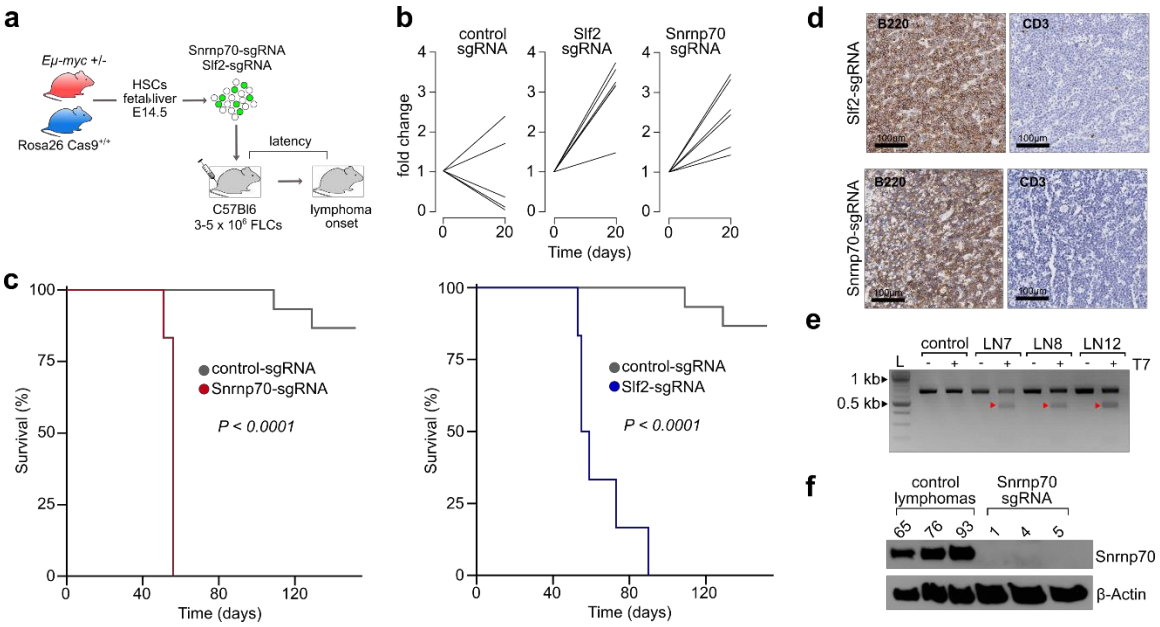

Figure 17. *Snrnp70* and *Slf2* restrict murine B-cell lymphomagenesis *in vivo*. (a) Transduction-transplantation strategy to generate chimeric mice stably expressing GFP-tagged sgRNAs in hematopoietic cells. Fetal liver hematopoietic stem/progenitor cells (HSPC) were transduced with the indicated sgRNAs. **(b)** Enrichment of B220+/EGFP+ cells representing sgRNA expressing B-cells in the peripheral blood 20 days after transplantation. Fold change of all EGFP+ cells at the time of transplantation and the B220+/EGPF+ population at day 20 are shown for either 5 mice (control) or 6 mice (Snrnp70 and Slf2) per group. (c) Kaplan-Meier curves for survival of mice transplanted with *Eμ-myc;Rosa26*^{Cas9} HSPCs transduced with sgRNAs targeting *Slf2* or *Snrnp70*. Slf2, n = 6; Snrnp70, n = 5; control, n = 15; P < 0.0001, log-rank (Mantel-Cox) test. (d) Representative histological and immunohistochemical analysis of Slf2-sgRNA and Snrnp70-sgRNA lymphomas out of three analyzed lymphomas. (e) *In vitro* T7 nuclease assay showing cutting efficacies of the Slf2-sgRNA in lymphomas from *in vivo* validation experiment. (f) Immunoblot analysis of Snrnp70-sgRNA lymphomas in comparison to control lymphomas with the indicated antibodies. [Data from (d) provided by K. Steiger].

chemistry straining for B220 (Figure 17d) and as expected, we could either detect insertions and deletions (InDels) at the targeted gene loci or loss of protein expression indicating efficient CIRPSR/Cas9 gene editing (Figure 17e and f).

In summary, we show that *Snrnp70* and *Slf2* are functional relevant tumor suppressor genes in mice, which might also be relevant in human BCLs. Notably, despite of *SNRNP70* being part of a large amplification, we found that SNRNP70 protein expression is absent or reduced in a fraction of DLBCL patients. In combination with the functional data from mice this

points towards a post-translational mechanism and underscores the power of functional screening for the interpretation of sequencing data from human cancer patients.

3.4 SENP6 is a tumor suppressor of B-cell lymphomagenesis

3.4.1 Identification of *Senp6* as a putative tumor suppressor gene

The *in vivo* transposon mutagenesis approach allows positive selection of driver alterations for B-cell lymphomagenesis. Hypothesizing that several of the identified CIS genes converge in common pathways during B-cell lymphomagenesis, we performed pathway enrichment analysis using the GeneTrail2 1.6 web service (Stockel et al., 2016) and the Reactome database. Among the 41 significantly enriched pathways were several pathways with well-defined roles in cancer and during lymphomagenesis, including the *"VEGFA-VEGFR2"* pathway, and the *"Antigen activates B-cell Receptor (BCR) leading to generation of second messengers"* pathway (Figure 18a; full list of enriched pathways, see section 7.2). Notably, *"SUMOylation of DNA damage response proteins" ($P = 7.81 \times 10^{-5}$)* scored among the top altered pathways (Figure 18a) prompting us to hypothesize that proteins cooperating with MYC in lymphomagenesis, and more generally in cancer pathogenesis, are part of the DDR network and are preferentially deregulated by the SUMO modification system. This hypothesis is supported by the frequent finding that aberrant SUMOylation is linked to a particular robust cancer phenotype, treatment resistance and poor prognosis (Seeler and Dejean, 2017). Furthermore, activated SUMOylation has been linked to MYC activity (Hoellein et al., 2014; Kessler et al., 2012).
To investigate which specific genes in the positive or negative regulatory SUMOylation path-

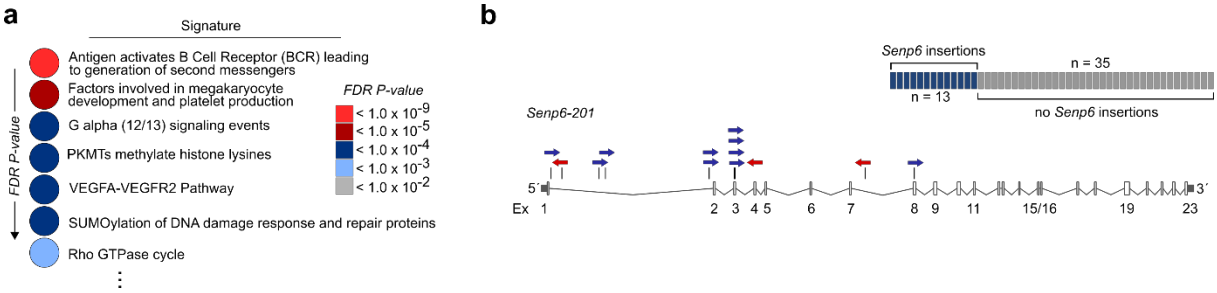

Figure 18. *Senp6* is a putative tumor suppressor of MYC-driven B-cell lymphomagenesis. (a) *Eμ-myc* CIS genes were analyzed using the Reactome database. Color-coded FDR *P-value* is shown for the top seven pathways. **(b)** Transposon insertion pattern in *Senp6* indicating tumor suppressor function and the number of affected tumors. Only the dominant insertion per tumor is shown.

way were integration sites within the transposon screen, we searched the CIS genes identified in the *A/R/M* screen and identified the SUMO protease *Senp6* as a putative cancer driver gene (see section 7.1). SENP6 belongs to the family of SUMO deconjugating cysteine proteases

and preferentially acts by dismantling SUMO chains (Kunz et al., 2018). The transposon insertion pattern of *Senp6* was characterized by scattered and bidirectional insertions, suggesting a role as a tumor suppressor gene (Figure 18b).

In summary, we identified dysregulated SUMOylation as a critical pathway in BCL pathogenesis and the SUMO protease *Senp6* as a candidate tumor suppressor gene in mice.

3.4.2 *SENP6* is recurrently deleted in human BCLs

To assess the relevance of this finding for human lymphomagenesis, we next queried human sequencing datasets for *SENP6* alterations.

While we found only infrequent somatic mutations in *SENP6* (1% in (Chapuy et al., 2018)), we found recurrent focal deletions of 6q14.1/*SENP6* in DLBCL patients with frequencies ranging from 13% (38/304) (Chapuy et al., 2018) to 23% (11/48) (TCGA DLBCL dataset) (Figure 19a), underscoring the relevance of the murine screen for human lymphomas. Moreover, genomic loss of *SENP6* was associated with reduced abundance of *SENP6* transcripts (Figure 19b). To stress the association of *SENP6* loss with MYC signatures, we performed gene set enrichment analysis (GSEA) and found that 6 out of 7 tested gene sets reflecting activated MYC signaling were significantly enriched in the subgroup of patients harboring *SENP6* deletions (Figure 19c and d).

Moreover, we also identified *SENP6* deletions in a broad range of BCL subentities, including marginal zone, MCL, FL and BL, indicating a possible role of SENP6 or the SUMOylation pathway in other lymphomas (Figure 19e). To investigate whether *SENP6* deletions might also occur in solid tumors, we searched TCGA datasets (https://www.cbioportal.org/) and identified *SENP6* deletions in several solid cancers like pancreatic adenocarcinoma (PDAC), prostate adenocarcinoma and uveal melanoma (Figure 19f).

Thus, functional analysis and mining large-scale OMICs studies revealed that *SENP6* deletions occur in a broad spectrum of hematopoietic and solid cancers and might have a general function in suppression of these malignancies.

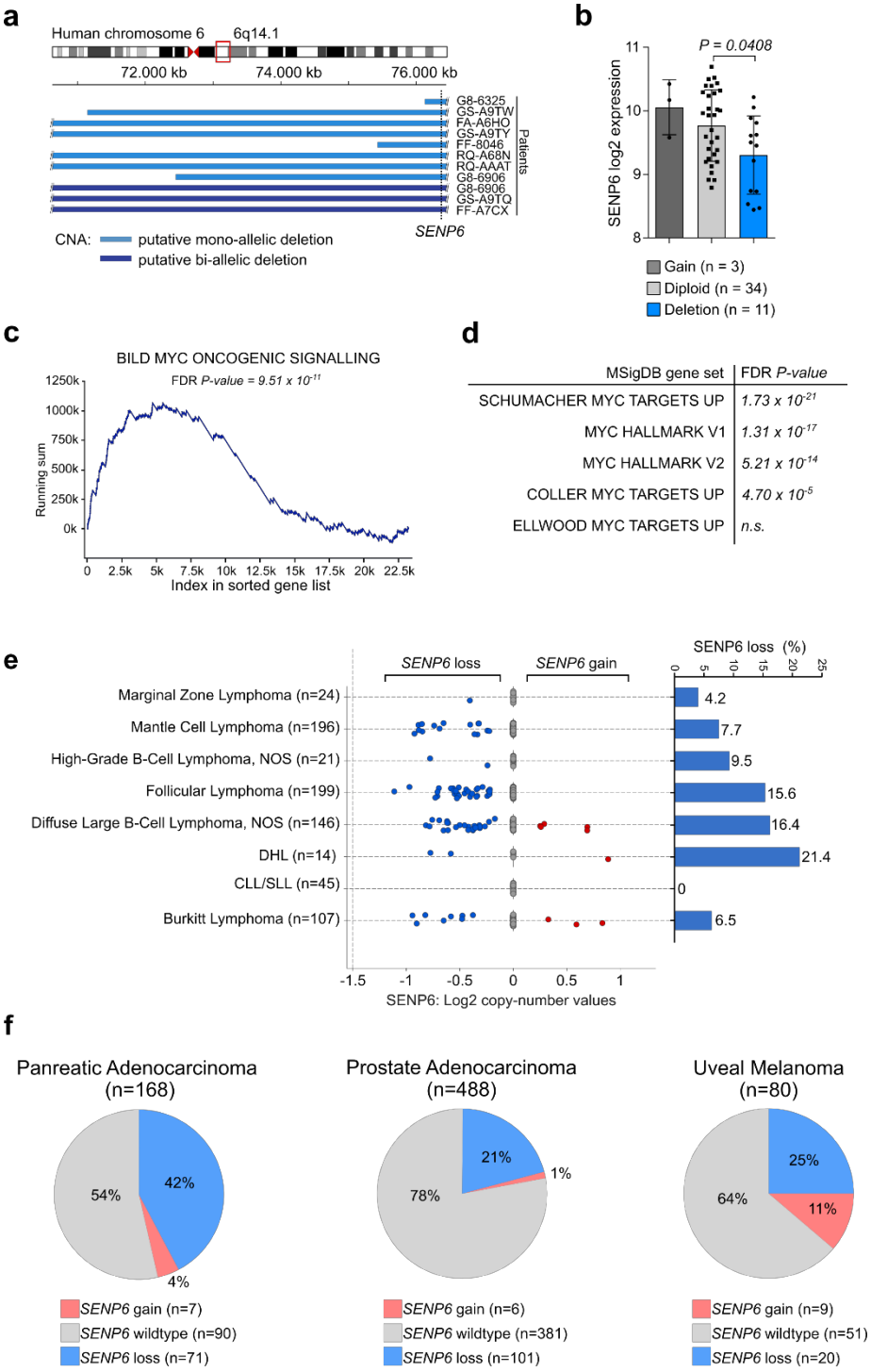

Figure 19. *SENP6* is recurrently deleted in human BCLs and non-hematopoietic cancers. (a) The red box indicates the region 6q14.1 on human chromosome 6, which is shown in detail below. Putative mono-allelic and putative bi-allelic deletions affecting the *SENP6* locus in human DLBCL patients are shown as horizontal bars and the respective color indicates the type of CNA. The dotted line indicates the genomic position of the *SENP6* gene. CNA, copy number alteration. Kb, kilobase. **(b)** Expression analysis of *SENP6* mRNA in DLBCL patients (n=48). Groups were classified according to their SENP6 copy number status. *P-value* determined by ANOVA, Tukey`s post hoc test. **(c, d)** GSEA of expression data derived from primary DLBCL patient samples described in Figure 19a and Figure 19b. Groups were classified according to their SENP6 copy number status. **(e)** *SENP6* copy number status in different mature B-cell lymphomas derived from https://www.cbioportal.org/. **(f)** *SENP6* copy number status in pancreatic adenocarcinoma, prostate adenocarcinoma and uveal melanoma (upper panel) and transcript abundance in patients groups classified according to the *SENP6* copy number status. Data were derived from https://www.cbioportal.org/ and are part of the TCGA consortium. *P-value* determined by ANOVA, Tukey`s post hoc test.

3.4.3 Genetic deletion of *Senp6* promotes B-cell lymphomagenesis

Finally, to prove a functional role for Senp6 loss in an established model of B-cell lymphomagenesis *in vivo*, we applied the CRISPR/Cas9 platform described above (Figure 15). To this end, we generated hematopoietic stem cell grafts from *Eμ-myc;Rosa26*^{Cas9} mice. E13.5 fetal liver-derived hematopoietic stem and progenitor cells (FL-HSPC) were transduced with a lentivirus encoding a sgRNA targeting *Senp6* as described in section 3.2.2. (Figure 20a). Syngeneic wildtype mice receiving *Senp6* sgRNA FL-HSPC grafts were monitored for lymphoma onset. Loss of Senp6 promoted B-cell lymphomagenesis *in vivo* (Figure 20b), validating the findings from the *PB* screen for this specific gene. As expected, we detected InDels with associated loss of Senp6 protein in Senp6-sgRNA lymphomas (Figure 20c and d).

Thus, this *in vivo* experiment proved that loss of Senp6 accelerated MYC-driven lymphomagenesis in mice, providing for the first time direct experimental evidence that deregulated SUMOylation accelerates cancer formation.

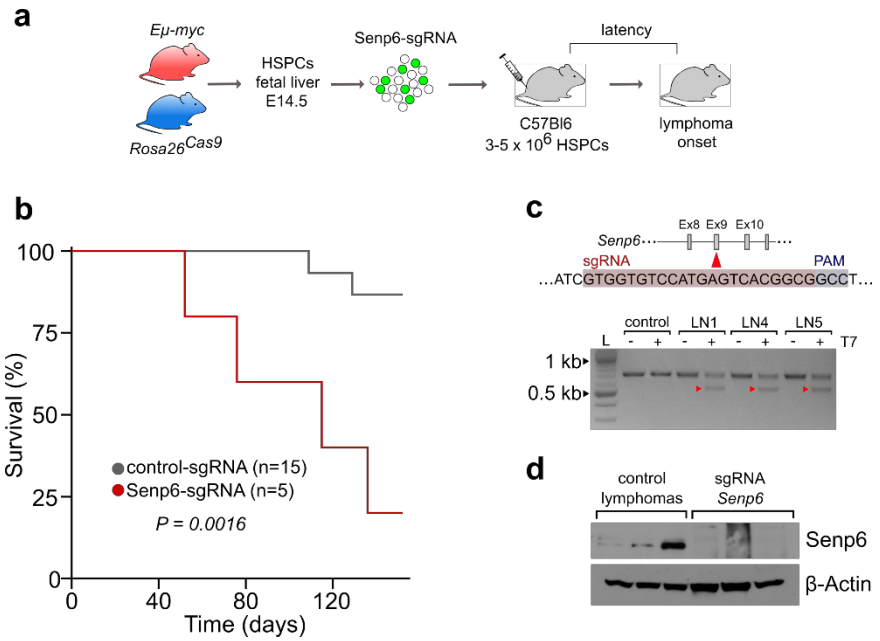

Figure 20. Genetic deletion of Senp6 promotes B-cell lymphomagenesis. (a) Tansduction-transplantation strategy to generate chimeric mice stably expressing GFP-tagged sgRNAs in hematopoietic cells. Fetal liver hematopoietic stem/progenitor cells (HSPC) were transduced with the Senp6-sgRNA. **(b)** Kaplan-Meier curves of overall survival in mice transplanted with *Eμ-myc;Rosa26*^{Cas9} HSPCs transduced with sgRNAs targeting *Senp6.* Senp6, n = 5; control n = 15; *P = 0.0016*, log-rank (Mantel-Cox) test. **(c)** *In vitro* T7 nuclease assay showing cutting efficacies of the Senp6-sgRNA in lymphomas from *in vivo* validation experiment. **(d)** Western blot analysis of Senp6-sgRNA lymphomas (n=3) and control lymphomas (n=3) with the indicated antibodies.

3.4.4 Ectopic SENP6 expression is sufficient to suppress BCL growth

To gain insight into the associated mechanisms in human BCL, we explored the Cancer Cell Line Encyclopedia (https://portals.broadinstitute.org/ccle) in search for model cell lines and identified DLBCL cell lines with (SU-DHL-5) and without (SU-DHL-8, Oci-Ly1, Oci-Ly3, DB)

genomic *SENP6* loss. Next, we performed immunoblot analysis to assess SENP6 protein levels in these cell lines and found reduced SENP6 protein expression in the *SENP6*-deleted SU-DHL-5 cell line (Figure 21a, upper panel) compared to expression in the control cells without *SENP6* loss. Next, we performed lentiviral transductions to reconstitute SENP6 expression in *SENP6*-deleted SU-DHL-5 cells and analyzed the cellular consequences of reduced and reconstituted SENP6 levels. As expected, SENP6 protein expression was substantially increased in reconstituted cells in comparison to the empty vector transduced cells (Figure 21a, lower panel and Figure 21b, insert). Importantly, reconstituted SENP6 expression in SU-DHL-5 cells resulted in significantly reduced cell growth (Figure 21b), which was associated with increased cell death (Figure 21c). Moreover, transcriptome profiling and subsequent GSEA indicated enriched expression of genes associated with apoptosis and depletion of MYC-signaling in cells with reconstituted SENP6 expression further empowering the association of genomic *SENP6* loss and MYC-signaling (Figure 21d and e).

Thus, we show that the SENP6 status is sufficient to suppress BCL growth and that SENP6 is a tumor suppressor in human BCL

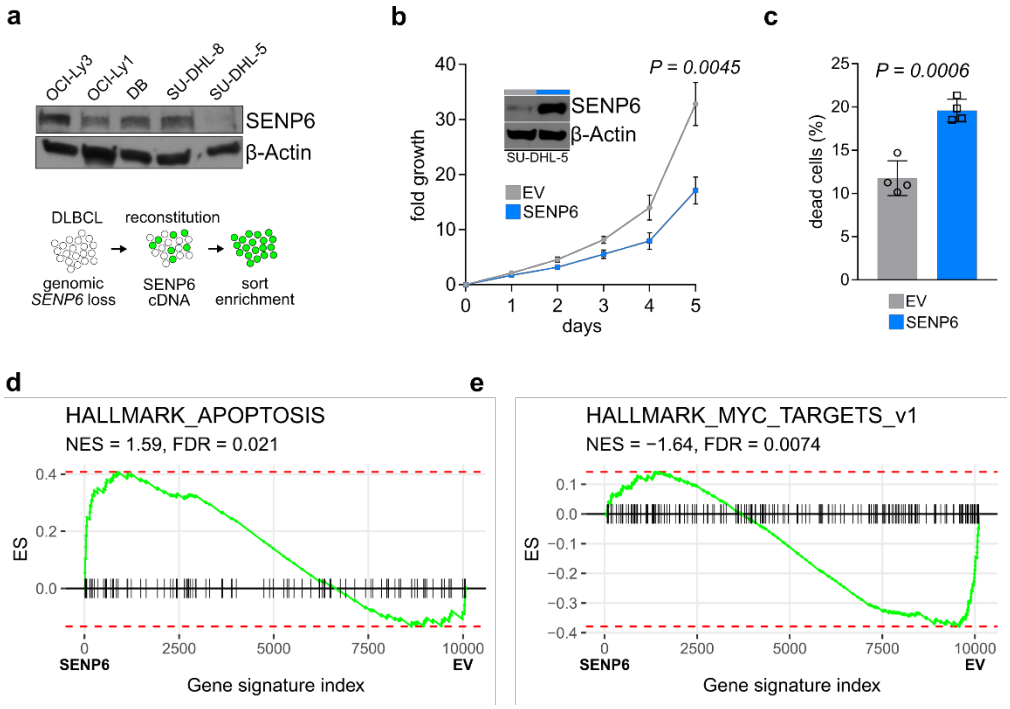

Figure 21. The SENP6 status is sufficient to suppress BCL growth *in vitro*. (a) Immunoblot analysis of SENP6 expression of human DLBCL cell lines with different *SENP6* copy number status and experimental workflow of lentiviral SENP6 reconstitution. **(b)** Immunoblot analysis of cells after SENP6 reconstitution and analysis of SU-DHL-5 proliferation upon SENP6 reconstitution versus empty vector (EV) transduced control cells (n=3). *P-value* determined by unpaired t-test. **(c)** Flow cytometry analysis of cell death of the cell lines described in Figure 21a using propidium iodide staining (n=4). *P-value* determined by unpaired t-test. **(d, e)** GSEA of expression data derived from whole transcriptome analysis of SU-DHL-5 described in Figure 21b. [Data from (d) and (e) provided by C. Maurer].

3.4.5 Low SENP6 expression is associated with adverse prognosis

In order to probe the association of SENP6 expression with an aggressive tumor phenotype in human BCL patients, we generated a tissue microarray derived from 58 DLBCL patients, who have been treated at the Klinikum rechts der Isar of the Technical University of Munich. We split the patients into two groups of either long-term remission (n=16) or early relapse (<1 year)/refractory disease (n=42) and performed IHC with an antibody specifically detecting SENP6 protein. SENP6 expression was significantly lower in the relapse/refractory group as compared to the long-term remission group (Figure 22a), indicating that low SENP6 levels were associated with inferior prognosis. In support of the human data pointing to an adverse association of SENP6 expression and treatment efficacy (Figure 22a), the SU-DHL-5 DLBCL cell line showed increased cell death upon doxorubicin (DRB) treatment after reconstitution of SENP6 expression (Figure 22b).

Taken together, these data reveal a function of SENP6 in mediating the efficacy of chemotherapeutic treatment and suggest that BCLs lacking SENP6 expression are less sensitive to standard lymphoma therapies.

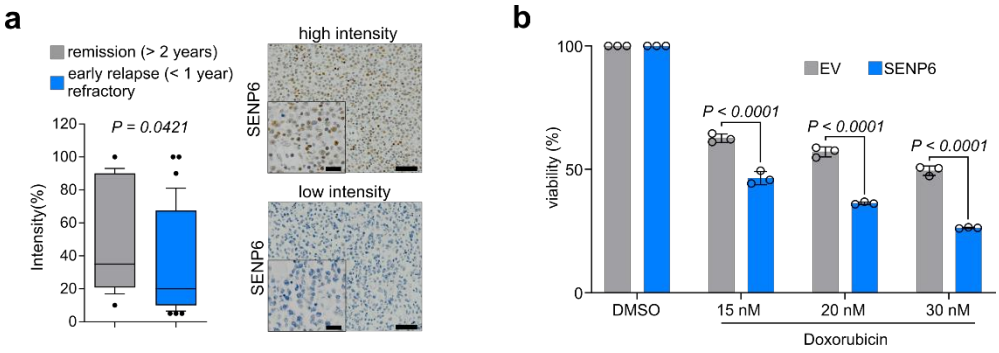

Figure 22. Low SENP6 expression is associated with adverse prognosis in DLBCL. (a) Tissue microarray analysis of primary DLBCL samples with a specific SENP6 antibody. *P-value* determined by Wilcoxin signed rank test. Remission (>2 years), n=16; early relapse/refractory, n=38). **(b)** Viability of cell lines described in Figure 21b after 48h doxorubicin treatment with the indicated doxorubicin concentrations. Viability was determined by propidium iodide staining and flow cytometry measurement. *P-value* determined by ANOVA; Bonferroni's multiple comparisons test. [Data from (a) provided by K. Steiger and J. Slotta-Huspenina].

3.5 SENP6 is the critical determinant of SUMO homeostasis in BCL

3.5.1 The SENP6 level is critical for the SUMO state in BCL

SUMO proteases are essential regulators of the SUMO equilibrium in mammalian cells. Whereas SENP1, SENP2, SENP3 and SENP5 act as maturation enzymes and deconjugases of SUMO, the closely related enzymes SENP6 and SENP7 cannot catalyze SUMO maturation and preferentially cleave poly-SUMO2/3 chains (Kunz et al., 2018).

To test, if Senp6 is critical for the SUMOylation state in early hematopoietic progenitor cells, we transduced *Eμ-myc* Hoxb8-FL cells with either a shRNA targeting Senp6 or an empty vector (Figure 23a). Next, we performed qPCR analysis of *Senp6* expression. *Senp6* expression was substantially reduced in progenitor cells transduced with the *Senp6* shRNA (Figure

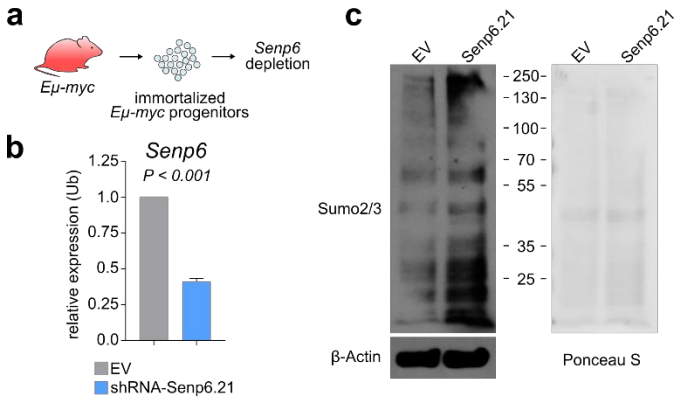

Figure 23. Senp6 is a critical regulator of the SUMO state in *Eμ-myc* Hoxb8-FL progenitor cells. (a) Experimental workflow for the immortalization of *Eμ-myc* progenitor cells and *Senp6* depletion. **(b)** *Senp6* expression in *Eμ-myc* Hoxb8-FL cells transduced with a shRNA targeting *Senp6* or empty vector (EV). Senp6 expression was normalized to *Ubiquitin*. **(c)** Immunoblot analysis of overall SUMOylation with the indicated antibodies and Ponceau S staining. *Eμ-myc* Hoxb8-FL cells transduced with a shRNA targeting *Senp6* were compared to empty vector transduced cells.

23b). We then performed immunoblot analysis of *Senp6* depleted progenitor cells and compared them to control cells. The level of Sumo2/3 conjugated target proteins was increased (Figure 23c) revealing that cell lacking Senp6 are characterized by a high level of SUMOylated proteins.

To test whether Senp6 is crucial for regulating the SUMO state in MYC-driven lymphoma, we performed immunoblot analysis of Senp6-depleted lymphomas derived from the *in vivo* validation experiments described above (Figure 20b). Remarkably, the high level of SUMOylated proteins in *Eμ-myc* lymphomas was further enhanced upon deletion of *Senp6* (Figure 24a). The effect was more pronounced on Sumo2/3 than Sumo1 conjugates underscoring the preference of Senp6 for Sumo2/3 (Figure 24a). To investigate whether reconstitution of SENP6 is sufficient for effectively controlling the level of global protein SUMOylation in human BCL, we analyzed the level of SUMO2/3 conjugated proteins in the SU-DHL-5 DLBCL cell line after reconstitution of SENP6 expression and found a strong reduction of SUMO2/3 conjugates

(Figure 24b). Moreover, CRISPR/Cas9-mediated deletion of *SENP6* led to decreased SENP6 protein expression accompanied by an increase in SUMO2/3-conjugated proteins (Figure 24c).

In summary, we conclude that the SENP6 level is a critical determinant of the overall SUMOylation state in murine and human BCL.

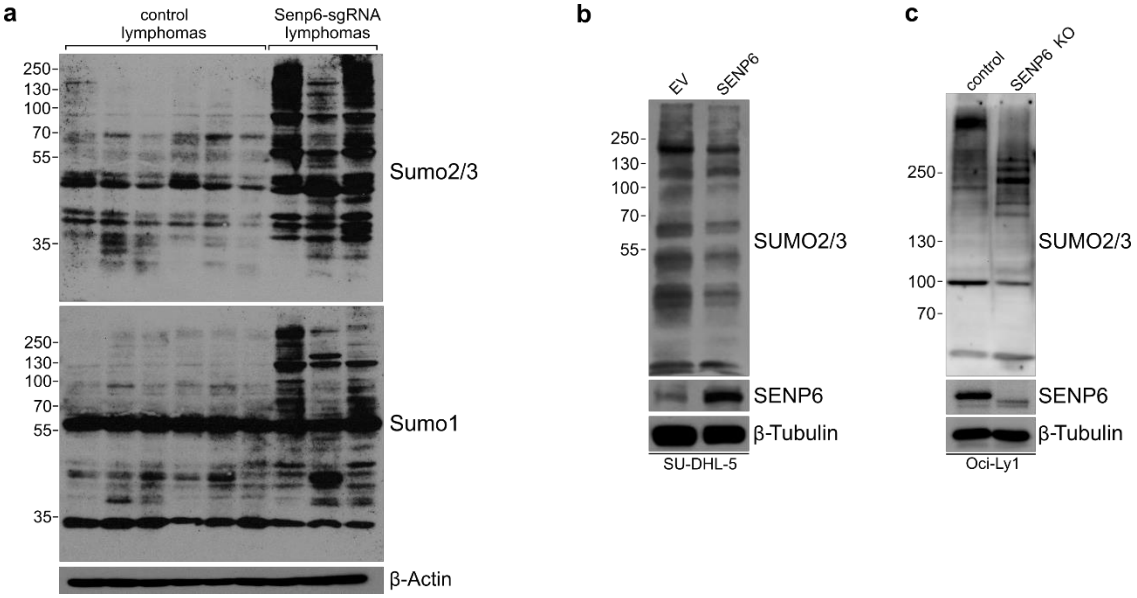

Figure 24. SENP6 is a critical regulator of the SUMO state in BCLs. (a) Immunoblot analysis of overall SUMOylation with the indicated antibodies. *Eμ-myc* control lymphomas (n=6) were compared to Senp6-sgRNA lymphomas (n=3) derived from *in vivo* validation experiments described in Figure 20b. **(b)** Immunoblot analysis of human SU-DHL-5 cell lines after reconstitution of SENP6 expression described in Figure 21b with the indicated antibodies. EV, empty vector control. **(c)** Immunoblot analysis of human Oci-Ly1 cell lines following CRISPR/Cas9-mediated SENP6 depletion with the indicated antibodies. KO, knockout.

3.5.2 SENP7 is suppressed during BCL pathogenesis

Considering that the SENP6-related isopeptidase SENP7 also primarily functions in trimming of SUMO chains we expected that the closely related enzyme SENP7 might, at least partly, rescue the effects of SENP6 depletion on SUMO deconjugation.

To delineate a potential interplay of both isopeptidases in tumor suppression, we first investigated *Senp7* levels during murine B-cell lymphomagenesis in the *Eμ-myc* model. Notably, *Senp7* was suppressed during lymphomagenesis on transcript level and Senp7 protein was absent in *Eμ-myc* lymphomas (Figure 25a and b). To confirm this result in human BCL,

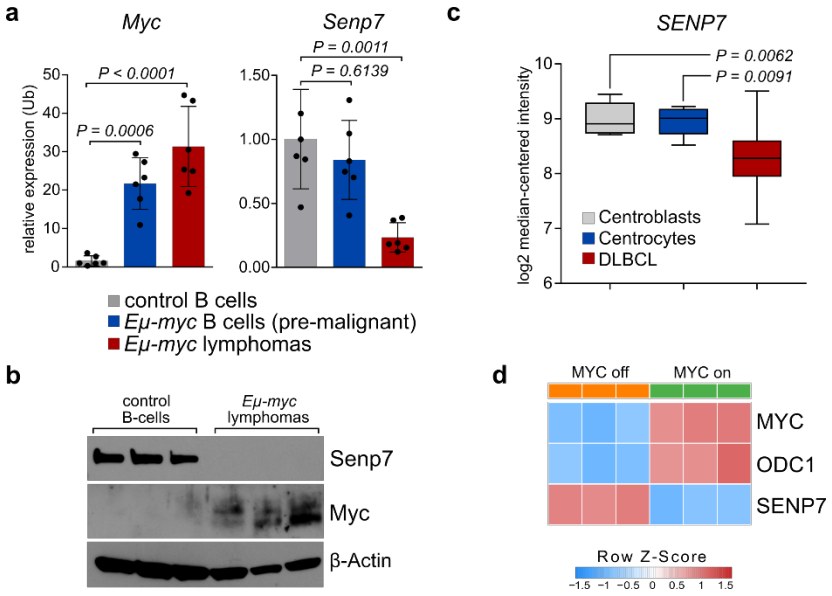

Figure 25. SENP7 is suppressed during B-cell lymphomagenesis. (a) *Senp7* and *MYC* expression in CD19+ B-cells derived from wild type mice (n=6), CD19+ B-cells from premalignant *Eμ-myc* mice (n=6) and *Eμ-myc* lymphomas (n=6). *Senp7* and *MYC* expression was normalized to *Ubiquitin*. *P-value* determined by ANOVA; Tukey`s post hoc test. **(b)** Immunoblot analysis of the indicated proteins comparing splenic CD19+ control B-cells (n=3) and *Eμ-myc* lymphomas (n=3) using the indicated antibodies. **(c)** *SENP7* expression compared in control B-cells (centroblasts, n=5; centrocytes, n=5) and primary DLBCL patient samples (n=73). Assessed was GSE12195. *P-value* was determined by ANOVA; Tukey`s post hoc test. **(d)** *MYC, ODC1* and *SENP7* expression after repression of *MYC* for 24h in the human P493-6 cell line carrying a tet-repressible *MYC* transgene. Assessed was GSE32219. [Data from (d) was provided by C. Maurer].

we analyzed a gene expression data set of human DLBCL samples in comparison to germinal center derived control B-cells (GSE12195) (Compagno et al., 2009). *SENP7* was also suppressed in human DLBCL (Figure 25c) and the broad spectrum of *SENP7* expression in human DLBCL patients suggested that *SENP7* might be eminently suppressed by specific genetic lesions.

To test this, we analyzed the effects of *MYC*, the primary genetic lesion in our screen, on *SENP7* expression in a dataset of the human P493-6 lymphoma model cell line (GSE32219) (Ji et al., 2011) carrying a tetracycline-repressible *MYC* transgene. Indeed, *SENP7* was rapidly upregulated upon repression of *MYC* (Figure 25d).

In summary, our data suggest that the suppression or inactivation of the related SUMO isopeptidase SENP7 contributes to the hyperSUMOylation phenotype in MYC-driven lymphomas observed after SENP6 depletion.

3.6 SENP6 is required for DNA damage checkpoint activation

3.6.1 SENP6 is activated in response to MYC-induced replicative stress

The DDR promotes checkpoint activation following DNA damage or enforced oncogene expression, which typically causes replicative stress. Activated checkpoints limit tumorigenesis by allowing DNA repair in order to maintain genomic integrity (Halazonetis et al., 2008). Ectopic MYC expression alone is insufficient to induce cellular transformation, because it triggers checkpoint activation, cell-cycle arrest and apoptosis through intrinsic tumor-suppressive pathways (Dominguez-Sola and Gautier, 2014).

To test if SENP6 is involved in the response to MYC-induced oncogenic stress, we analyzed Senp6 protein expression in murine MYC-driven lymphomas. Senp6 protein expression was substantially elevated in *Eμ-myc* lymphomas in comparison to control B-cells (Figure 26a). Furthermore, enforced MYC expression rapidly activated SENP6 protein expression (Figure 26b) in a human cell line with doxycycline-inducible MYC.

Thus, SENP6 may be involved in the response to MYC-induced replicative stress and in an intrinsic tumor suppressive pathway.

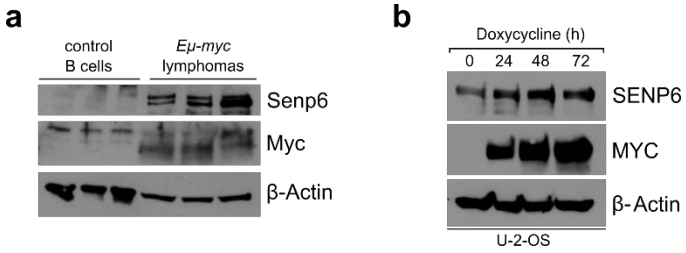

Figure 26. SENP6 is activated by MYC-induced replicative stress. (a) Immunoblot analysis of the indicated proteins comparing splenic CD19+ B-cells (n=3) purified from wild type mice and *Eμ-myc* lymphomas (n=3). **(b)** Immunoblot analysis of U-2-OS cells after induction of MYC for the indicated times.

3.6.2 SENP6 is crucial for CHK1 activation and the DDR in BCL

Cleavage of poly-SUMO chains by SENP6 plays a general role in the DDR (Dou et al., 2010; Gibbs-Seymour et al., 2015; Kunz et al., 2018) and SENP6 was linked to checkpoint activation (Wagner et al., 2019).

To test the role of Senp6 in DNA repair in non-tumor cells, we lentivirally transduced murine NIH 3T3 fibroblasts with three different shRNAs targeting *Senp6* and an empty vector control. Subsequently, we performed qPCR analysis. *Senp6* expression was substantially reduced in cells transduced with shRNA constructs (Figure 27a). To assess the role of Senp6 in regulating DDR checkpoints in NIH 3T3 cells, we treated the cells with DRB to promote checkpoint activation. Phosphorylation of the effector kinase Chk1 was substantially reduced in cells with

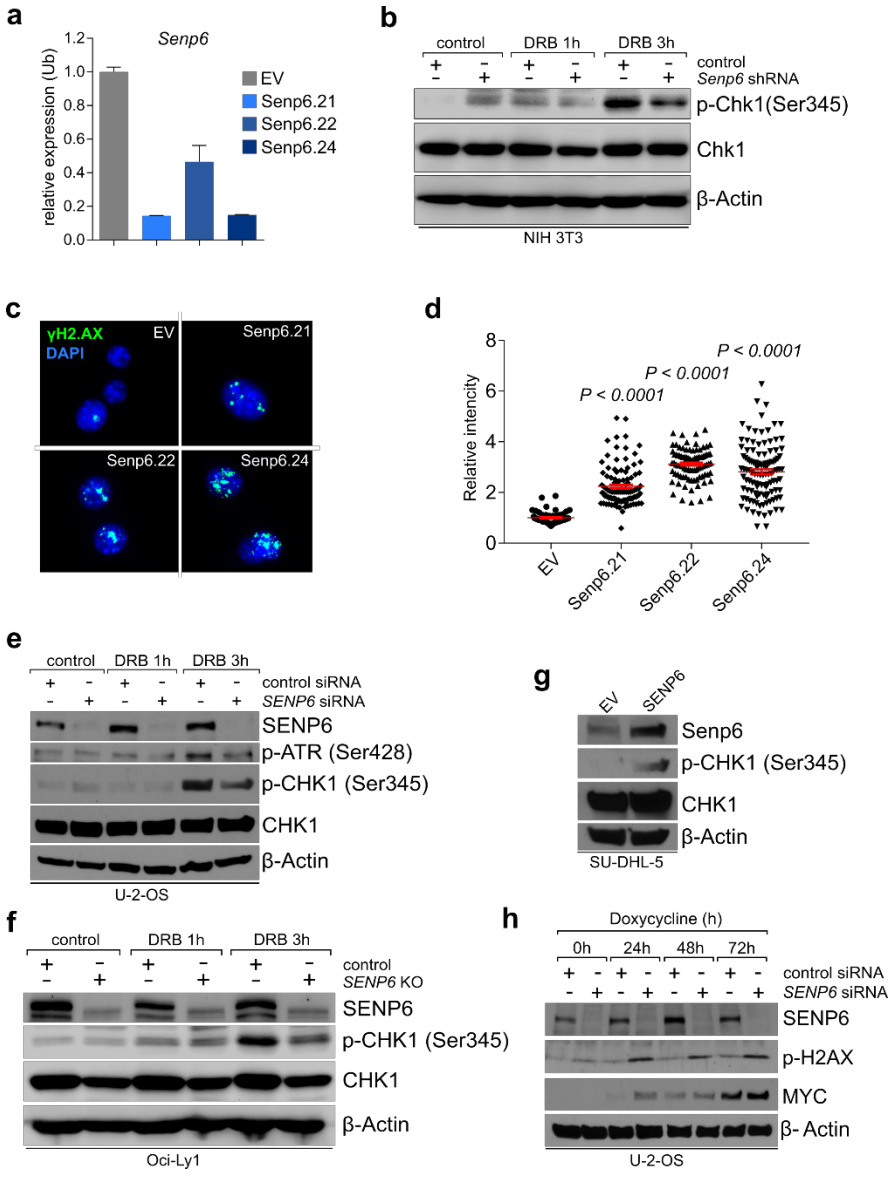

Figure 27. Loss of SENP6 is associated with compromised DNA damage checkpoint activation defective DNA repair. (a) *Senp6* mRNA expression of NIH-3T3 cells after transduction with either empty vector or three Senp6 shRNA constructs. *Senp6* expression was normalized to *Ubiquitin*. EV, empty vector. **(b)** Immunoblot analysis of cells described in Figure 27a after DRB treatment for the indicated time points. DRB, doxorubicin. **(c)** Immunofluorescence staining of γH2.AX expression of cells described in Figure 27a. **(d)** Quantification of Immunofluorescence staining described in Figure 27c. *P-value* determined by ANOVA, Tukey`s post hoc test. **(e)** Immunoblot analysis of U-2-OS cells after transfection with specific *SENP6* siRNA or control siRNA and doxorubicin (DRB) treatment for the indicated times. **(f)** Immunoblot analysis of human DLBCL cell lines following CRISPR/Cas9-mediated SENP6 depletion and DRB treatment for the indicated times with the indicated antibodies. **(g)** Immunoblot analysis of human DLBCL cell lines described in Figure 21b with the indicated antibodies. EV, empty vector control. **(d)** Immunoblot analysis of U-2-OS cells after transfection with specific *SENP6* siRNA or control siRNA and induction of MYC for the indicated times. *[Data from (c) and (d) provided by R. Istvanffy].*

reduced Senp6 expression (Figure 27b). Moreover, shRNA mediated depletion of *Senp6* in murine NIH-3T3 fibroblasts induced DSBs as monitored by increased γH2AX phosphorylation and foci formation (Figure 27c and d). In summary, we concluded that Senp6 has a critical function in DNA repair and DNA damage checkpoint activation in non-tumor cells.

To assess the role of SENP6 in regulating DDR checkpoints in human cells, we depleted *SENP6* transcripts in U-2-OS cells with a specific siRNA and treated the cells with DRB to promote checkpoint activation. Importantly, when compared to control cells, ATR phosphorylation was compromised upon depletion of SENP6. Accordingly, phosphorylation of the downstream kinase CHK1 was reduced (Figure 27e). To stress this finding in human BCL, we treated the SENP6-depleted human Oci-Ly1 DLBCL cell line with DRB and showed that SENP6 loss was associated with defective CHK1 phosphorylation (Figure 27f). Accordingly, ectopic SENP6 expression in the SU-DHL-5 DLBCL cell line promoted CHK1 phosphorylation even without an additional external stimulus (Figure 27g).

Next, we tested whether the cellular SENP6 status affects genome integrity in response to MYC-induced replicative stress. To this end, we depleted SENP6 expression and concomitantly induced MYC expression in U-2-OS cells. Cells lacking SENP6 showed a strong accumulation of DSBs indicated by H2AX phosphorylation (Figure 27d).

Altogether, these data show a critical function of SENP6 in DNA repair and specifically DNA damage-induced checkpoint activation during lymphomagenesis. Moreover, SENP6 depleted cells have a reduced DNA repair capacity.

3.6.3 The *SENP6* status is critical for maintenance of genome integrity *in vivo*

To investigate if *Senp6* loss affects genome stability in murine BCLs *in vivo*, we performed low coverage whole genome sequencing (WGS) of *Senp6*-deficient murine lymphomas derived from the *in vivo* validation experiments and analyzed somatic copy number alterations (SCNAs). Intriguingly, in comparison to control lymphomas, *Senp6*-sgRNA lymphomas showed a significantly larger genome fraction with SCNAs (Figure 28a and b). Moreover, we detected increased Chk1 and H2AX phosphorylation in these lymphomas suggesting that the Senp6-mediated defect in DDR activation leads to an increased level of DNA damage (Figure 28c).

To investigate this finding in human BCL patients, we investigated the effects of the *SENP6* status on genomic stability in a dataset of 304 DLBCL patients (Chapuy et al., 2018). Patient groups were classified according to their *SENP6* copy number status (38/304 with loss of 6q14.1/*SENP6*) and the total number of co-occuring somatic copy number alterations (SCNAs) were assessed (Figure 28d, upper panel). Notably, primary DLBCL samples harboring *SENP6* deletions showed significantly higher number of SCNAs (Figure 28d, lower panel),

suggesting that SENP6 serves as a gatekeeper of genome stability in both murine and human BCLs.

In summary, these data identify SENP6 as the critical deSUMOylating enzyme, which controls genome stability during oncogene-induced replicative stress in BCL.

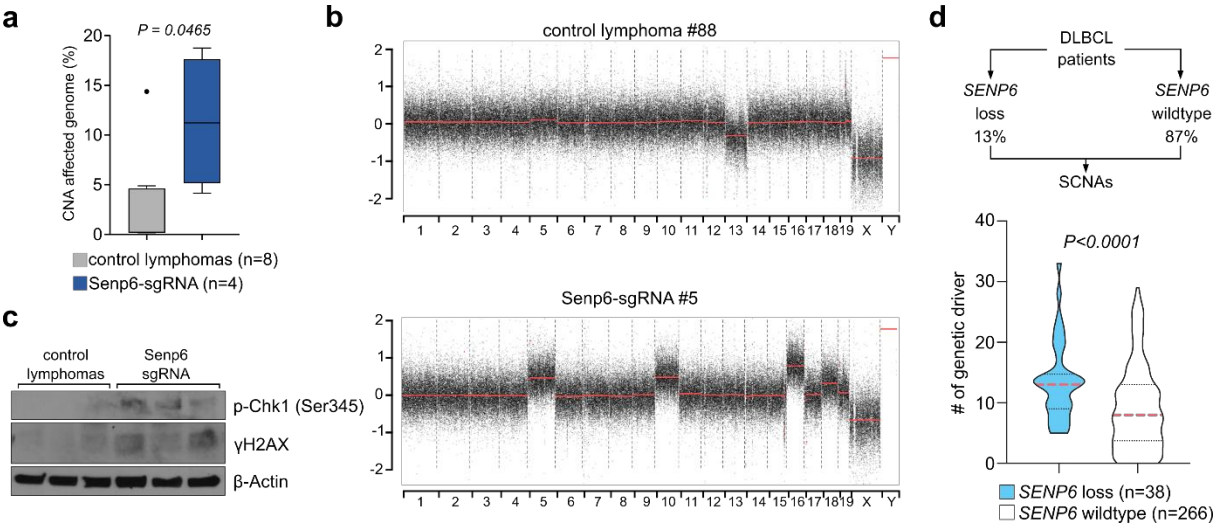

Figure 28. SENP6 controls genome integrity in BCLs *in vivo*. (a) Copy number alterations of control and Senp6-sgRNA lymphomas were analyzed by low coverage WGS and the fraction of CNA affected genome was compared. X and Y chromosomes have been excluded from analysis. *P-value* determined by Wilcoxin signed-rank test. **(b)** Copy number plots of one *Eμ-myc* control and one Senp6-sgRNA lymphoma derived from *in vivo* validation experiments as determined by low coverage WGS. **(c)** Immunoblot analysis using the indicated antibodies. *Eμ-myc* control lymphomas (n=3) are compared to Senp6-sgRNA lymphomas (n=3) derived from *in vivo* validation experiments described in Figure 20b**. (d)** Analysis of SCNAs in human DLBCL patients (n=304). Groups were classified according to their *SENP6* copy number status (upper panel). P-value determined by Mann-Whitney U test (lower panel). [Data from (d) provided by B. Chapuy].

3.7 SENP6 acts as key signaling hub of DNA repair pathways

3.7.1 Ectopic SENP6 expression does not affect the proteome in BCL

The SUMO protease SENP6 has been shown to counteract the formation of SUMO2/3 chains. SUMO2/3 chains are substrates of StUbLs like RNF4 and can trigger subsequent ubiquitination and degradation of substrates (Rojas-Fernandez et al., 2014).

To test, if the reconstitution of SENP6 expression in the SU-DHL-5 DLBCL cell line affects the stability of proteins, we performed mass-spectrometry based proteome analysis. We next performed bioinformatics analysis and identified more than 5000 proteins. Notably, only four proteins were significantly regulated in SENP6 reconstituted cells when compared to control cells. Besides that, seven proteins were exclusively detected in reconstituted and one in control cells (Figure 29).

In summary, we conclude that the level of SENP6 expression is not critical for the overall proteome in BCL and that effects might be highly dynamic on a substrate level or more pronounced in subcellular fractions.

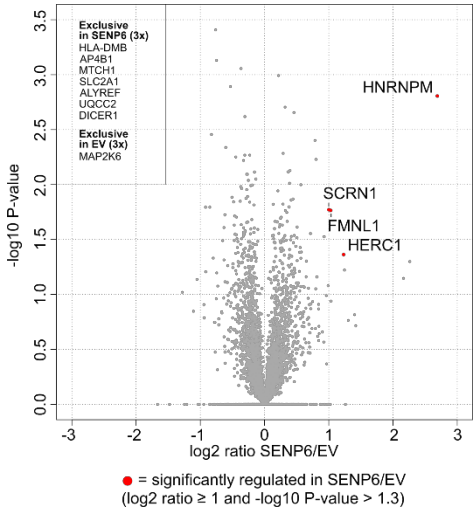

Figure 29. Ectopic SENP6 expression does not affect the overall proteome in BCL. Volcano plot summarizing the results of quantitative MS analysis from the SU-DHL-5 DLBCL cell line after reconstitution of SENP6 expression described in Figure 21b. Proteins considered as significantly enriched are colour-coded (cut-offs are indicated in the figure). The experiment was performed in triplicates. [Data provided by K. Schunck].

3.7.2 SENP6 controls CDC5L localization to regulate CHK1 activation

Unrestricted SUMO chain formation at chromatin can disturb the chromatin residency of chromatin-associated protein complexes through activation of the RNF4 pathway (Gibbs-Seymour et al., 2015; Liebelt et al., 2019; Psakhye et al., 2019; Wagner et al., 2019). Given the role of RNF4, we hypothesized that in conjunction with SENP6 deletion this affects chromatin association of DDR factors.

Of note, we found an increase of chromatin-bound SENP6 in the context of MYC-induced replicative stress (Figure 30a) revealing that SENP6 functions primarily at chromatin. A recently identified SENP6-regulated factor is CDC5L, a core component of the mammalian hPSO4 complex (Wagner et al., 2019). This complex promotes activation of DNA damage checkpoint and DNA repair and particularly contributes to the maintenance of genome integrity in response to replication stress (Abbas et al., 2014).

For this reason, we explored if the hPSO4 complex is also a critical downstream mediator of SENP6 in lymphoma. Importantly, siRNA-mediated depletion of CDC5L from U-2-OS cells phenocopied the defect on CHK1 activation observed upon loss of SENP6 (Figure 30b). To test if SENP6 controls chromatin residency of CDC5L during oncogene-induced replicative stress, we isolated chromatin from SENP6-depleted and control cells following induction of

MYC expression. In this context, SENP6 depletion substantially reduced CDC5L levels in the chromatin fraction (Figure 30c).

These data indicate that SENP6 controls chromatin association of CDC5L, but not its overall turnover. In summary, our mechanistic data support the critical role of SENP6 in regulating chromatin residency of CDC5L and link loss of SENP6 to defective DDR control in lymphoma.

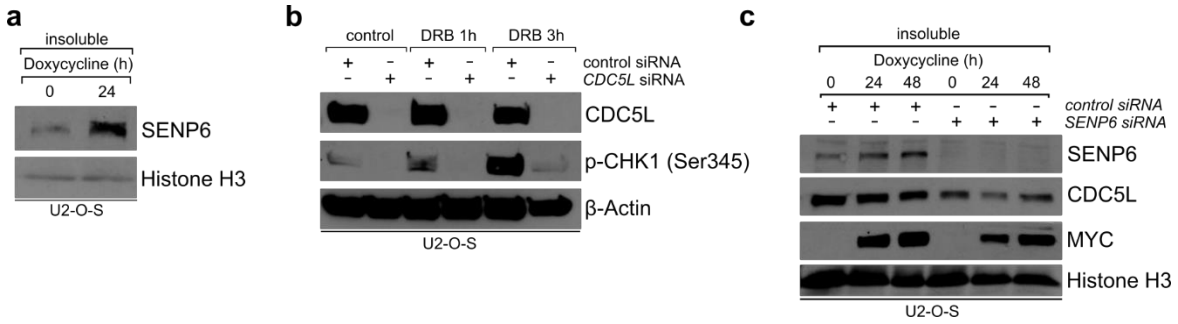

Figure 30. SENP6 controls the chromatin localization of CDC5L to control DNA damage checkpoint activation. (a) Immunoblot analysis of U2-O-S cells after MYC induction for the indicated time points with the indicated antibodies. **(b)** Immunoblot analysis of whole cell lysates of U-2 OS cells after transfection with specific CDC5L siRNA or control siRNA and DRB treatment for the indicated time points. DRB, Doxorubicin. **(c)** Immunoblot analysis of the insoluble (chromatin) fraction of U2-O-S cells after transfection with specific *SENP6* siRNA or control siRNA after induction of MYC for the indicated time points with the indicated antibodies.

3.7.3 SENP6 controls the SUMO/chromatin landscape in BCL

Our data support the idea that SENP6 controls the SUMOylation status of chromatin-associated proteins and protein complexes.

To directly test whether alterations in SENP6 expression affect SUMOylation at chromatin, we performed ChIPseq analysis with specific antibodies against SUMO1 and SUMO2/3 in the parental SU-DHL-5 DLBCL cell line and the cells reconstituted with SENP6 expression. Inspection of browser tracks revealed reduction of SUMO1 (Figure 31a) and SUMO2/3 modified proteins (Figure 31b) on individual genes in SENP6 re-expressing cells and analysis of the peaks called for SUMO1 showed substantial reduction in the number of peaks after reconstitution of SENP6 expression (Figure 31c). Additionally, reduced binding of SUMO1 modified proteins was found for the common peaks when SENP6 is expressed (Figure 31c). Similar results were noted for binding of SUMO2/3 modified proteins as well (Figure 31d).

In summary, this suggests that SENP6 restricts SUMOylation of chromatin-bound proteins in BCL in a global manner.

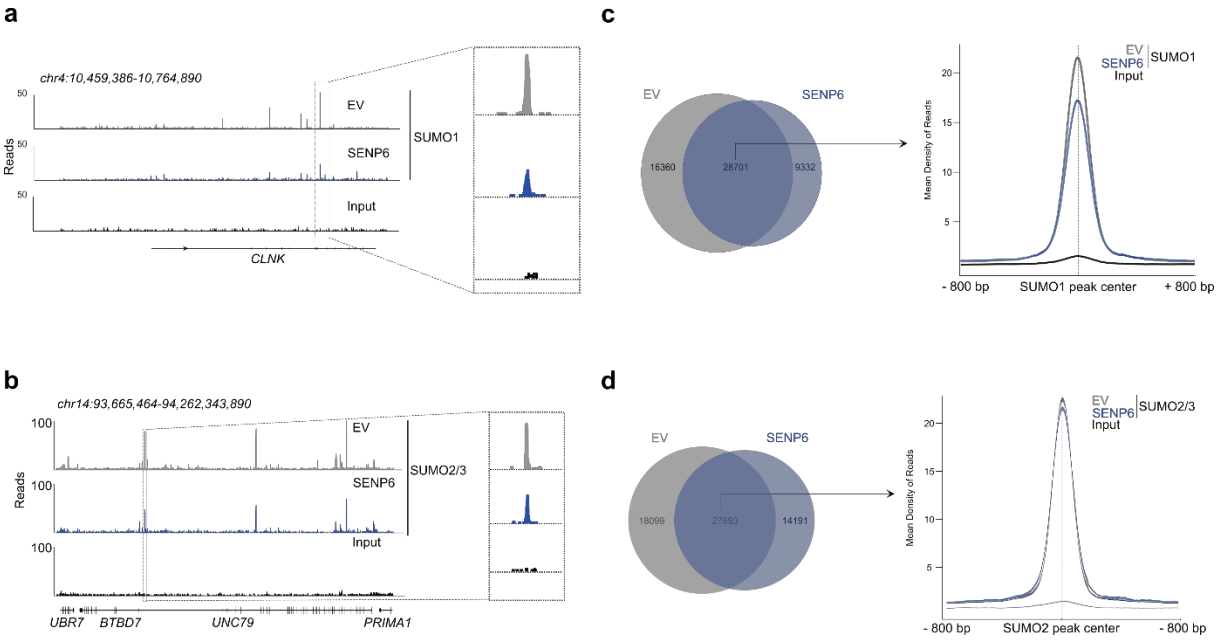

Figure 31. SENP6 controls the SUMO/chromatin landscape in BCL. (a, b) Genome browser picture of read normalized SUMO1 (a) or SUMO2/3 (b) ChIPseq profiles from SU-DHL-5 cells with low SENP6 expression (EV, grey) or reconstituted for SENP6 expression (SENP6, blue) described in Figure 21b. Input is shown in black. **(c, d)** Venn diagram (left) showing overlap of SUMO1 (c) or SUMO2/3 (d) peaks in SU-DHL-5 cells with low SENP6 expression (EV, grey) or reconstituted for SENP6 expression (SENP6, blue) described in Figure 21b. Density plot centered at common SUMO1 (c) or SUMO2/3 (d) peaks (right). Input is shown in black. [Data provided by A. Baluapuri and J. Hofstetter].

3.7.4 The cohesin complex is a tumor-relevant target of SENP6

To identify additional critical SENP6 targets that mediate its tumor suppressive role, we scrutinized two recent proteomics studies with defined SENP6 targets. These studies suggested that SENP6 regulates the SUMOylation status of a larger network of proteins primarily involved in chromatin organization, DNA repair and genome maintenance (Figure 32a) (Liebelt et al., 2019; Wagner et al., 2019).

In order to extract additional candidate tumor-relevant substrates of SENP6 from these dataset, we intersected it with the putative cancer genes identified in our transposon mutagenesis screen. Following this approach, we identified 17 SENP6 targets, which also scored in the *PB* screen (Figure 32a and b).

To get insight into the biological function of these common SENP6 targets and explore if they converge on a given pathway, we next performed pathway enrichment analysis using the Reactome database. Among the six significantly enriched pathways *"SUMOylation of DNA damage response and repair proteins"* ranked highest (Figure 32c). Notably, the same pathway scored among the top hits in the pathway enrichment analysis of the 958 cancer genes identified in our transposon mutagenesis screen (Figure 18a), suggesting that the function of

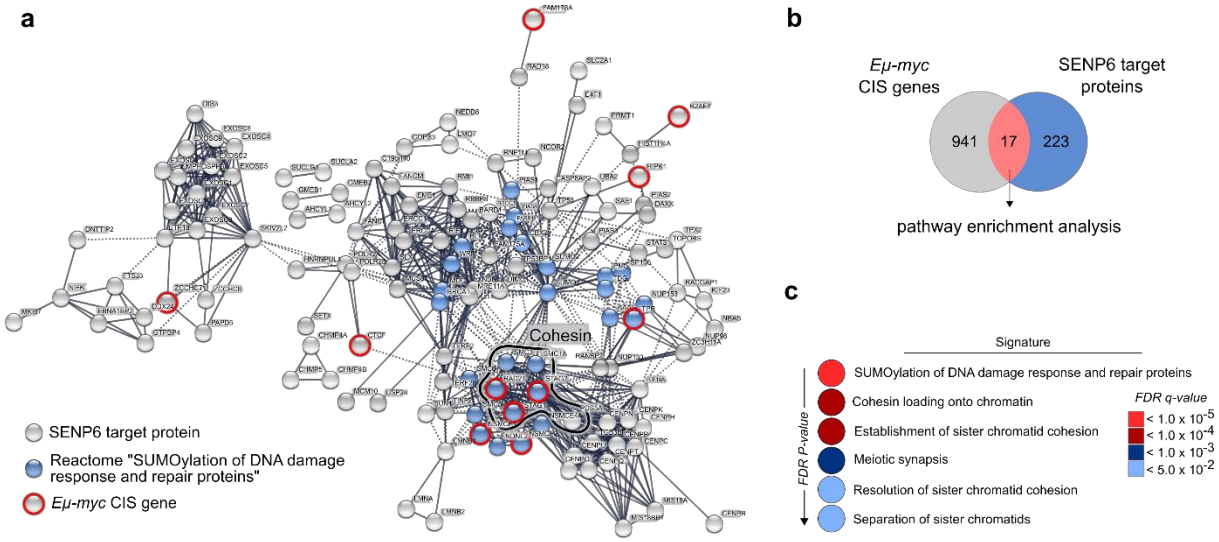

Figure 32. The cohesin complex is a tumor-relevant target of SENP6. **(a)** STRING network analysis depicting the interconnection of SENP6 targets and the resulting clusters. For STRING analysis both recently described SENP6 targetomes (Liebelt et al., 2019; Wagner et al., 2019) were combined. The highest confidence filter (0.9) was applied and only connected proteins are visualized. **(b)** Venn diagram showing the overlap between CIS genes derived from the *Eμ-myc* transposon mutagenesis screen and SENP6 target proteins (Liebelt et al., 2019; Wagner et al., 2019). **(c)** Overlapping candidates from (Figure 32c) were analyzed using the Reactome database. Color-coded *FDR P-value* is shown for all significantly enriched pathways.

specific CIS genes is post-translationally regulated by SENP6-dependent deSUMOylation. Four out of the five remaining pathways were associated with the cohesin pathway (Figure 32c) and all cohesin complex components (RAD21, STAG1, STAG2, SMC3 and SMC1A) are SENP6 targets (Figure 32a). Of those, we identified *Rad21*, *Stag1* and *Stag2* as putative cancer genes in our screen (Figure 33a). The transposon insertion pattern was bi-directional and scattered for all three genes indicating tumor-suppressor function (Figure 33a). In addition to that, transcript expression of *RAD21*, *STAG2* and *STAG1* was suppressed in human BCL when compared to healthy GC derived B-cells (Figure 33b). This is in line with the well-known tumor suppressor role of *RAD21*, *STAG1* and *STAG2* in human cancers as listed in the COSMIC Cancer Gene Census (Sondka et al., 2018).

In support of our data, recent work supports the notion that lack of SENP6 leads to reduced chromatin association of the two cohesin complex member, RAD21 and STAG2 (Wagner et al., 2019). To test if this concept is also valid in BCL, we performed cellular fractionation of control and SENP6 KO Oci-Ly1 cells and analyzed soluble and chromatin-bound proteins by immunoblot analysis. Indeed, STAG2 and RAD21 levels were reduced at chromatin and shifted to the soluble fraction, linking unbalanced SUMOylation with defects in chromatin-residency and loss of function of cohesin complex members in BCL.

From this, we conclude that the cohesin subunits STAG1, STAG2 and RAD21 are tumor-relevant substrates of SENP6 to restrict B-cell lymphomagenesis.

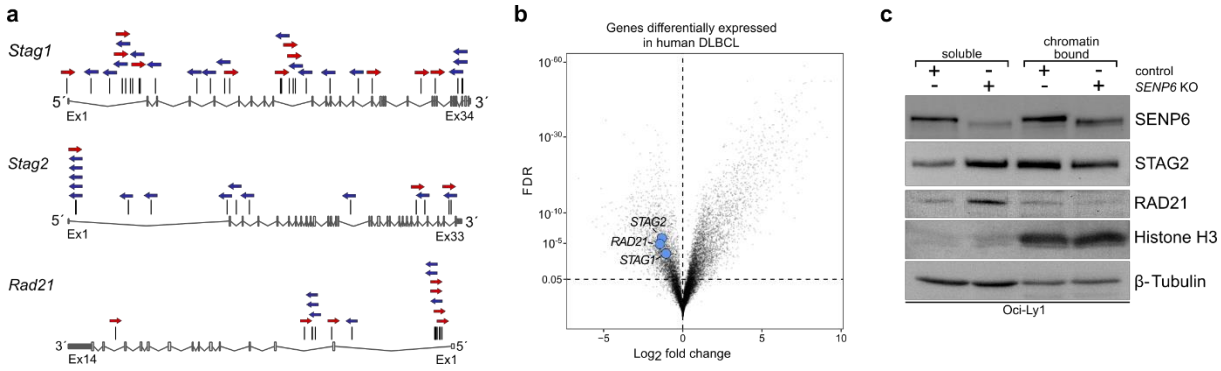

Figure 33. The cohesin complex subunits STAG1, STAG2 and RAD21 are putative tumor suppressor genes in mice and suppressed in human BCL. (a) Transposon insertion pattern in *Stag1*, *Stag2* and *Rad21* indicating tumor suppressor function. Only the dominant insertion per tumor is shown. **(b)** Volcano plot summarizing the results of dysregulated genes in human DLBCL in a published dataset (Compagno et al., 2009). *STAG1*, *STAG2* and *RAD21* are highlighted. **(c)** Immunoblot analysis of soluble and chromatin-bound proteins of control and SENP6 KO Oci-Ly1 cells with the indicated antibodies. [Data from (b) provided by C. Maurer].

3.8 SENP6 loss is associated with sensitivity to PARP inhibition

Next we sought out to explore the translational potential of our findings for targeted therapies. The concept of synthetic lethality-based tumor therapy is best exemplified by the clinical success of poly (ADP-ribose) polymerase (PARP) inhibitors in patients suffering from BRCA1/BRCA2-mutated breast or ovarian cancer (Lord and Ashworth, 2012).

Importantly, it has been demonstrated that tumor cells harboring mutations in the cohesin complex are sensitive to PARP inhibition (PARPi) (Bailey et al., 2014). Based on our finding that SENP6 deletion affects cohesin functions, we asked whether PARPi exploits a specific vulnerability for SENP6-deficient DLBCL cells. To this end we used the Oci-Ly1 DLBCL cell line model and treated SENP6 knockout and control cells with varying concentrations of olaparib, a selective PARP inhibitor. Strikingly, when compared to the control cells, the SENP6 knockout cells exhibited significantly stronger sensitivity towards PARPi and a substantially reduced GI_{50} concentration (control: 15.8 µM vs. SENP6 KO: 5.5µM) (Figure 34a). Moreover, SENP6 loss significantly induced apoptosis following PARPi treatment (Figure 34b and c) further empowering the critical role of the SENP6 status for efficacy of PARP inhibition. To stress this finding, we then treated the SU-DHL-5 DLBCL cell line model with olaparib. Fully in line with our previous findings, SENP6 reconstitution reduced the sensitivity to olaparib (Figure 34c).

Altogether these data show that SENP6 deficiency drives synthetic lethality to PARP inhibition and indicate that inhibition of PARP could be a therapeutic option in the subgroup of SENP6-deficient BCL.

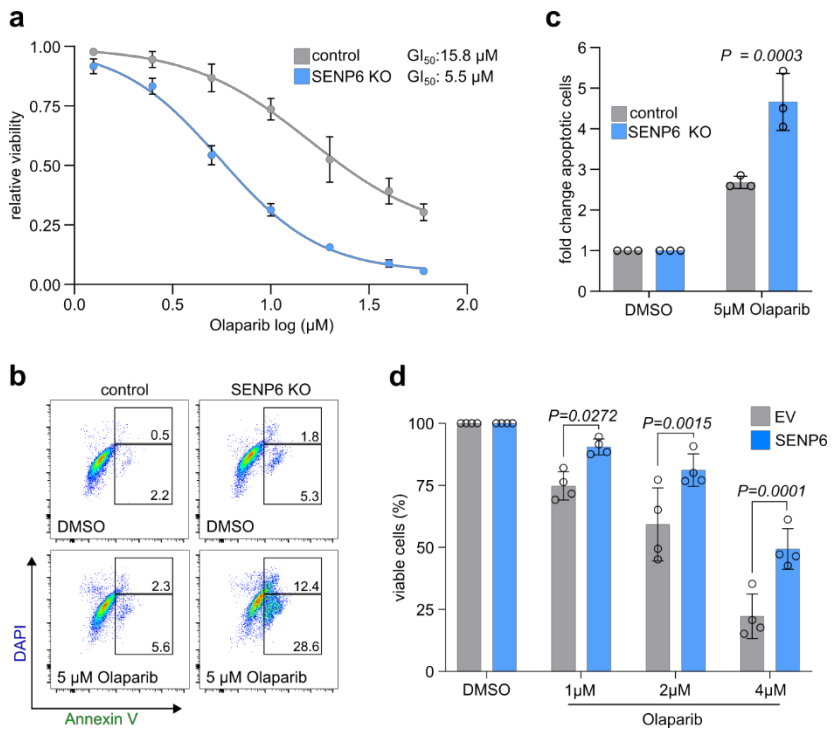

Figure 34. SENP6 loss is associated with sensitivity to PARP inhibition. (a) Analysis of GI_{50} values of control Oci-Ly1 and *SENP6* knockout (SENP6 KO) Oci-Ly1 cells. Cells were treated with indicated olaparib concentrations or respective DMSO concentrations for 72h. Viability was assessed by flow cytometry and Annexin V/DAPI staining. **(b,c)** Analysis of apoptotic cells as AnnexinV+/DAPI- cell population determined by FACS analysis. Control Oci-Ly1 cells and *SENP6* knockout (SENP6 KO) Oci-Ly1 cells were treated with 5 µM olaparib or DMSO for 72 h **(d)** Viability of cell lines described in Figure 21b after 48h olaparib treatment with the indicated concentrations. Viability determined by DAPI staining and flow cytometry measurement. *P-value* determined by ANOVA; Bonferroni's multiple comparisons test.

3.9 Therapeutic targeting of activated SUMOylation in BCLs

3.9.1 Assessment of *in vivo* toxicity of SUMOi

SUMOylation is an essential pathway in all cells (Seeler and Dejean, 2017) and successful therapeutic targeting of this pathway with a small molecule inhibitor of SUMOylation (SUMOi) seemed unlikely as genetic experiments showed that the E1 and E2 enzymes are essential for cell survival. This prompted the fear of severe toxic side-effects on non-tumor cells when targeting this pathway *in vivo*, however, for a long time experimental testing was limited due to the lack of clinically suitable agents to inhibit SUMOylation (Seeler and Dejean, 2017).

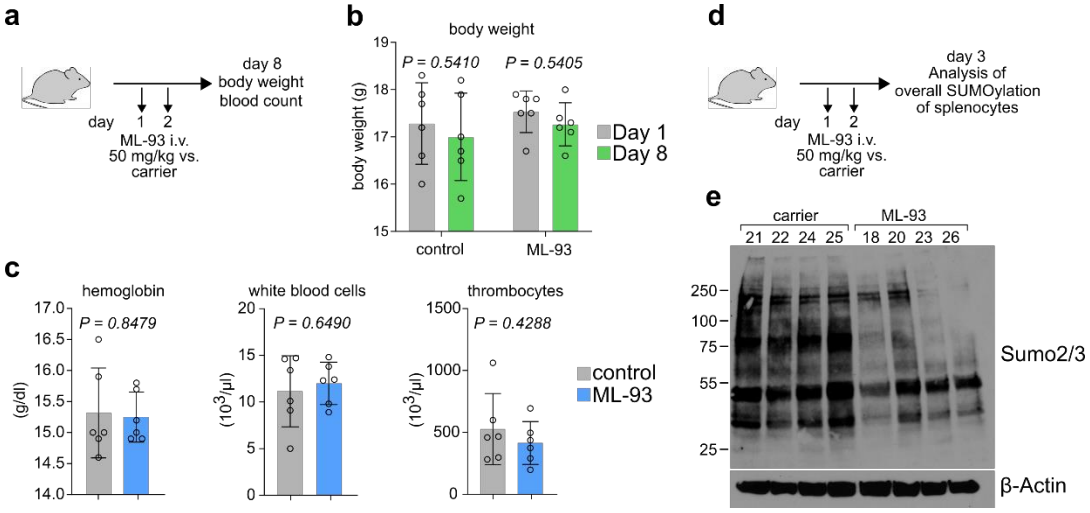

Figure 35. *In vivo* testing of ML-93 efficacy and toxicity. (a) ML-93 treatment schedule used for the *in vivo* toxicity analysis in *C57BL/6* mice. **(b)** Body weight of control (n=6) and ML-93 (n=6) treated mice at day 1 and day 8. *P-value* determined with unpaired t-test. **(c)** Blood cell parameters, hemoglobin, white blood cells, and thrombocytes of control and ML-93 treated mice at day 8. *P-values* determined with unpaired t-test. **(d)** ML-93 treatment schedule to determine on-target efficacy of ML-93 in protein lysates of splenocytes. **(e)** Immunoblot analysis of splenocyte lysates of four control and four ML-93 treated mice with the indicated antibodies.

Based on the recently described potent SUMOi ML-792 and the follow up compound ML-93 with optimized parameters for *in vivo* application (Biederstadt et al., 2020; He et al., 2017), we aimed to test the toxicity of SUMOi in immunocompetent mice. To determine *in vivo* toxicity of ML-93, we treated wildtype mice on two consecutive days and performed analysis on day eight (Figure 35a). No significant change in body weight (Figure 35b), haemoglobin concentration, white blood cell or platelet counts were detected (Figure 35c).

To test, if ML-93 efficiently inhibits protein SUMOylation *in vivo*, we treated wildtype mice on two consecutive days and harvested splenocytes on day three to perform immunoblot analysis (Figure 35d). Overall SUMOylation was dramatically reduced in splenocytes of SUMOi treated mice revealing *in vivo* on target activity of ML-93 (Figure 35e).

From this we conclude that the SUMOi ML-93 efficiently reduces protein SUMOylation *in vivo* and can be applied to wildtype mice without severe toxic side-effects.

3.9.2 Therapeutic targeting of activated SUMOylation in BCL

The surprisingly moderate toxic effects of SUMOi after *in vivo* application prompted us to test its potential to therapeutically target BCL cells in a preclinical model. MYC-driven BCL cells derived from *Eμ-myc* mice are highly dependent on the SUMO pathway and genetic inhibition of SUMOylation triggers cell death (Hoellein et al., 2014).

Therefore, we used primary lymphoma cells derived from diseased *Eμ-myc* mice to serially transplant CD45.1 recipient mice. Transplanting lymphoma cells derived from *Eμ-myc* mice expressing CD45.2 into CD45.1 recipients allowed tracking of lymphoma cells. Seven days after transplantation first mice showed lymph node infiltration and all mice were subsequently treated with either carrier control or SUMOi (Figure 36a). Two days after treatment we performed full analysis of the experimental cohort. Spleen size and weight was significantly lower in mice treated with SUMOi, indicating efficient eradication of lymphoma cells (Figure 36b and c). Next, we performed flow cytometry analysis to determine the number of remaining lymphoma cells. Lymphoma cells (CD45.2+ cells) were virtually fully eradicated in mice treated with SUMOi, whereas a clear lymphoma cell population was present in carrier treated mice (Figure 36d and e), indicating efficient anti-tumor effect of the SUMOi *in vivo*.

In summary, we show that SUMOi can be used for efficient therapeutic targeting of activated SUMOylation in MYC-driven BCLs *in vivo*.

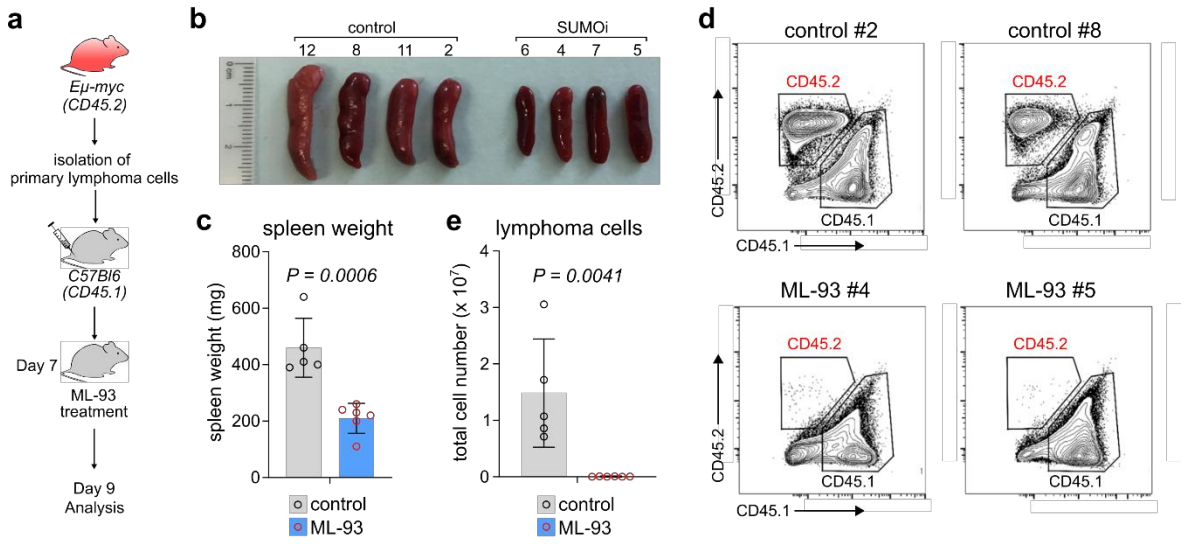

Figure 36. *In vivo* testing of SUMOi anti-tumor efficacy. (a) Experimental workflow for assessment of *in vivo* efficacy of SUMOi ML-93. Primary *Eμ-myc* lymphoma cells have been transplanted into syngeneic *C57Bl6 (lCD45.1)* recipient mice. **(b)** Spleens of mice treated with ML-93 (SUMOi) or carrier (control). **(c)** Spleen weight of carrier (control) and ML-93 (SUMOi) treated mice. Control, n=6; SUMOi, n=6. *P-value* determined with unpaired t-test. **(d)** FACS analysis of lymphoma cell infiltration in recipient mice after control or ML-93 treatment. Lymphoma cells have been assessed as CD45.2+ cells in CD45.1+ recipient mice. **(e)** Total number of lymphoma cells in spleens of carrier (control) or ML-93 (SUMOi) treated mice. Control, n=6; SUMOi, n=6. *P-value* determined with unpaired t-test.

3.9.3 Therapeutic targeting of activated SUMOylation in PDAC

The association of MYC and activated SUMOylation has been described in several human malignancies (Hoellein et al., 2014; Kessler et al., 2012). To test this mechanistic concept in PDAC, a human cancer with dismal prognosis, we analyzed transcriptome profiles.

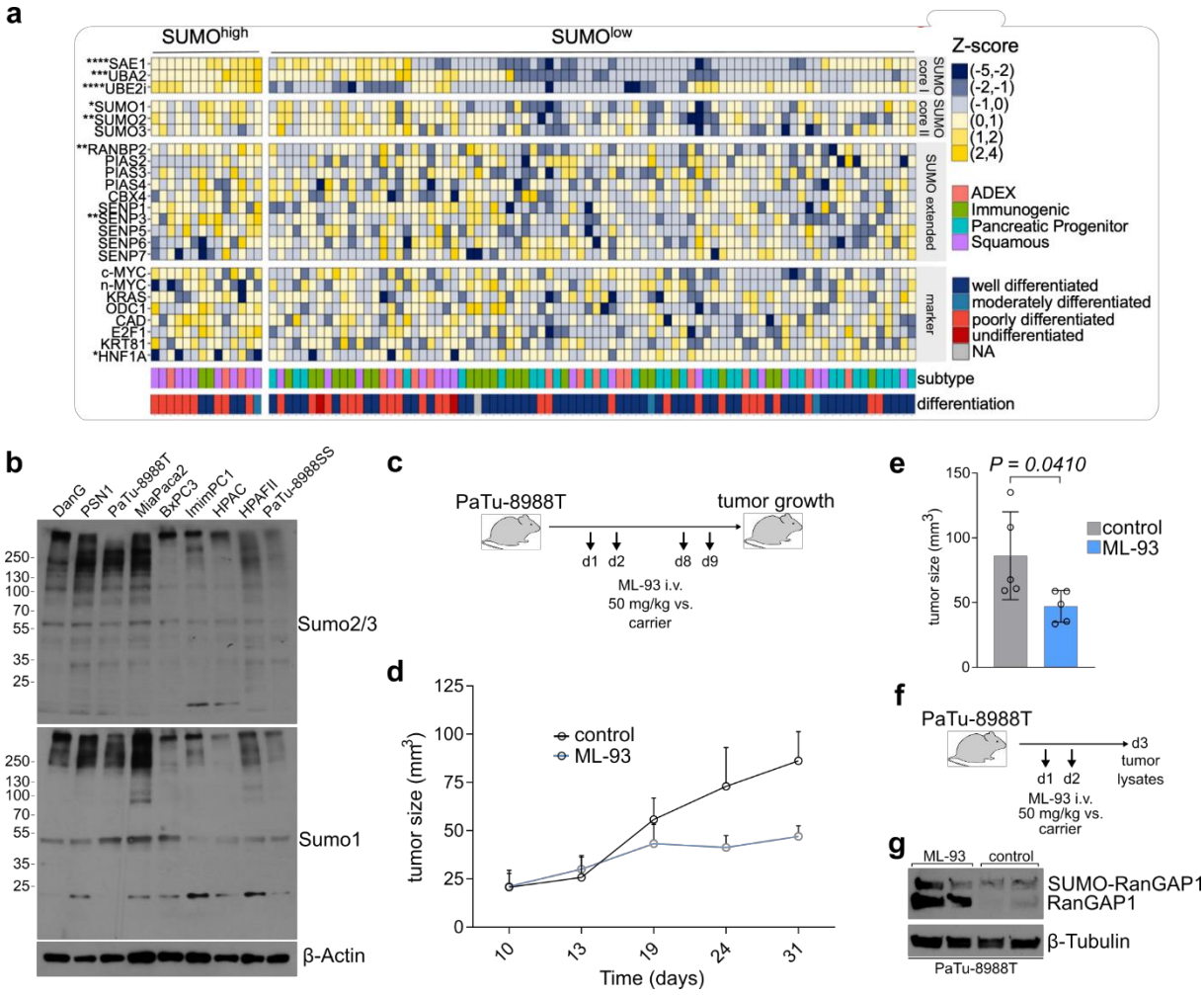

Figure 37. Therapeutic targeting of activated SUMOylation in PDAC. (a) Manual curation of a publicly available gene expression dataset of PDAC patients (n=96) (Bailey et al., 2016) was used to define a SUMO-high population, characterized by positive z-scores for SAE1, UBA2 and UBE2I (n=14). **(b)** Representative immunoblot analysis with antibodies detecting SUMO1 and SUMO2/3 in human PDAC cell lines. **(c)** The human PDAC cell line PaTu-8988T was used to generate murine xenograft models in NOG mice. Mice were treated with 50 mg/kg ML-93 intravenously on d1,2 and d8,9 and **(d)** tumor size was measured over time. **(d)** Tumor size at d31 of ML-93-treated PaTu-8988T-derived xenograft mice revealed significant reduction in tumor size in treated mice (n=5 mice in each group). *P-value* assessed using an unpaired t-test. **(f)** Two days after the first injection (d3), tumors were harvested and protein lysates were analyzed for SUMOylated and un-SUMOylated RanGAP1 by immunoblot analysis. **(g)** Immunoblot analysis of ML-93 and carrier treated PaTu-8988T xenograft tumors with the indicated antibodies. [Data in (a) were provided by Lara Schneider and data in (d) were provided by Jonas Nilsson]

Indeed, we identified a SUMO^{high} subgroup, which was associated with activated MYC signalling and an aggressive PDAC subtype (Figure 37a). To test, if increased transcript levels of the SUMO conjugation machinery also converge on increased protein SUMOylation, we performed western blot analysis of human PDAC cell lines. The level of SUMOylated proteins was substantially increased in a subgroup of cell lines (Figure 37b), which were also characterized by high levels of MYC expression.

To test *in vivo* efficacy of ML-93, we performed xenograft transplantation of the human SUMO^{high} PDAC cell line PaTu-8988T s.c. into immunocompromised NOG mice and treated tumor-bearing mice with ML-93 (Figure 37c). Growth of PaTu-8988T xenografts was inhibited by ML-93 treatment (Figure 37d). To investigate the efficacy of SUMO inhibition *in vivo*, we analyzed SUMOylation of RanGAP following acute ML-93 treatment (Figure 37f) and observed reduced SUMOylation of RanGAP1 revealing on target efficacy of ML-93 (Figure 37g).

Together, our data reveal that targeting of activated SUMOylation might be a therapeutic strategy in the aggressive subtype of PDAC.

4 DISCUSSION

DLBCL is the most common aggressive BCL in adults and although more than half of all patients achieve long-term remission, the majority of the remaining patients develops progressive disease and succumbs to DLBCL (Reddy et al., 2017).

Large-scale sequencing studies provide a precise characterization of the genetic landscape of DLBCL and elucidate the high molecular and structural complexity of the disease. Many of the identified recurrent alterations occur with low frequencies and their biological and functional relevance is largely understudied (Chapuy et al., 2018; Pasqualucci et al., 2011; Reddy et al., 2017). Accordingly, several large phase 3 trials have failed to advance the therapeutic standard beyond classical immuno-chemotherapy (R-CHOP) towards mechanism-based novel therapies (Ryu et al., 2018) underscoring the urgent need for functional studies interpreting the complex genetic and molecular background of DLBCL.

Starting from a genome-scale cancer gene discovery screen in a murine model of MYC-driven B-cell lymphomagenesis, we identified recurrent *SENP6* deletions in human BCL causing unrestricted poly-SUMOylation and provide direct experimental evidence that SENP6 loss accelerates lymphomagenesis. Moreover, we applied a multiOMICs approach to link *SENP6* deletions to a defective DDR. We demonstrate that SENP6 loss triggers extraction of protein complexes required for response to DNA damage stress from chromatin, ultimately promoting genomic instability. Notably, SENP6 loss confers synthetic lethality to PARP inhibitors pointing to novel therapeutic options in a subgroup of BCL patients. Beyond this specific vulnerability, we prove that targeting the SUMO pathway is an efficient therapeutic strategy in MYC-dependent cancers.

The key achievements of this study are:

1. Providing a catalogue of previously unappreciated drivers of B-cell lymphomagenesis and *in vivo* validation of *Slf2* and *Snrnp70* as tumor suppressor genes
2. Identification of dysregulated SUMOylation and *SENP6* deletions as recurrent functional drivers of human B-cell lymphomagenesis
3. Providing first-time experimental evidence that unrestricted poly-SUMOylation caused by SENP6 deficiency directly contributes to cancer pathogenesis
4. Linking of *SENP6* deletions to a defective DDR and demonstration that SENP6 governs genome stability *in vivo* in murine and human BCLs
5. Demonstration that SENP6 controls the chromatin residency of DNA repair factors such as CDC5L and the cohesin complex
6. Identification of synthetic lethality of PARP inhibition that is conferred by SENP6 loss
7. *In vivo* investigation of SUMOi as a therapeutic strategy in MYC-driven cancers

4.1 Identification of previously unappreciated drivers of BCL

Previous work has proven the applicability and value of somatic transposon mutagenesis to identify and validate putative cancer genes (de la Rosa et al., 2017; Rad et al., 2010; Weber et al., 2019). We have combined transposon mutagenesis with the well-characterized *Eμ-myc* mouse model of MYC-driven B-cell lymphomagenesis.

Our screening approach conceptually parallels a RIM screening, which discovered oncogenes in the *Eμ-myc* mouse model (Mikkers et al., 2002; Uren et al., 2005) and a shRNA screening, which identified tumor suppressor genes in the same model (Bric et al., 2009). We compared the hits described in all three screens and clearly showed, that the screens are not redundant and complement to each other. Our screening identified the largest fraction of putative cancer genes and does not overlap with the genes uncovered in the shRNA screening. In the shRNA screening, candidates were pre-selected based on a list comprising putative human cancer genes mainly based on recurrent mutations (Witt et al., 2006). On one hand, this approach allows the testing of candidates in the *in vivo* screening with the certainty that every positive hit is also relevant in human cancers. However, the vast majority of genes altered in human cancers is transcriptionally dysregulated or part of long copy number alterations and moreover, this often is true for thousands of genes per cancer cell (Chapuy et al., 2018; Pasqualucci and Dalla-Favera, 2018; Pasqualucci et al., 2011). Thereby the focus on genetic mutations can be misleading. On the other hand, transposon mutagenesis, the system we used in our screen, allows the genome-wide discovery of cancer genes in a random fashion and ideally covers the entire mouse genome. Of note, transposon mutagenesis provides a first biological validation of the identified hits as cancer-causing events in relevant disease models. However, an unbiased genome-wide screening in mice bears the risk of finding cancer genes without relevance in humans. Arguing against this, more than 50% of the CIS genes identified in our screening approach, were also dysregulated in human B-cell lymphomas by means of mutations, copy number alterations or differential gene expression revealing potential translational relevance of the alterations identified in the murine screen. Moreover, we identified several well-described human oncogenes and tumor suppressor genes among the top hits of our screen, providing evidence for the relevance of the identified CIS genes and the quality of the model. Thus, we conclude that the BCL model used in this study is modelling human B-cell lymphomagenesis in an appropriate way to identify novel human cancer genes.

In particular, transposon mutagenesis is a powerful tool to identify drivers, which are not altered by genetic mechanisms like mutations (Friedrich et al., 2017). Here we identified *SNRNP70* and *SLF2* as tumor suppressor genes, which have both not been associated with cancer before. Moreover, we proved their biological relevance in cancer pathogenesis. *SLF2* deletions occur in BCL patients with low frequencies like hundreds of genes (TCGA DLBCL cohort). Thereby, our *in vivo* screening was vital to pinpoint SLF2 loss as a cancer causing

event. As the mechanisms of SLF2 inactivation in human cancers are not understood yet, the relevance of transcriptional dysregulation and of the rare mutations occurring in the *SLF2* gene need to be assessed in future studies (Sondka et al., 2018).

The *SNRNP70* gene is part of a long amplification in DLBCL (Chapuy et al., 2018) suggesting a role as oncogene. Against this background, applying the functional information from our transposon mutagenesis screen, we showed that *SNRNP70* is a tumor suppressor gene. From there on the analysis of DLBCL histology samples showed the absence of SNRNP70 protein in a subgroup of patients pointing to a potential post-translational inactivation mechanism. Moreover, this provided potential relevance of SNRNP70 as tumor suppressor in DLBCL patients.

In summary, this shows the enormous benefit of transposon mutagenesis for interpreting NGS data and how the results from our screening can be used to identify driver alterations of B-cell lymphomagenesis.

4.2 The biological relevance of *SENP6* deletions in tumorigenesis

Recurrent deletions of *SENP6* in human BCL were found with frequencies from 13 to 23%. Of note, comprehensive sequencing studies showed that hundreds of genes are altered in DLBCL with frequencies comparable to *SENP6* deletions (Chapuy et al., 2018). In order to interpret and translate findings from such sequencing studies into novel mechanism-based therapeutic strategies for patients, functional studies thus seem indispensable. In our study, we experimentally show for the first time that loss of SENP6 initiates tumorigenesis and suggest, that genetic *SENP6* loss is a tumor initiating event in B-cell lymphomas.

Whereas we combined genetic deletion of *Senp6* with oncogenic MYC signalling as primary lesion in the described validation experiments, it remains unclear if loss of Senp6 causes tumorigenesis without cooperating with an additional driver. Testing this heavily relies on the availability of a genetic mouse model as the transplantation models used in this study are limited by the lifespan of irradiated recipient mice. Therefore these models do not allow long aging of experimental mice and thereby the identification of subtle effects. Moreover, only four out of five mice from the *in vivo* validation experiment developed tumors, and we cannot exclude that beyond MYC activation and Senp6 loss a tertiary alteration is needed to malignantly transform B-cells.

Studies in cell culture models showed that balanced regulation of SUMO chains is critical for proliferation and that SENP6 depletion leads to severe mitotic failures and reduced cell survival (Hattersley et al., 2011; Mukhopadhyay and Dasso, 2010). Against this background, we show that loss of Senp6 led to more aggressively growing lymphomas in mice and could substantially deplete SENP6 in a human DLCBL cell line. Notably, the cell line was growing

stable without effect on cell proliferation. Altogether this suggests that SENP6 acts context-specific. This could either be attributed to an altered target proteins landscape in specific cancer cells or to compensatory mechanisms (e.g. transcriptional dysregulation), which are activated following SENP6 loss to protect specific target proteins (e.g. the ones involved in cell proliferation) from chromatin extraction or degradation triggered by unrestricted poly-SUMOylation. Of note, this shows that proposed strategies to target SENP6 therapeutically to treat cancers (Liebelt et al., 2019) should not be considered for aggressive human BCLs and need to be assessed critically for other entities.

Although our study elucidated a defective DDR associated with *SENP6* deletions in DLBCL, these deletions might have broader implications. Beyond the deletions in DLBCL, we identified *SENP6* deletions in MCL and FL, two BCL sub-entities with a described role of MYC and in various types of solid cancers like uveal melanoma, prostate adenocarcinoma and pancreatic adenocarcinoma. Indeed, our mechanistic investigations in NIH 3T3 and U-2-OS cells showed functionality of the discovered mechanism in non-hematopoietic cells and non-lymphoma cells respectively. Hereby we provide a mechanistic framework to assess the pathway downstream of SENP6 deletions in different cancer entities as well.

4.3 Dysregulated SUMOylation and tumor initiation

SUMOylation is an essential pathway for all cells. Whereas several studies provided evidence that SUMO conjugation is activated in human cancers (Hoellein et al., 2014; Kessler et al., 2012; Seeler and Dejean, 2017) a specific role in causing tumorigenesis has not been described so far. Of note, loss of function mutations of enzymes involved in the SUMO pathway have not been considered potential mechanisms of transformation due to the central role of SUMOylation in all cell types (Seeler and Dejean, 2017).

Against this background, we here experimentally show for the first time that unrestricted poly-SUMOylation caused by loss of *SENP6* directly promotes tumorigenesis *in vivo*. SENPs are key determinants of the SUMO machinery and control the SUMOylation status of target proteins. With regard to MYC-dependent cancers, we found a strong SENP6-dependent increase of SUMO2/3 conjugates, revealing that SENP6 acts as a critical determinant of the SUMO homeostasis in BCLs. This was corroborated by genetic experiments in BCL cell lines and is in line with the previous described role of SENP6 in balancing the SUMO status of target proteins in non-cancer cell types (Kunz et al., 2018).

SENP6 and SENP7 are the most divergent members of the SENP family. Both are specific for SUMO2/3 isoforms and have a preference for cleaving SUMO chains (Alegre and Reverter, 2011). Whereas SENP7 is expressed in typical *in vitro* model systems like U2-O-S or Hela cells (Gonzalez-Prieto et al., 2015), we here show that SENP7 is suppressed during

B-cell lymphomagenesis and that SENP6 is the only remaining enzyme of this SENP family in BCLs further underscoring the critical role in controlling the level of poly-SUMOylated proteins. Thereby we also exclude the possibility that SENP7 could compensate the function of SENP6 after loss of SENP6. Moreover, it is not known so far if SENP7 and SENP6 have common substrates. Of note, a recent study showed that SENP7 is not able to functionally compensate for SENP6 absence (Liebelt et al., 2019), which indicates that the biological roles are at least not fully overlapping and it remains to be experimentally tested if SENP7 does restrict or contribute to tumorigenesis.

SENP6 specifically acts as SUMO chain trimmer and counteracts the StUbL pathway (Keiten-Schmitz et al., 2019). Ubiquitination of poly-SUMOylated substrates by StUbLs like RNF4 or RNF111 typically causes either proteasomal degradation or proteasome-independent extraction from chromatin (Gibbs-Seymour et al., 2015; Liebelt et al., 2019; Wagner et al., 2019). Activation of MYC drives the expression of the E1 enzymes SAE1/UBA2, the E2 ligase UBC9 and all SUMO isoforms in BCLs (Hoellein et al., 2014). UBC9 is the critical enzyme for

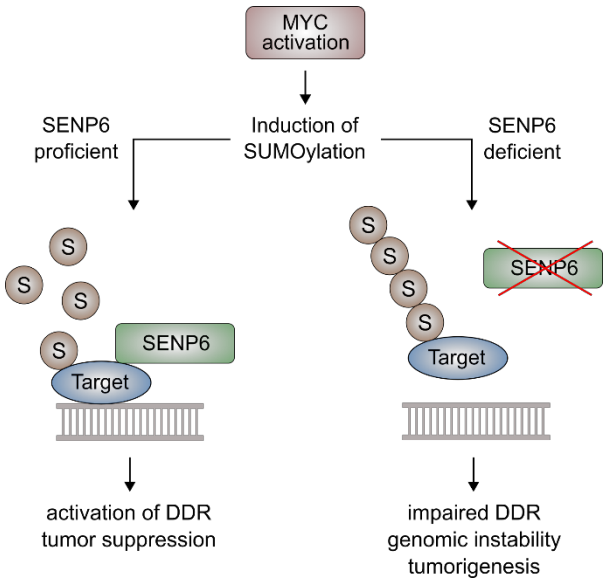

Figure 38. Model of SENP6-mediated suppression of B-cell lymphomagenesis. Activation of oncogenic MYC signaling drives the SUMOylation of target proteins. Overall a substantial fraction of SENP6 substrates is part of the DDR and SENP6 is considered to play a key role as signaling hub in DDR pathways. Under *SENP6* wildtype conditions (SENP6 proficient) SENP6 is located on chromatin and stabilizes its substrates in an un-SUMOylated/ mono-SUMOylated form which leads to chromatin localization and thereby functional DDR and tumor suppression. Under conditions of *SENP6* loss (SENP6 deficient) the poly-SUMOylated form of its substrates accumulates. Consequently substrates are extracted from chromatin leading to impaired DDR, genomic instability and tumorigenesis. S, SUMO.

promoting poly-SUMOylation (Garvin and Morris, 2017) and we conclude that by inducing UBC9, MYC also activates poly-SUMOylation. Thereby MYC promotes a signal priming a broad spectrum of proteins for StUbL-mediated degradation or chromatin extraction. We show that SENP6, which is rapidly activated in the context of oncogene-induced replicative stress, is located at chromatin and protects its substrates from this faith by trimming the poly-SUMO chains and thereby avoiding ubiquitination (Figure 38). From this we conclude that SENP6 acts

as a safeguard deSUMOylase localized at chromatin to protect proteins, which are essential in the context of replicative stress. This is in line with the described role of SENP6 in the DDR (Wagner et al., 2019) and we extend this concept to SENP6 being activated as intrinsic tumor suppressive pathway.

The fate of poly-SUMOylated proteins following StUbL-mediated ubiquitination needs to be further investigated as StUbLs can mediate K63 as well as K48 ubiquitination (Keiten-Schmitz et al., 2019). However, our MS-based proteome analysis argues for a not proteolytic signal as the overall proteome was only moderately affected after editing the SENP6 status in a DLBCL cell line, whereas the change in overall SUMOylation was dramatic. By this time, we also cannot exclude that the tumor initiating effect of enhanced SUMOylation could also be accomplished by activated SUMO-conjugation and thereby increasing the amount of poly-SUMO modified proteins, which needs to be addressed experimentally.

Previous work suggested that enhanced SUMOylation in MYC-driven tumors is needed for a distinct gene expression programm (Kessler et al., 2012). However, our proteomic analysis did not reveal major differences in protein expression patterns when comparing SENP6-deficient cells to normal cells. This is most likely due to the fact that enhanced polySUMOylation primarily affects genome stability, but not gene regulation. This is also corroborated by the SENP6 substrate landscape, which primarily comprises DNA damage associated proteins (Liebelt et al., 2019; Wagner et al., 2019).

Of note, a recent publication showed increased P53 expression upon Senp6 depletion in mouse chondrocytes (Li et al., 2018). However, we did not detect differences in P53 expression in our proteome experiment, which might be explained by context or tissue specifity of this effect.

4.4 Tumor-relevant substrates of SENP6

Two recent studies comprehensively defined the substrates of SENP6 for dynamic poly-SUMOylation (Liebelt et al., 2019; Wagner et al., 2019). These approaches provided a list of candidate substrates critical for the biological functions of SENP6 and revealed a network of proteins involved in chromatin organization and the DDR (Keiten-Schmitz et al., 2019).

In order to identify the tumor relevant molecular substrates of SENP6 we integrated the functional data from the transposon-based screen with proteomic data of candidate SENP6-controlled SUMO target proteins (Liebelt et al., 2019; Wagner et al., 2019). This analysis clearly pointed towards the cohesin complex and in particular the subunits RAD21, STAG1 and STAG2 as potential prime targets of SENP6-mediated tumor suppression. All three corresponding murine genes, *Rad21*, *Stag1* and *Stag2*, were identified as tumor suppressor genes in the murine *Eμ-myc* transposon mutagenesis screen providing direct *in vivo* evidence, and

the corresponding human genes are well-known tumor suppressors in human cancers (Sondka et al., 2018). Cohesins hold sister chromatids together until metaphase to anaphase transition. In addition, cohesin is present at replication sites and promotes restart of stalled forks thereby promoting replication stress tolerance. Finally, cohesins are also involved in homologous recombination-mediated DSB repair (Litwin et al., 2018). We demonstrate impaired chromatin association of RAD21 and STAG2 in a human BCL cell line deficient for *SENP6* indicating loss of cohesin function in the absence of SENP6.

Impaired chromatin association upon loss of SENP6 was also observed for CDC5L, exemplifying that unrestricted SUMOylation after loss of SENP6 is affecting the chromatin association of various target proteins. CDC5L is a core component of the hPSO4/PRP19 complex, which is associated with DNA damage checkpoint activation (Mahajan, 2016). The observed removal of CDC5L from chromatin during oncogene-induced replicative stress after depletion of SENP6 provides a molecular rational for compromised DNA damage checkpoint activation.

Based on these data, we assume that SENP6-dependent deSUMOylation affects several DDR and genome maintenance associated pathways and acts as a central signaling hub controlling critical DDR signaling pathways. For this reason, we conclude that the caretaker function of SENP6 in these pathways is linked to its role as a rheostat of chromatin occupancy. Poly-SUMOylation in conjunction with RNF4-mediated ubiquitination normally initiates the release of genome maintenance factors from sites of DNA damage upon termination of the DDR. In the early response phase SENPs counterbalance SUMOylation to avoid premature release. Our data suggest that in analogy to what was proposed for SENP2, SENP6 is required to restrict an “over before it has begun” repair response (Garvin et al., 2019). SENP6 loss consequently impairs DNA repair and causes genomic instability.

4.5 *SENP6* deletions and genomic instability

Insights into the cellular caretaker mechanisms allowing tumor cells to handle increased levels of DNA damage are crucial for the rational development of mechanism-based therapy strategies. This is of particular interest in BCL, in which DNA double strand breaks represent a physiological process during formation and revision of specific antigen receptors and where failure of repair often leads to malignant transformation (Pasqualucci and Dalla-Favera, 2018). Initially, SENP6 was associated with DNA repair by controlling the SUMOylation state of RPA70. Only in the absence of SENP6, RPA70 accumulates in its SUMOylated form and recruits Rad51 to the site of DNA damage to initiate DNA repair (Dou et al., 2010). Moreover, two recent mass-spectrometry studies identified a broad set of factors involved in the DNA repair pathway as *bona fide* SENP6 targets (Liebelt et al., 2019; Wagner et al., 2019). Fully in line with these recent studies, we expand the biological role of SENP6 as a key signaling hub

at the interface of several DDR pathways and implicate a much broader function than described initially. Of note, a recent study described a premature aging phenotype in mice with Senp6 depletion in osteochondroprogenitors, which resembles the phenotypes described in mice deficient for DNA repair or DDR associated genes (Hoeijmakers, 2009; Li et al., 2018) and further strengthens the concept of SENP6 as central regulator of the DDR.

Defects in cellular genome caretaker mechanisms often lead to accumulation of DNA damage and ultimately to an increase in genome instability. Genome instability leads to the acquisition of advantageous genotypes and is a characteristic that causally contributes to tumorigenesis (Hanahan and Weinberg, 2011). Notably, we provide first *in vivo* evidence that the SENP6 status is critical for maintenance of genome integrity in murine as well as in human lymphomas and extend the biological function of SENP6 towards a caretaker of genome stability. Considering the spectrum of molecular DNA repair mechanisms controlled by SENP6, deregulation of several DNA repair pathways might contribute to genomic instability in SENP6 depleted lymphomas. However, the aneuploidy, which we detected in *Eμ-myc* lymphomas following SENP6 loss is in line with studies describing genome instability and aneuploidy in human cancers harboring inactivating mutations or deletions affecting the cohesin subunit STAG2 (Barber et al., 2008; Solomon et al., 2011). STAG2 regulates the separation of sister chromatids and defects in sister chromatid cohesin are considered a major cause of genome instability (Barber et al., 2008; Solomon et al., 2011). This points towards STAG2 potentially being the prime target for genomic instability mediated by SENP6 loss. Of note, genetic deletion of Ulp2, the yeast homologue of SENP6, leads to aneuploidy in yeast (Ryu et al., 2018). In this light our study expands this observation to mammalian cells and suggests a highly conserved mechanism.

Moreover, we found that low SENP6 expression is associated with adverse outcome after standard of care BCL treatment and that the SENP6 status is crucial for sensitivity to chemotherapy treatment. Considering that many chemotherapeutics like cyclophosphamide or DRB induce a DDR, a defective DDR following loss of SENP6 might influence the effects of chemotherapy and explain this result.

Thus, we here implicate SENP6 as a global-acting deSUMOylase regulating DNA repair and governing genome integrity and reveal the mechanism, which enables cells to circumvent DNA damage checkpoint activation after endogenous as well as exogenous DNA damage stimuli.

4.6 SENP6 as biomarker for mechanism-based cancer treatment

Initially, we set out for dissecting the mechanisms of BCL pathogenesis to ultimately identify novel tumor vulnerabilities. Whereas SENP6 limits tumorigenesis and could not directly be

targeted therapeutically, our investigations allow the mechanism-based targeting of the tumor biology driven by *SENP6* deletions.

Hereby, a striking observation is the sensitivity of SENP6-deficient BCL cells to PARPi. Following the initial discovery of synthetic lethality of PARPi and BRCA deficiency, other cancer types that harbor mutations in genes functioning in the DDR and DNA repair networks were shown to be sensitive to PARPi (Lord and Ashworth, 2012). One key example are tumor cells containing mutations in cohesin components. Thus, it has been proposed that inhibition of replication fork stability by PARPi creates a targetable synthetic lethality in STAG2-deficient cancer cells (Mondal et al., 2019). The finding that loss of SENP6 impaired cohesin function is therefore in perfect agreement with the observed sensitivity of the SENP6-deficient DLBCL cell line to PARPi. Since several PARP inhibitors are clinically approved drugs, PARPi could provide a therapeutic option for the subgroup of SENP6-deficient lymphoma patients. Data about the clinical application of PARPi in B-cell malignancies are limited. However, evidence for clinical activity of the PARPi veliparib was reported in patients with B-NHL (Soumerai et al., 2017).

Therefore, our findings on the tumor biology driven by *SENP6* deletions allow stratification of DLBCL patients for PARPi treatment and may lead to a novel therapy approach to be tested in clinical trials.

4.7 Therapeutic targeting of dysregulated SUMOylation

SUMOylation is an essential pathway in all cells and therapeutic targeting of this critical pathway seemed unlikely for a long time (Seeler and Dejean, 2017) until first studies identified that loss of the E1 enzymes SAE1/2 drives synthetic lethality with MYC in human breast cancer cells *in vitro* (Kessler et al., 2012). Based on this pivotal study, SUMOylation was identified as a vulnerability in MYC-driven B-cell lymphomas in various cell model systems (Hoellein et al., 2014). However, the lack of a specific compound inhibiting SUMOylation did compromise experimental *in vivo* testing (Seeler and Dejean, 2017).

Here, we set out to test a specific small molecule inhibitor targeting SUMOylation *in vivo*. Against the common assumption that inhibition of SUMOylation is associated with highly toxic effects, we show that repeated *in vivo* application of the SUMOi ML-93 is associated with manageable toxicity and did not affect *C57Bl6* immunocompetent wildtype mice. This reveals a therapeutic window allowing specific killing of cancer cells with SUMOi, which are highly dependent on SUMOylation for example driven by MYC (Hoellein et al., 2014; Kessler et al., 2012). Moreover, the striking reduction of overall SUMOylation in SUMOi-treated splenocytes argues for a certain range of differential SUMOylation, which healthy cells can tolerate without a dramatic loss in viability. This range is much smaller for tumor cells and allows specific killing, which we show using MYC-driven B-cell lymphoma cells.

The efficient killing of MYC-driven tumor cells is fully in line with studies proving that MYC activity is connected to increased sensitivity to pharmacological SUMO inhibition (He et al., 2017; Hoellein et al., 2014; Kessler et al., 2012). However, our experiment shows for the first-time *in vivo* synthetic lethality of SUMO E1 inhibition and MYC activation in BCL. Moreover, we provide a clear rationale for the future development of SUMOylation inhibitor-based therapies for cancers with activated SUMOylation.

Of note, inhibition of SUMOylation in PDAC does not have comparable efficacy with SUMOi in MYC-driven B-cell lymphoma and the molecular basis of these results and potential biomarkers indicating sensitivity to SUMOi treatment urgently need to be identified (Biederstadt et al., 2020). The toxicity effects in human patients of the advanced SUMOi TAK-981 are currently tested in a phase I clinical trial (ClinicalTrials.gov Identifier: NCT03648372). Based on the results of this trial strategies for patient stratification need to be tested.

5 MATERIALS

5.1 Instruments

Analytical balance Kern 770	*Kern & Sohn GmbH*
Cage systems IVC	*Tecniplast*
Cell incubator (Heraeus Hera cell 240)	*Heraeus*
Electrophoresis chamber	*Bio-Rad Laboratories*
Elphoscan ES2000 Plus device	*Sarstedt*
Flow cytometer (Cyan ADP Lx P8)	*Coulter-Cytomation*
FACSAria™ III cell sorter	*BD Biosciences*
Fridges and lab freezers	*Liebherr Hausgeräte GmbH*
Dissecting instruments	*Fine Science Tools GmbH*
Epson Perfection 4990 Photo Scanner	*Epson*
GelDoc System Universal Hood II	*Bio-Rad Laboratories*
Glas ware	*Labware SCHOTT AG*
Infrared lamp	*Breuer GmbH*
Light microscope Olympus CK40 and CKX41	*Olympus*
Light microscope Axiovert 25	*Carl Zeiss*
Liquid nitrogen tank Biosafe® MDβ	*Cryotherm*
MACS MultiStand	*Miltenyi Biotec*
Microfuge Heraeus Biofuge fresco	*Heraeus*
Microfuge Heraeus Megafuge 16 RS	*Heraeus*
Microfuge Heraeus Multifuge 3s	*Heraeus*
Microfuge MiniSpin	*Eppendorf AG*
Microcentrifuge Mikro22R	*Hettich Zentrifugen*
MidiMACS™ Separator	*Miltenyi Biotec*
Multi-Channel Pipettes Research Plus®	*Eppendorf AG*
NanoDrop 2000c	*ThermoFisher Scientific*
Neubauer hemocytometer	*Paul Marienfeld GmbH*
OPTIMAX X-ray Film Processor	*PROTEC GmbH & Co KG*
pH-meter SevenEasy™	*Mettler Toledo*
Pipetboy	*Integra Biosciences AG*
Pipettes Research Plus®	*Eppendorf AG*
Power Pac 200	*Bio-Rad Laboratories*
Power Pac P25T	*Biometra*
Precision balance Kern EG 2200-2NM	*Kern & Sohn GmbH*
Repeater 4780 and M4	*Eppendorf AG*
qRT-PCR Cycler (ABI Prism 7900 HT)	*Applied Biosystems*
Safety cabinet HERAsafe® HSP18	*Heraeus*
Scil Vet ABC Blood Counter	*ScilAnimal Care*

SDS-Gelelectrophoresis chamber (Multigel Long)	*Biometra GmbH*
Smart Spec Plus™ Spectrophotometer	*Bio-Rad Laboratories*
SONOPLUS Homogenisator (HD 2070)	*Bandelin electronic*
Sunrise Microplate Reader	*Tecan Life Sciences*
Thermal Cycler Veriti™ 96-well	*ThermoFisher Scientific*
Thermal Cycler BIOER Gene Touch	*Biozym Scientific GmbH*
Thermomixer comfort	*Eppendorf AG*
Vortex Mixer Genie2	*Scientific Industries*
Vortex Mixer IKA MS1 and Lab Dancer	*IKA® Werke GmbH & Co. KG*
Water bath	*Memmert*
Water bath SUB	*Grant Instruments*
Wet-transfer device	*Bio-Rad Laboratories*

5.2 Consumables

6 *well*-plates	*Greiner Bio-One GmbH*
12 *well*-plates	*Greiner Bio-One GmbH*
BD Plastipak™ 1 ml Sub-Q insulin syringes	*BD Biosciences*
Blood lancets supra	*Megro GmbH & Co KG*
Cell culture dishes	*TPP*
Cell culture flasks T125, T75, T25	*Greiner Bio-One GmbH*
Cell strainers 100 µm	*BD Bioscience*
Combitips advanced® 10 ml	*Eppendorf AG*
CoolCell™ FTS30 Freezing container	*Sigma Aldrich*
Cryo Tubes™	*Corning*
CyAn ADP Lx P8	*Beckman Coulter*
Discardit™ II disposable syringes	*BD Biosciences*
Eppendorf tubes, 1.5 ml and 2 ml	*Sarstedt*
FACS tubes, 5 ml	*BD Biosciences*
Filter vacuum driven bottle top filter	*Millipore*
Kodak films	*ThermoFisher Scientific*
MACS LS Columns	*Miltenyi Biotech*
Microvette tubes	*Sarstedt*
Parafilm	*Pechiney Plastic Packaging*
PCR-Strips Single Cap 8er-Soft-Strips 0.2 ml	*Biozym Scientific GMBH*
Pipette tips	*Sarstedt*
Pipette filter tips	*Starlab*
PVDF-Membrane	*Bio-Rad Laboratories*
S-Monovette®, EDTA	*Sarstedt*
Sterican® disposable needles	*B. Braun Melsungen AG*
Whatman® Filter Unit Puradisc FP30 0.2 µm and 0.45 µm	*GE Healthcare Life Sciences*

Whatman® Paper	*Biometra*

5.3 Chemicals and reagents

2-Mercaptoethanol, 50 mM	*ThermoFisher Scientific*
Acetic acid	*Carl Roth GmbH*
ACK Lysis buffer	*ThermoFisher Scientific*
Acrylamide/Bis-acrylamide solution [30%]	*Carl Roth GmbH*
Agarose NEEO ultra-quality Roti®Garose	*Carl Roth GmbH*
Ammonium persulfate (APS)	*Sigma-Aldrich*
Aprotinin	*Roth*
Bovine Serumalbumin (BSA)	*Sigma-Aldrich*
Bromphenol blue	*Sigma-Aldrich*
Complete Mini (Protease Inhibitor Cocktail)	*Roche*
Deionized water	*B. Braun Melsungen AG*
Dimethyl sulfoxide (DMSO)	*Serva*
dNTP Mix, 10 mM	*Fermentas*
Dithiothreitol (DTT)	*Sigma-Aldrich*
Dulbecco's phosphate buffered saline (DPBS)	*ThermoFisher Scientific*
Dulbecco's Modified Eagle Medium (DMEM)	*ThermoFisher Scientific*
Ethanol	*Carl Roth GmbH*
Ethidiumbromid (EtBr) solution [1%]	*Carl Roth GmbH*
Ethylendiamintetraacetate (EDTA)	*Carl Roth GmbH*
Fetal Calf Serum (FCS)	*PAA Laboratories GmbH*
Formaldehyde solution [36%]	*Fluka*
Formalin solution [10%]	*Sigma-Aldrich*
Glycerol	*Sigma-Aldrich*
Glycine	*Carl Roth GmbH*
Hank's Balanced Salt Solution, 10x (HBSS)	*ThermoFisher Scientific*
4-(2-hydroxyethyl)-1-piperazineethanesulfonic acid (HEPES)	*ThermoFisher Scientific*
Isoflurane CP® [1 mg/ml]	*CP-Pharma*
Isopropanol	*Carl Roth GmbH*
Leupeptin	*AppliChem*
Lipofectamin® 2000	*ThermoFisher Scientific*
L-Glutamin, 200 mM	*ThermoFisher Scientific*
Magnesium chloride ($MgCl_2$)	*Sigma-Aldrich*
Methanol	*J.T. Baker*
ML-93	*Takeda*
N-Ethylmaleimide	*Sigma-Aldrich*
Non-essential amino acids (NEAA)	*ThermoFisher Scientific*
Oligo(dT)12-18 Primer	*ThermoFisher Scientific*

Opti-Mem® I Reduced Serum Media	*ThermoFisher Scientific*
Osteosoft®	*Sigma-Aldrich*
Penicillin/Streptomycin (Pen/Strep)	*ThermoFisher Scientific*
Pepstatin A	*Roth*
Phenylmethylsulphonyl fluoride (PMSF)	*Sigma-Aldrich*
Phosphate buffered saline (PBS)	*ThermoFisher Scientific*
Polybrene (Hexadimethrine bromide)	*Sigma-Aldrich*
Ponceau S	*Sarstedt*
Propidium Iodide (PI)	*ThermoFisher Scientific*
RNase OUT	*ThermoFisher Scientific*
Sheep red blood cells (SRBC)	*ThermoFisher Scientific*
Skim milk powder	*Sigma-Aldrich*
Sodium dodecylsulfate (SDS)	*Sigma-Aldrich*
Sodium chloride (NaCl)	*Carl Roth GmbH*
Sodium fluoride (NaF)	*Sigma-Aldrich*
Sodium orthovanadate (Na3VO4)	*Sigma-Aldrich*
Sodium tetraborate decahydrate (Borax)	*Sigma-Aldrich*
SuperSignal West (Pico/Dura/Femto)	*Pierce*
N,N,N′,N′-Tetramethylethan-1,2-diamin (TEMED)	*Sigma-Aldrich*
Tris(hydroxymethyl)aminomethane (TRIS)	*Carl Roth GmbH*
Trypan blue stain solution [0.4%]	*ThermoFisher Scientific*
Trypsin-EDTA-Solution, 10x	*ThermoFisher Scientific*
Tween 20	*Sigma-Aldrich*
Ultra Pure Distilled Water (Aqua dest.)	*ThermoFisher Scientific*

5.4 Solutions and buffers

All buffers were prepared with deionized water (diH_2O) and stored at 4°C if not specified otherwise.

HF2$^+$ buffer:
10% HBSS, 10x
2% FCS (heat inactivated)
1% HEPES
1% Pen/Strep
diH_2O
0.22 µm sterile filtered

FACS buffer:
PBS

	0.5% BSA
Tail buffer:	1% SDS 0.1 M NaCl 0.1 M EDTA 0.05 M Tris (pH 8) 315 ml diH_2O
NaB buffer (1x):	0.19% Borax diH_2O
Agarose gel (1%):	1% Agarose NaB buffer (1x) Boiled in microwave until completely dissolved. 1 µg/ml EtBr
Protein lysis buffer:	50 mM HEPES 150 mM NaCl 1 mM EDTA pH 7.5 2.5 mM EGTA pH 7.5 0.1% Tween 20 1 mM PMSF 1 mM NaF 0.1 mM NaVO4 20 mM NEM 10% of one Roche Mini-Complete tablet dissolved in diH_2O
PBS-Tween (PBS-T):	0.1% Tween 20 PBS
APS (10%):	10% Ammoniumpersulfat diH_2O

SDS-PAGE separating gel buffer (1×):	1.5 M Tris/HCl, pH 8.8
SDS-PAGE stacking gel buffer (1×):	0.5 M Tris/HCl, pH 6.8
SDS-PAGE loading buffer (5x):	3.88 g DTT 250 mM Tris/HCl 1M ph 6.8 5 g SDS 6.25 g Bromphenol blue (1%) 50% Glycerol 50 ml diH_2O
SDS running buffer (10x):	14.4% Glycine 3% Tris 1% SDS diH_2O
SDS transfer buffer:	20% Methanol 10% SDS-Running buffer (10x) diH_2O
Stripping buffer (Western Blot):	10% Methanol 10% Acetic acid 80% diH_2O
4% Formalin solution:	40% Formalin solution [10%] 60% PBS
Lysis buffer (Chromatin extraction):	10 mM HEPES pH 7.4 10 mM KCl 0.05% NP-40 2 µg/ml Aprotinin 1 µg/ml Pepstatin A 2 µg/ml Leupeptin PMSF 1mM 1 mM NaF

0.1 mM Na_3VO_4
20 mM NEM
diH_2O

Low salt buffer (Chromatin extraction): 10 mM Tris-HCl pH 7.4
0.2 mM $MgCl_2$
2 µg/ml Aprotinin
1 µg/ml Pepstatin A
2 µg/ml Leupeptin
PMSF 1mM
1 mM NaF
0.1 mM Na_3VO_4
20 mM NEM
diH_2O

Neutralization buffer (Chromatin extraction): 1 M Tris/HCl pH 8

Lysis buffer I (ChiP seq): 5mM PIPES pH 8
85 mM KCl
0,5% NP40
10 mM Glycine
diH_2O

Lysis buffer II (ChiP seq): 10 mM Tris/HCl pH 7.5
150mM NaCl
1mM EDTA
1% NP-40
1% Deoxycholic acid sodium salt
0.1% SDS
diH_2O

Washing buffer I (ChiP seq): 20 mM Tris HCl pH 8.1
150 mM NaCl
2mM EDTA
0,1% SDS
1%Triton-X-100

	diH_2O
Washing buffer II (ChiP seq):	20 mM Tris HCl pH 8.1
	500 mM NaCl
	2mM EDTA
	0.1% SDS
	1%Triton-X-100
	diH_2O
Washing buffer III (ChiP seq):	10 mM Tris/HCl pH 8.1
	250 mM LiCl
	1 mM EDTA
	1% NP-40
	1% Deoxycholic acid sodium salt
	diH_2O
Elution buffer (ChIP seq):	1% SDS
	0.1 M $NaHCO_3$
	diH_2O

5.5 Enzymes

Alkaline Phosphatase, Calf Intestinal (CIP)	*New England Biolabs*
BglII	*New England Biolabs*
BsmBI	*New England Biolabs*
DNAse I	*Qiagen*
EcoRI	*New England Biolabs*
RNAse A	*Qiagen*
Phusion High Fidelity DNA Polymerase	*ThermoFisher Scientific*
Proteinase K	*Ambion*
T4 DNA Ligase	*New England Biolabs*

XhoI	*New England Biolabs*

5.6 Antibodies

5.6.1 Immunblotting

SUMO1 (4930)	*Cell Signaling*
SUMO2/3 (8A2)	*Cell Signaling*
c-MYC (sc-764)	*Santa Cruz*
β-Actin (A5316)	*Sigma-Aldrich*
RAD21 (4321)	*Cell Signaling*
p-ATM (4526)	*Cell Signaling*
p-ATR (2853)	*Cell Signaling*
p-CHK1 (2348)	*Cell Signaling*
p-CHK2 (2197)	*Cell Signaling*
CHK1 (sc-56291)	*Santa Cruz*
CHK2 (3440)	*Cell Signaling*
yH2AX (ab11174)	*Abcam*
CDC5L (ab51320)	*Abcam*
PRPF19 (ab126776)	*Abcam*
Histone-H3 (4499)	*Cell Signaling*
SENP6 (HPA024376)	*Sigma-Aldrich*
SENP7 (ab58422)	*Abcam*
β-Tubulin (E7)	*DSHB*
mouse IgG HRP (NA931V)	*GE Healthcare*
rabbit IgG HRP (NA934V)	*GE Healthcare*

5.6.2 Immunohistochemistry

SENP6 (HPA024376)	*Sigma-Aldrich*
IgM (BD 553435)	*BD Biosciences*
B220 (BD 550286)	*BD Biosciences*

5.6.3 Flow cytometry

CD45 (FITC, 30-F11),	*eBioscience*

B220 (PE-Cyanine7, RA3-6B2)	*eBioscience*
IgM (PE, eB121-15F9)	*eBioscience*
IgD (eFluor450, 11-26c(11-26)	*eBioscience*
c-Kit (APC-eFluor780, 2B8)	*eBioscience*

5.6.4 ChIP sequencing

SUMO1 (ab32058)	*Abcam*
SUMO2/3 (ab81371)	*Abcam*

5.7 Kits

Bio-Rad Protein Assay	*Bio-Rad Laboratories*
CD19 MicroBeads, mouse	*Miltenyi Biotec*
Platinum SYBR Green qPCR SuperMix-UDG	*Invitrogen*
Qiagen® DNeasy Blood & Tissue Kit	*Qiagen*
Qiagen® Omniscript RT Kit	*Qiagen*
Qiagen® Qiashredder	*Qiagen*
Qiagen® RNeasy Plus Mini Kit	*Qiagen*

5.8 Oligonucleotides

5.8.1 Genotyping primers

Eμ-myc	fw: 5`-ACCTCTCCGAAACCAGGCACCGCAA-3` rv: 5`-TCTTGCTCGCGCGCTAGTCCTTTCC-3`
ATP2-H32	fw: 5`-CTCGTTAATCGCCGAGCTAC-3` rv: 5`-GCCTTATCGCGATTTTACCA-3`
Rosa26^{PB}	fw1: 5`-CCAAAGTCGCTCTGAGTTGTTATCAG-3` fw2: 5`-GCTGGGGATGCGGTGGGCTC-3` rv: 5`-GGCGGATCACAAGCAATAATAACCTGTAGTTT-3`
Rosa26^{Cas9}	fw1: 5`-AAAGTCGCTCTGAGTTGTTAT-3` fw2: 5`-GCCACACTGATTCATCAGTCAA-3` rv: 5`- ATTTTACACCTGTTCAATTCCCC-3`

5.8.2 Cloning oligonucleotides

Senp6-sgRNA

Fw: 5`-GTCGTCTCCCACCGAGAGGAAAGTCCAGCAGAAGGTTTCGAGACGTG-3`
Rv: 5`-CACGTCTCGAAACCTTCTGCTGGACTTTCCTCTCGGTGGGAGACGAC-3`

Snrnp70-sgRNA

Fw: 5`-GTCGTCTCCCACCGTGAACGGCGACAGCAGGAAGGTTTCGAGACGTG-3`
Rv: 5`-CACGTCTCGAAACCTTCCTGCTGTCGCCGTTCACGGTGGGAGACGAC-3`

Slf2-sgRNA

Fw: 5`-GTCGTCTCCCACCGGTGGTGTCCATGAGTCACGGGTTTCGAGACGTG-3`
Rv: 5`-CACGTCTCGAAACCCGTGACTCATGGACACCACCGGTGGGAGACGAC-3`

5.8.3 CRISPR/Cas9 sgRNA sequences for transfection

SENP6Ex2_g2: 5`-AGATCAGAGTCTAAGAGAGA-3`
SENP6Ex2_g3: 5`-GGAGATACAGATAAAGAGTA-3`

5.8.4 PCR amplification of CRISPR/Cas9 target regions.

Senp6.mm2	fw: 5`-CTATAGCAAAGATCATGAG-3`
	rv: 5`-GATGCATTGATAAATTCTG-3`
Slf2.mm2	fw: 5`-CAAACATATGTTGGATTC-3`
	rv: 5`-GAGAGATTACTCTTCCCA-3`

5.8.5 qPCR primers

MYC (murine)	fw: 5`-TTCCTTTGGGCGTTGGAAAC-3`
	rv: 5`-GCTGTACGGAGTCGTAGTCG-3`
Senp6 (murine)	fw: 5`-CGGCACTGTAGCACTTACCA-3`
	rv: 5`-GGCTTGTCGGCAATTTCTT-3`
Senp7 (murine)	fw: 5`-GGATGTTCTTGCTCAGTCACC-3`
	rv: 5`-ACCTTGCTGGGAGCACATAA-3`

Ubiquitin (murine)	fw: 5`-GCAAGTGGCTAGAGTGCAGAGTAA-3`
	rv: 5`-TGGCTATTAATTATTCGGTCTGCAT-3`

5.8.6 shRNA identifier

Senp6.21	TRCN0000031019, Sigma Aldrich, Mission Library
Senp6.22	TRCN0000031022, Sigma Aldrich, Mission Library
Senp6.23	TRCN0000031023, Sigma Aldrich, Mission Library

5.9 Plasmids

MSCV-IRES-GFP (MIG)	Addgene (#9044), William Hahn
MSCV-IRES-GFP-Bcl-2	Prof. Ulrich Keller
pLKO.1-puro	Sigma Aldrich
pLKO.1-puro-Senp6.21	Sigma Aldrich
pLKO.1-puro-Senp6.22	Sigma Aldrich
pLKO.1-puro-Senp6.23	Sigma Aldrich
pLKO5.sgRNA.EFS.GFP	Addgene (#57822), Benjamin Ebert
pLKO5.sgRNA.EFS.GFP-sgRNA-Trp53	Julia Weber
pLKO5.sgRNA.EFS.GFP-sgRNA-LacZ	Julia Weber
pLKO5.sgRNA.EFS.GFP-sgRNA-Senp6	this study, cloned by M. Schick
pLKO5.sgRNA.EFS.GFP-sgRNA-Slf2	this study, cloned by M. Schick
pLKO5.sgRNA.EFS.GFP-sgRNA-Snrnp70	this study, cloned by M. Schick
pHIV-EGFP	Addgene (#21373), Bryan Welm
pHIV-EGFP-SENP6	this study, cloned by M. Schick
psPAX2	Addgene (#12260), Didier Trono
pMD2.G	Addgene (#12259), Didier Trono

5.10 Standards for DNA and protein electrophoresis

GeneRuler 1kb DNA Ladder	Thermo Scientific
PageRuler Plus Prestained Protein Ladder	Thermo Scientific

5.11 Bacteria

DH5α	gift, Tim Ammon

5.12 Cell lines

NIH 3T3	murine fibroblast cell line	Prof. Ulrich Keller
Eμ-myc Hoxb8	Hoxb8-FL cells	gift, Tim Ammon
Eμ-myc;Rosa26^{Cas9} Hoxb8	Hoxb8-FL cells	gift, Tim Ammon
HEK293T	human embryonic kidney cell line	Prof. Ulrich Keller
Phoenix Eco	retrovirus producer cell line	Prof. Ulrich Keller
SU-DHL-5	human DLBCL cell line	DSMZ (ACC 571)
SU-DHL-8	human DLBCL cell line	DSMZ (ACC 573)
Oci-Ly1	human DLBCL cell line	gift, Björn Chapuy
Oci-Ly3	human DLBCL cell line	DSMZ (ACC 761)
DB	human DLBCL cell line	DSMZ (ACC 539)
U-2-OS	human osteosarcoma cell line	DSMZ (ACC 832)

5.13 Mice

Eμ-myc	The Jackson Laboratory
ATP2-H32	gift, Prof. Roland Rad
Rosa26^{PB}	gift, Prof. Roland Rad
C57Bl6/J	Charles River Laboratories

5.14 Software and database tools

Excel	*Microsoft Office*
FlowJo Version 10	*Tree Star Inc.*
GraphPad Prism Version 7	*GraphPad Inc*
Inkscape Version 0.92	*Inkscape Community*
Word	*Microsoft Office*

6 METHODS

6.1 Molecular biology techniques

6.1.1 Polymerase chain reaction (PCR)

The reaction for standard PCRs contained 50 ng of template DNA, 0.5 µM each of forward and reverse primers, 0.5 µl dNTPs (10mM each), 0.5 µl Phusion High-Fidelity DNA Polymerase and 2.5 µl of the 10 x reaction buffer in a final volume of 25 µl. The temperature for denaturation was set to 95 °C, annealing temperatures were between 45-68 °C depending on the primers and elongation was carried out at 72 °C for 1-2 min depending on the length of the sequence. Typically, PCR reactions were performed with 30 cycles.

6.1.2 Digestion of DNA with restriction enzymes

For analytical purposes, 0.5 µg DNA (plasmids and/or inserts) were digested using 5 units of restriction enzyme in the respective buffer for 1 h at 37 °C. For preparative purposes, 5 µg DNA were digested using 20 units of restriction enzyme in the respective buffer for 2 h at 37 °C. Buffers for double digests were chosen according to the manufacturer's instructions. To dephosphorylate digested plasmids, 10 units of calf intestinal alkaline phosphatase (CIP) were added and incubated for 1 h at 37 °C followed by 20 min incubation at 80 °C for inactivation.

6.1.3 Ligation

For ligation, insert and plasmid were mixed at molar ratio of 2:1 to 5:1 with 50 ng of the digested and dephosphorylated vector. For the ligation, DNA was mixed with the according buffer and T4 ligase in a total volume of 10 µl for 5 min at RT or 16 °C overnight.

6.1.4 Transformation of competent bacteria

In this study, chemically competent DH5α were used for transformations. For transformation, either 2 µl of ligation reaction (see 6.1.3) or 100 ng plasmid DNA (for re-transformation) was added to 50 µl bacteria. Bacteria were then incubated on ice for 30 min. Next, heat shock was performed at 42 °C for 45 sec followed by 2 min incubation on ice. Subsequently, bacteria were plated on LB agar plates containing the respective antibiotic (depending on the plasmid) and incubated at 37 °C overnight. Next, single clones were picked and inoculated in LB medium with antibiotic and cultured at 37 °C for 12-16 h on a shaker.

6.1.5 Isolation of DNA from bacteria

For the purification of amplified plasmid DNA from bacteria, commercially available kits were used. Depending on the amount of bacterial culture, either the Qiagen Plasmid Maxi or Mini Kit was used according to the manufacturer's instructions. For long-term storage of positive clones, glycerol was added to bacterial cultures at a final concentration of 40% and the mix was stored at -80 °C.

6.1.6 Agarose gel electrophoresis and gel purification

To separate DNA fragments according to their size, agarose gels (0.8 – 1.5%) were used. To this end, agarose was dissolved in the appropriate volume electrophoresis buffer (1 x NaB), boiled and supplemented with EtBr. The solution was poured into a gel chamber. DNA samples were then loaded into gel pockets for electrophoresis and EtBr stained DNA was visualized with UV-light.

6.1.7 Isolation of genomic DNA from tumor material

Genomic DNA was extracted using the Blood and Tissue Kit (Qiagen) according to manufacturer's instructions.

6.1.8 RNA extraction from eukaryotic cells

Tissue or cell lysates were first homogenized using a QIAshredder (Qiagen). Next, total RNA was extracted using the RNeasy Mini Kit Plus (Qiagen) according to the manufacturer's instructions. The final RNA concentration was determined spectrophotometrically with a NanoDrop (ThermoFisher Scientific).

6.1.9 Reverse transcription (RT)

For the generation of cDNA, 400-1000 ng of RNA was reversely transcribed using the Omniscript RT Kit (Qiagen) with oligo(dT) primers, for specific transcription of mRNA by binding to polyA-tails following the manufacturer's protocol.

Reaction mix: 400-1000 ng RNA in 12 µl RNase-free H_2O
2 µl 10x RT buffer
2 µl dNTPs
2 µl oligo-dT (20 µM)

1 µl RNase inhibitor (10 units/µl)
1 µl Reverse Transcriptase
20 µl total reaction volume

6.1.10 Quantitative real time PCR (qRT-PCR)

qRT-PCR analysis was performed on an ABI Prism 7900HT cycler using the Platinum SYBR-Green Q PCR SuperMix according to the manufacturer's instructions. For data analysis, Ct values were compared to a control sample and normalized to the expression of *Ubiquitin*.

Primer sequences are listed in section 5.8.5.

Reaction mix:	15.6 µl	Power SYBR Green PCR Master Mix
	0.5 µl	ROX
	1 µl	Forward Primer
	1 µl	Reverse Primer
	1.8 µl	cDNA
	5.1 µl	H_2O
	25 µl total reaction volume	

Program: 1: 95 °C 1 min
2: 95 °C 15sec
3: 60 °C 1 min
4: to 1 (40 x)

6.2 Cell culture and cell-based assays

6.2.1 Culture of suspension and adherent cell lines

NIH-3T3, HEK293T, U-2-OS and Poenix-Eco cells were cultured in DMEM with 10% FCS. Human DLBCL cell lines were cultured in RPMI-1640 or IMDM medium supplemented with 20% FCS and 2 mM L-Glutamine. SU-DHL-5, SU-DHL-8, DB and Oci-Ly1 cells were purchased from DSMZ (Leibniz Institute DSMZ-German Collection of Microorganisms and Cell Cultures). U-2-OS cells with inducible MYC expression were used as described (Walz et al., 2014).

6.2.2 Freezing and thawing of cells

For long term storage, cells were pelleted and re-suspended in freeze medium (FCS supplemented with 10% DMSO) and transferred into cryotubes. The maximum concentration was 1 x 10^8 cells/ml. Tubes were then transferred to a – 80 °C freezer in a freezing container for at least 24 h. The cells were then transferred to liquid nitrogen for long-term storage. For re-culturing, cells were rapidly thawed at 37 °C and DMSO was washed out with the respective culture medium.

6.2.3 Transfection of eukaryotic cells

For the generation of ecotropic retroviral particles, PhoenixEco cells were seeded at a density of 4 x 10^6 cells in 5 ml PhoenixEco media in a 10 cm cell culture dish. Per approach, 30 µl of Lipofectamine 2000 were mixed with 1500 µl Opti-MEM® I Reduced Serum Media and 20 µg plasmid DNA. The mixture was incubated for 30 min at RT. Media was removed from PhoenixEco cells and replaced by 3.5 ml fresh PhoenixEco medium and 1500 µl transfection mix per dish was added. For the generation of lentiviral particles, HEK293T cells were co-transfected with the indicated lentiviral plasmids and helper virus plasmids equally. After 6 h incubation, the media was replaced by PhoenixEco medium. Supernatant containing viral particles was collected after 24, 36, and 48 h post transfection and filtered through a 0.45 µm Whatman® Filter Unit to avoid contamination with virus producer cells.

6.2.4 Viral transduction

Virus supernatants were collected after transfection and used to transduce the indicated cell lines in the presence of 1 µg/ml polybrene (Sigma-Aldrich). Suspension cells were transduced using spin-transduction at 1,500 RPM for 1 h at 32 °C.

6.2.5 CRISPR/Cas9-based gene editing

For depletion of SENP6 in human DLBCL cell lines, exon 2 of the SENP6 open reading frame was removed by CRISPR/Cas9 gene editing. To this end, 150.000 Oci-Ly1 cells were transfected with 500 ng of each of the sgRNA`s (sgRNA sequences are listed in 5.8.3) and 1 µg Cas9 protein (PNA Bio) with a Neon Transfection System (ThermoFisher/Invitrogen) (parameters: 1450 V; 10 ms; 4 pulses). The cleavage efficacy was tested 24 h following transfection with the Terra™ PCR Direct Card Kit and primers flanking exon 2. Cells were then separated

to single cells by serial dilution. Cell clones were screened for efficient gene editing and selected clones were analyzed for SENP6 protein expression by immunoblot analysis.

6.2.6 Analysis of CRISPR/Cas9 target regions.

Genomic DNA from infiltrated lymph nodes was isolated using the Qiagen Blood and Tissue kit. PCR amplification of targeted loci was carried out with Q5R Hot Start High Fidelity 2 x Master Mix. Afterwards the PCR products were analyzed using Engen T7 Endonuclease I following to the manufacturer's protocol. Primer pairs used for amplification of target regions are listed in section 5.8.4.

6.2.7 Flow cytometry

Flow cytometry analysis was performed following standard protocols. Primary cell suspensions from lymph nodes were directly labelled with fluorescently labelled antibodies against the following surface proteins: CD45, B220, IgM, IgD. For exclusion of dead cells either PI or DAPI was used. Data were acquired using a BD Cyan flow cytometer and analyzed by FlowJo software (FlowJo LLC). For subsequent data analysis viable CD45-positive positive cells have been gated following the gating strategy (Figure 39).

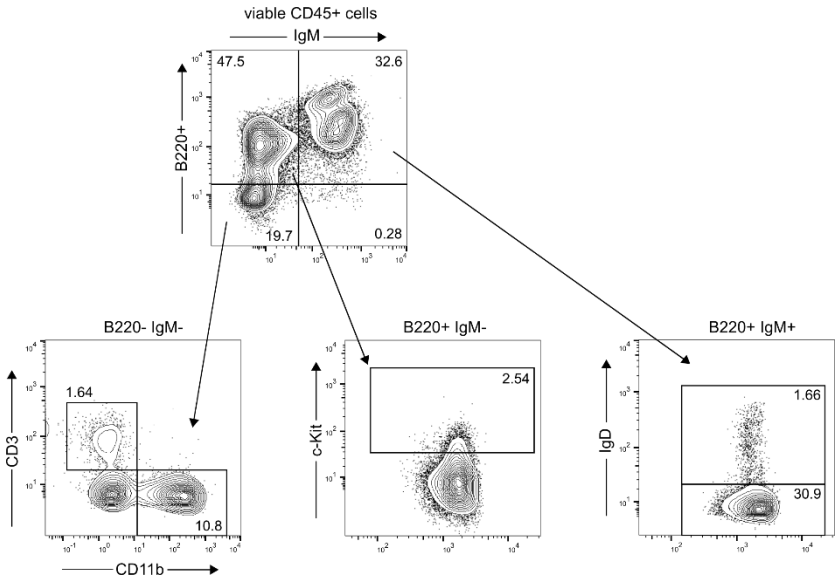

Figure 39. Gating strategy for the flow cytometry based phenotyping of B-cell lymphomas arising in *Eμ-myc* mice. Viable CD45+ cells have been analyzed for T-cells (CD3+), myeloid cells (CD11b+), pro-B-cells (B220+/c-Kit+), pre-B-cells (B220+/IgM-/c-Kit-), immature B-cells (B220+/IgM+/IgM-) and mature B-cells

6.2.8 Fluorescence microscopy

Cells were cultured on poly-L-lysine-coated slides for three days and fixed with 4% paraformaldehyde (Merck Millipore) in PBS. After this cells were blocked with 10% FCS (PAA, Germany), 0.1% Triton-X (Carl Roth) in PBS and stained with primary phospho-Histone H2A.X (Ser139) (Millipore). As secondary antibody, we used goat anti-Mouse IgG (H+L) Superclonal™ Secondary Antibody, Alexa Fluor 488 (ThermoFisher**).** All stains were counterstained with SlowFadeR Gold Antifade Reagent with DAPI (ThermoFisher). Staining was assessed on a Leica DM RBE fluorescent microscope (Leica). Fluorescence intensities of stained cells were quantified in total pixels from at least 15 cells after background correction using ImageJ (NIH). Each stain included a negative Ig control, the detected pixels of which were deducted from the total pictures as background. Fluorescence microscopy experiments were performed in a collaboration by Rouzanna Istvanffy, Technical University of Munich.

6.3 Protein Biochemistry

6.3.1 Cell lysis

Cell pellets were lysed in ice-cold lysis buffer for 30 min on ice followed by sonication (4 cycles with 10 sec at 30% power). Samples were then centrifuged at full speed for 15 min at 4 °C in a microcentrifuge to remove cell debris. The supernatant was collected and protein concentration was quantified using the Bio-Rad Protein Assay Dye Reagent according to the manufacturer's instructions. 15 to 100 µg protein was mixed with 1 x SDS loading buffer and boiled at 95 °C for 5 min.

6.3.2 Cell fractionation

Cell fractionation was performed as described (Huang et al., 2009). In brief, cell pellets have been resuspended in lysis buffer and incubated for 20 min on ice. After centrifugation at full speed for 10 min at 4 °C the supernatant (cytoplasmic fraction) was discarded and the remaining pellet was washed once in lysis buffer. Next, the pellet containing the nuclei was resuspended in low salt buffer + 1% Triton-X 100 and incubated on ice for 15 min. After centrifugation at full speed for 10 min at 4 °C the supernatant containing nucleoplasmatic proteins (soluble fraction) was collected. The chromatin (insoluble) fraction was purified by resuspending the final pellet in 0.2 N HCl and incubating for 20 min on ice. Afterwards the suspension was neutralized with Tris-HCl (pH 8). Antibodies specific for β-Tubulin and Histone H3 were used as loading controls for the soluble and insoluble fraction and as control for proper fractionation.

6.3.3 SDS polyacrylamide gel electrophoresis (SDS-PAGE)

Gels were purchased from Bio-Rad and stored at 4 °C. Protein samples (15-100 µg per slot) and a molecular weight marker were loaded onto a SDS-polyacrylamide gel and were electrophoretically separated in SDS-PAGE running buffer in an electrophoresis chamber at 60-130 V. Afterwards, gels were transferred to a membrane for immunoblot analysis.

6.3.4 Immunoblot analysis (Western Blot)

The gel was then transferred onto a PVDF membrane (0.45 µm) after methanol-activation in a wet-transfer chamber in transfer buffer at 4 °C and 1000 mA for 2-4 h. The membrane was then blocked with either 5% BSA in PBS-T or 5% skim milk in PBS-T for 1 h at RT. Membranes were incubated with primary antibodies in either 5% BSA in PBS-T or 5% skim milk in PBS-T on a shaker overnight. Afterwards membranes were washed three times with PBS-T for 10 min and incubated with a HRP-conjugated secondary antibody for 45 min at RT. After three 10 min washing steps in PBS-T, membranes were visualized on films with Pierce™ ECL Western Blotting Substrate according to the manufacturers' instructions.

6.3.5 Stripping of membranes

For re-probing of PVDF membranes with further antibodies the membranes were stripped with stripping buffer for 10 min at RT. The membranes were then washed three times for 10 min in PBS-T and incubated with new antibodies after blocking.

6.4 Mass spectrometric analyses

Mass spectrometric proteome analysis was carried out in a collaboration and was performed by Kathrin Schunck, Mueller Lab, University of Frankfurt.

6.4.1 Sample preparation for proteome analysis

Cells were lysed in 2% SDS lysis buffer, shortly heated to 95 °C, then sonicated and centrifuged at 16000 g for 5 min. In the following, protein content was determined using the DC Protein Assay Kit from BioRad. For in-solution digestion, 20 µg of each sample were precipitated using 4 volumes of acetone for 1 h at -20 °C. After centrifugation a wash step with 90% acetone was included. The precipitated pellet was shortly dried at room temperature and then resuspended in 6M urea/2M thiourea. Proteins were reduced with DTT, following an alkylation

step using chloroacetamide. Digestion was performed in only 2M urea with the endopeptidase Lys-C (Wako) in combination with trypsin (sequence grade, Promega) overnight at 37 °C. Digestion was stopped by acidifying. Finally, peptides were desalted and concentrated by the STAGE tipping technique (Stop and Go Extraction) (Rappsilber et al., 2007).

6.4.2 Liquid chromatography and mass spectrometry

For LC-MS/MS analysis, an Easy-nLC 1200 was coupled via a nano-electrospray ionization source to the Q Exactive HF mass spectrometer. Peptide separation by hydrophobicity was carried out on an in-house packed 17 cm long 75 µm ID column with 1.9 µm C18 beads (Dr Maisch GmbH). The binary buffer system used consisted of solution A: 0.1% formic acid and solution B: 80% acetonitrile, 0.1% formic acid. A gradient of 150 min was used for proteome analysis (0-123 min, linear up to 38% B). Then the concentration of solution B was increased to 60% in 12 min and finally increased to 95% in 5 min with a following re-equilibration to 5% B. Q Exactive HF settings: MS spectra were acquired with a maximal injection time of 20 ms, a resolution of 60000 at 300 - 1650 m/z and 3x106 as an AGC target. MS/MS spectra of the top 15 most intense peaks were obtained by higher-energy collisional dissociation (HCD) fragmentation. The maximal injection time was set to 25 ms, with an AGC target of 1x105 and a resolution of 15000.

6.5 Mouse breeding

ATP2-H32 transgenic mice were crossed to *Eμ-myc* mice to generate the *ATP2-H32;Eμ-myc* line. The resulting line was crossed to *Rosa26*^{PB} mice to generate triple-transgenic *Eμ-myc;ATP2-H32;Rosa26*$^{PB/+}$ mice. *Eμ-myc* (002728) mice were purchased from the Jackson Laboratory. Mice were examined twice a week and sacrificed as soon as lymph nodes were well palpable (5 mm diameter) or any of the approved thresholds was reached. The survival data in each experiment were analyzed using the Kaplan-Meier method and log-rank (Mantel-Cox) test was applied to test statistical significance. All animal experiments were performed in accordance to local authorities (Regierung von Oberbayern, Munich, Germany).

6.6 Genotyping

For genotyping of mice DNA was isolated from ear punches or embryonic tissue by digestion in tail buffer with 200 µg/ml Proteinase K at 55 °C in a thermo shaker. After at least 5 h the reaction was stopped by heat inactivation at 98 °C for 5 min. The supernatant containing DNA

was collected after centrifugation for 10 min at full speed in a table centrifuge. 1 µl of the supernatant was used as a template for genotyping. Genotyping of *Eμ-myc* mice was performed as described (Harris et al., 1988). Genotyping of *ATP2-H32*, *Rosa26*^{PB} and *Rosa26*^{Cas9} mice has been performed following standard protocols (Weber et al., 2019).

Primers used for genotyping are depicted in section 5.8.1.

6.7 Histology

Mouse lymph nodes were fixed in 10% neutral-buffered formalin solution for min. 48 h, dehydrated under standard conditions (Leica ASP300S, Wetzlar, Germany) and embedded in paraffin. Serial 2 µm-thin sections prepared with a rotary microtome (HM355S, ThermoFisher Scientific, Waltham, USA) were collected and subjected to histological and immunohistochemical analysis. Hematoxylin-Eosin (H.-E.) staining was performed on deparaffinized sections with Eosin and Mayer's Haemalaun according to a standard protocol. Histology has been performed in a collaboration by Katja Steiger, Pathology, Technical University of Munich.

6.8 Immunohistochemistry

Immunohistochemistry on human TMAs and whole slide specimen as well as on murine tissues was performed using a Bond RXm system (Leica, Wetzlar, Germany, all reagents from Leica) with primary antibodies listed in section 5.6.2. Briefly, slides were deparaffinized using deparaffinization solution and pretreated with epitope retrieval solution. Antibody binding was detected with a polymer refine detection kit without post primary reagent and visualized with DAB as a dark brown precipitate. Counterstaining was done with hematoxyline. Immunohistochemistry has been performed in a collaboration by Katja Steiger, Pathology, Technical University of Munich.

6.9 Quantitative transposon insertion site sequencing

Infiltrated lymph nodes from triple transgenic mice were harvested and snap frozen. Genomic DNA was extracted using the Qiagen blood and tissue kit according to manufacturer's instructions. Transposon insertion sites were recovered using the QiSeq pipeline as described earlier (Weber et al., 2019). Statistical analysis for CIS identification using CIMPL (Common Insertion site Mapping Platform) analysis based on a Gaussian kernel convolution framework was performed as previously reported (Weber et al., 2019).

6.10 Analysis of copy number alterations in murine BCLs

6.10.1 Low-coverage whole genome sequencing

Genomic DNA was isolated with DNeasy Blood & Tissue Kit. Library preparation was performed with 50 ng DNA per sample using the Illumina Nextera DNA Flex Library Prep Kit. Samples were sequenced single end with 75bp reads on an Illumina NextSeq system. Low-coverage whole genome sequencing has been performed in a collaboration by Rupert Oellinger, Technical University of Munich.

6.10.2 Analysis of sequencing data

Resulting sequencing data were processed using a standardized set of pipelines (Lange et al., 2019). Briefly, reads were trimmed using Trimmomatic and mapped to the mouse reference genome GRCm38.p6 using bwa mem. The GATK toolkit was used for base recalibration. Copy number alterations were called by HMMCopy, using data from the tail of backcrossed *C57BL/6J* mice as control. Analysis of low-coverage whole genome sequencing has been performed in a collaboration by Thomas Engleitner, Technical University of Munich.

6.11 ChIP sequencing

6.11.1 Spike-in ChIP sequencing

ChIP sequencing was performed as described previously (Baluapuri et al., 2019). In brief, 50 million SU-DHL-5 cells per IP condition were fixed using formaldehyde at 1% final concentration for 5 min at room temperature and fixation was stopped with addition of 125 mM glycine for 5 min at room temperature. After washing, cells were lysed in lysis buffer I and 6% murine T-lymphoma$^{MYC\text{-}Tet\text{-}Off}$ cells were added for exogenous spike-in. After 20 min lysis, nuclei were collected (1500 rpm, 15 min, 4 °C). Nuclei were incubated in lysis buffer II for 10 min. Cross-linked chromatin was fragmented by sonication (total duration: 20 min, pulse of 10 sec with 45 sec pausing). Efficient chromatin fragmentation was confirmed by agarose gel electrophoresis. Prior to immunoprecipitation, chromatin was cleared (20 min, 14000 rpm, 4 °C). Per IP reaction 100 µl Dynabeads (Protein A and Protein G 1:1 mixture, ThermoFisher Scientific) were incubated over night with 15 µg of corresponding antibody in presence of 5 g/L BSA in PBS: SUMO1 (abcam, ab32058) and SUMO2/3 (abcam, ab81371) antibodies. Chromatin corresponding to 50 million cells per IP reaction was added to the beads and IP was performed for 6 h on rotating wheel (4 °C). After IP, beads were washed with washing buffer I, washing buffer II, washing buffer III, and TE buffer three times each. Elution was performed twice in 150 µl

elution buffer each for 15 min on rotating wheel (room temperature). De-crosslinking of eluted samples and input samples was carried out overnight, and RNA and proteins were digested by adding RNase A and proteinase K, respectively. After chloroform-phenol extraction and ethanol precipitation, DNA concentration was determined using the Quant-iT PicoGreen dsDNA assay (ThermoFisher Scientific). For ChIP-seq library preparation the NEBNext ChIP-Seq Library Prep Master Mix Set for Illumina (New England Biolabs) was used according to the manual's instructions. Library quality was determined using the Fragment Analyzer (Advanced Analytical; NGS Fragment High Sensitivity Analysis Kit (1-6,000 bp; Advanced Analytical)) prior to being sequenced on the Illumina Next-Seq500. ChIP sequencing has been performed in a collaboration with Julia Hofstetter, University of Würzburg.

6.11.2 Analyisis of ChIP sequencing data

FASTQ files generation was carried out using Illumina CASAVA software within BaseSpace suit. Quality control of FASTQ files was performed using FASTQC. Reads were then aligned to hg19 build of human reference genome and mm10 child of mouse genome for calculating amount of spike in. Since the spike in reads were same in all samples, the files were read-normalized to the same depth and used for further analyzes after combining the input samples. The read-normalized bam files were converted to bedGraphs for visualization in genome browser. Peak calling was carried out using macs v1.4 and peak annotation was performed with bedtools v2.29.0 suit. The density plots were generated with deep tools v3.3.1. Analysis of ChIP sequencing data has been performed in a collaboration by Apoorva Baluapuri, University of Würzburg.

6.12 RNA sequencing

For RNA sequencing, total RNA of SU-DHL-5 cells was isolated using the Qiagen RNeasy Plus Mini Kit. Total RNA was quantified and used for RNA sequencing following quality control. RNA sequencing and data analysis was performed as described (Baluapuri et al., 2019). RNA sequencing has been performed in a collaboration by Apoorva Baluapuri, University of Würzburg.

6.13 Transduction-transplantation experiments

For the *in vivo* validation of tumor suppressor genes, single guide RNA (sgRNA) sequence was designed and selected with the CHOPCHOP (http://chopchop.cbu.uib.no/) sgRNA design resource and cloned into the pLKO5.sgRNA.EFS.GFP (Addgene #57822) construct. sgRNA

sequences are listed in 5.8.2. Transduction-transplantation experiments have been performed as described before (Weber et al., 2019). The transduction efficacy was typically between 15-25% and $2.5x10^5$ eGFP-positive HSPCs and $2x10^5$ CD45.1 bone marrow helper cells were transplanted into lethally irradiated (8.5 Gy) recipient mice. For all transplantation experiments female *C57Bl6/J* mice aged 6-8 weeks were used. Mice were purchased from Charles River. After transplantation mice were monitored daily for lymphoma development.

6.14 *In vivo* xenograft experiments

All animal experiments were performed in accordance with regional Gothenburg University animal ethics committee approval 100/16 and 5.8.18-01949/2018. The tumor cells were suspended in RPMI, mixed 1:1 with Matrigel (BD Biosciences) and transplanted subcutaneously onto the flanks of immunocompromised, non-obese severe combined immune deficient interleukin-2 chain receptor γ knockout mice (NOG mice; Taconic, Denmark). $1x10^6$ cells were used per mouse. Mice were weighted and tumors measured using calipers twice a week. The metric tumor volume (V) was calculated by measurements of length (L) and width (W) by applying the following equation: $V = 0.5 \times (L \times W^2)$. Treatments were started when the tumors were actively growing, judged by increasing volumes on repeated caliper measurements. ML-93 was dissolved in beta hydroxypropyl cyclodextrin and mice were dosed intravenously with 50 mg/kg body weight per dose. Dosing regimen for intravenous delivery were two consecutive days per week. Tumor size was measured until best response, or until no further effects could be expected. Mice were sacrificed before or when tumors reached ethical size limit. Xenograft experiments were performed in a collaboration by Lisa Nilsson, University of Gothenburg.

6.15 *In vivo* toxicity experiments

For in vivo testing of ML-93 toxicity, female *C57Bl6/J* mice were treated with 50 mg/kg ML-93 or vehicle control on day 1 and 2. On day 8 blood samples were analyzed on a blood counter (scil Animal Blood Counter, USA) and single cell suspensions from spleens were generated (100µM cell strainer). Following red blood cell lysis (ACK Lysing Buffer, GIBCO, ThermoFisher Scientific), splenocytes were snap frozen for consecutive western blot analysis and processed following the described protein lysis protocol.

6.16 Tissue microarray analysis of human DLBCL samples

For tissue microarrays (TMA) formalin fixed and paraffin embedded tissue from 58 patients suffering from DLBCL treated during a time period from 1991 to 2014 in the University Clinic

of the Technical University Munich, Division of Internal Medicine III, Haematology and Medical Oncology, were used. Corresponding to the remission status obtained by CT scan, patients were divided into two biological groups, either showing long term remission (duration of remission >2 years; 16 patients) or early relapse (<1 year)/refractory disease (42 patients). The responsible ethics committees of the Technische Universität München approved data analysis (ethics approval 498/17s). TMA analysis was performed in a collaboration by Julia Slotta-Huspenina, Pathology Technical University of Munich.

6.17 Statistical analysis

Statistical analyzes were performed using GraphPad Prism (GraphPad Software, La Jolla, CA). The error bars shown in the figures represent the standard deviation (SD), unless specified otherwise. In each experiment, the statistical tests used are indicated in the figure legends.

6.18 Bioinformatics analysis

6.18.1 Gene expression analysis

Gene expression data were retrieved from the Gene Expression Omnibus (GEO) using the accession numbers GSE44672 (Walz et al., 2014) and GSE12195 (Compagno et al., 2009), respectively. For the former, normalized counts supplied by the authors were log2 transformed before downstream analysis. For the latter, all CEL files were retrieved and normalized using the GCRMA R package. Differential gene expression (DEG) analysis between conditions was carried out using the limma framework (Ritchie et al., 2015) and a FDR < 0.1 was considered significant. Select DEG results were illustrated in a heatmap using the pheatmap R package after scaling all genes to have mean of 0 and a standard deviation of 1. Analysis of gene expression data sets was performed in a collaboration by Carlo Maurer, Technical University of Munich.

6.18.2 Pathway enrichment analysis and gene set enrichment analysis

Pathway enrichment analysis was performed by GeneTrail2 (Stockel et al., 2016) (using Reactome database) and was assessed using an over-representation analysis. Corresponding *P-values* are FDR-adjusted per database using the method of Benjamini and Yekutieli with a significance level of 0.05. Results obtained with Reactome have been visualized with Adobe Illustrator. Gene set enrichment analysis (GSEA) was performed with the H gene sets from MSigDB (http://www.broadinstitute.org/gsea/msigdb) by GeneTrail2. Gene sets related to

MYC signatures were selected. Gene set enrichment was assessed using the Kolmogorov-Smirnov test. Corresponding *P-values* were FDR-adjusted per database using the method by Benjamini and Yekutieli with a significance level of 0.05.

6.18.3 STRING network analysis

The freely available STRING database https://string-db.org (version 10.5) was used for the generation of string networks. The following criteria were used for network analysis: Recently described SENP6 target protein datasets were used as input (Liebelt et al., 2019; Wagner et al., 2019). The parameters were set to highest confidence and we used a MCL clustering with inflation of 3. All active interaction sources were enabled and non-connected proteins were excluded from the visible interaction network.

6.18.4 Analysis of copy number alterations in human BCLs

To assess the *SENP6* copy number in a recently published human dataset, we first queried if *SENP6* is targeted by a GISTIC2-identified recurrent SCNA using the provided GISTIC2 focal peak boundaries. This analysis revealed that *SENP6* resides in the focal peak at 6q14.1 that is perturbed in 38/304 tumors. Next, we dichotomized the patients in those with SENP6 haploinsuffiency and wildtype *SENP6* copy number and compared their *SENP6* transcript abundance and total SCNAs leveraging the respective data within this study. Differences between transcripts and total number of SCNAs were tested with a Mann-Whitney U test. The analysis was performed in a collaboration by Björn Chapuy, University of Göttingen.

7 SUPPLEMENTAL INFORMATION

7.1 *Eμ-myc* CIS genes

Rank	Gene Name	Rank	Gene Name	Rank	Gene Name
1	Bmi1	47	2310043O21Rik	93	Tbxas1
2	Myb	48	Ajuba	94	Arid1b
3	Sp3	49	Slc7a7	95	Dyrk1a
4	Setd2	50	A930006K02Rik	96	Gm13561
5	Ets1	51	Cnot1	97	Gsk3b
6	Fli1	52	Gm7860	98	Evi2
7	Gm47680	53	Trio	99	Platr6
8	Foxp1	54	Cux1	100	Sgk1
9	Bach2	55	Eml4	101	Add3
10	Zcchc7	56	Lrrc4c	102	Ccr7
11	Fgd2	57	Mcl1	103	Cd80
12	Gm26885	58	Rnls	104	Cdc42se2
13	Rasgrp1	59	Rprd2	105	Gm23649
14	9230111E07Rik	60	Plekha2	106	Krt222
15	A530013C23Rik	61	Csde1	107	Lbh
16	Gm14319	62	Sgms1	108	Sp140
17	Ptpn1	63	Stag1	109	A930007I19Rik
18	1810026B05Rik	64	Suz12	110	Aff1
19	Gm44124	65	5830428M24Rik	111	Baz2b
20	Il17ra	66	Gm23018	112	Celf2
21	Ptbp3	67	Gm42645	113	Cnot6l
22	Susd1	68	Gm43838	114	Mtss1
23	Api5	69	Pip4k2a	115	Phf21a
24	Snrnp70	70	Tbc1d1	116	Pkig
25	Ikzf1	71	A430072P03Rik	117	Tbcc
26	Srgap2	72	Galnt7	118	AC136376.1
27	4930519D14Rik	73	Gm6012	119	Ccnd3
28	Akap13	74	Raf1	120	Cd47
29	Elf1	75	2010300C02Rik	121	Gpatch8
30	Exoc2	76	Mef2c	122	Olfr750
31	Irf4	77	Mgat4a	123	Pten
32	Naa16	78	Pced1b	124	Dhx40
33	Nipbl	79	Wasf2	125	Fam69a
34	Gm3716	80	Wdtc1	126	Gm10800
35	Klf3	81	Gnb1	127	Lnpep
36	Gmds	82	3300005D01Rik	128	Mbnl1
37	Ptp4a2	83	Ankrd28	129	Pou2af1
38	Gm16225	84	Atp1b3	130	Rassf3
39	Phip	85	Btd	131	Swap70
40	Runx3	86	Kansl1	132	Zfp217
41	Syf2	87	Mnd1	133	A430110L20Rik
42	Gm32401	88	Rbpms	134	Bcl2l1
43	Nedd9	89	Rfx7	135	Cop1
44	Rbms1	90	Snx9	136	Cxxc5
45	Sos1	91	Hipk2	137	Gm15411
46	Vis1	92	Rabgap1l	138	Il12a

Rank	Gene Name	Rank	Gene Name	Rank	Gene Name
139	Irf2	192	Arih1	245	Srgn
140	Phf6	193	Atp10d	246	4933406I18Rik
141	Pou2f1	194	Coq2	247	Ankrd17
142	Ptprc	195	Cyth1	248	Ankrd44
143	Smim14	196	E130308A19Rik	249	Camk2g
144	Stk24	197	Ebf1	250	Dhx15
145	Aff3	198	Ezh2	251	Entpd7
146	Elmo1	199	Fam49b	252	Foxc1
147	Gm28643	200	Gm10138	253	Gm10095
148	Hnrnpc	201	Gm24402	254	Gm11464
149	Naa15	202	Gm43510	255	Gm23667
150	Nfatc1	203	Hnrnpu	256	Gm5373
151	Plek2	204	Med13l	257	H2-Eb2
152	Rpl30-ps6	205	Primpol	258	Map3k14
153	Smarcc1	206	Rapgef5	259	Map4k4
154	Ssh2	207	Rock2	260	Mtdh
155	Supt16	208	Snx30	261	Nsmce2
156	Tgfbr2	209	Tnfrsf13b	262	Plau
157	1700027J07Rik	210	1110059E24Rik	263	Rap1a
158	Atf7ip	211	Bhlhe41	264	Slf2
159	Cdk19	212	Cdk17	265	Sp1
160	Gm26616	213	Foxo1	266	Specc1l
161	Gm47734	214	Gfod1	267	Zfp207
162	Gm8013	215	Lrch1	268	Znrf1
163	Gm9034	216	Nr3c1	269	5330439M10Rik
164	Ikzf3	217	Pspc1	270	Arhgef3
165	Mctp2	218	Rpf1	271	Asap1
166	Milr1	219	Serp1	272	Cblb
167	Pecam1	220	Sh3kbp1	273	E2f2
168	Pik3c2b	221	Usp3	274	Epb41l4b
169	Ppp3ca	222	Vps37b	275	Fgfr2
170	Runx1	223	4632428C04Rik	276	Glo1
171	Smc4	224	Ccdc146	277	Gm13009
172	Arid1a	225	Cdk13	278	Gm18748
173	Fbxl17	226	Cytip	279	Gm44210
174	Nt5c2	227	Gata3	280	Jazf1
175	Sema4b	228	Gm28694	281	Map3k5
176	Slc35e3	229	Ivd	282	Med12l
177	Zfp710	230	Ptk2b	283	Stag2
178	Cmss1	231	Ralgps2	284	Stx8
179	Dym	232	Rhoa	285	Tec
180	Eif2d	233	Rps18-ps2	286	Tnrc6b
181	Cdkl3	234	Traf3	287	Ubac2
182	Matr3	235	Fam35a	288	Umad1
183	Gm32540	236	Fam43a	289	Cdk12
184	Gm44778	237	Gpbp1	290	Crebbp
185	Gm44956	238	Hjurp	291	Crtc3
186	Ptprj	239	Immt	292	Cxcr4
187	Sfi1	240	Jarid2	293	Dapp1
188	Smad7	241	Plekhf2	294	Dars
189	St8sia4	242	Ppp1r12a	295	Eps15l1
190	Tcf4	243	Rbm27	296	Frat1
191	Ipo7	244	Slc38a1	297	Gm12159

Rank	Gene Name	Rank	Gene Name	Rank	Gene Name
298	Gm15747	351	Rasa3	404	Hivep2
299	Gm22482	352	Serinc5	405	Hnrnpf
300	Gm47639	353	Snd1|Lrrc4	406	Hvcn1
301	Igkv4-51	354	Tmpo	407	Irf2bp2
302	Maml2	355	Tpr	408	Leprotl1
303	Man1a	356	Ylpm1	409	Ndst1
304	Msl1	357	2610307P16Rik	410	Nfkb1
305	Poli	358	AC117232.1	411	Picalm
306	Rcsd1	359	Arhgap11a	412	Qprt
307	Rreb1	360	B4galt5	413	Rhoq
308	Sema4d	361	Blnk	414	Rnf157
309	Slc20a2	362	Cdkal1	415	Sec24a
310	Smchd1	363	Cyfip2	416	She
311	Wdr66	364	Dgka	417	Slc39a13
312	Xpo4	365	Fam49a	418	Synpo
313	2310001H17Rik	366	Gm10088	419	Ube2d3
314	Atf7	367	Hist2h3c1	420	Vgll4
315	Bcor	368	Gm24913	421	Zfand3
316	Commd6	369	Gm37312	422	Sept9
317	Dennd4a	370	Ifng	423	AC093043.2
318	G3bp1	371	Inpp5d	424	Cabcoco1
319	Gm12503	372	Nfyc	425	Camk2d
320	Gm32633	373	Otud5	426	Ccdc125
321	Gm43674	374	Pcmtd1	427	Ccnd1
322	Gm5432	375	Pde3b	428	Cplx2
323	H2afy	376	Pik3r1	429	Ctnnb1
324	March1	377	Prag1	430	Etfbkmt
325	Mirt1	378	Prdm10	431	Fyttd1
326	Pan3	379	Prkce	432	Gata2
327	Prim2	380	Runx2	433	Gfi1b
328	Reln	381	Sell	434	Gga1
329	Ahnak	382	Tbca	435	Gm11292
330	Arid5b	383	Tbl1xr1	436	Gm15322
331	Cd38	384	Tfe3	437	Gm48652
332	Cnot2	385	Tspan14	438	Gm7804
333	Dirc2	386	Uhrf2	439	Gna13
334	Enthd1	387	Xylt1	440	Hikeshi
335	B3gnt2	388	Mllt10	441	Itpk1
336	Gm15228	389	Anp32b	442	None
337	Gm15232	390	Braf	443	Notch2
338	Sorl1	391	Cbl	444	Pabpc1
339	Irf8	392	Chd1	445	Pik3cd
340	Gm48876	393	Clec2g	446	Rgl1
341	Hist1h3d	394	Cul3	447	Scmh1
342	Jak1	395	Dtx2	448	Serbp1
343	Kpna3	396	Fam117a	449	Sf3b1
344	Mta3	397	Gm25866	450	Tpm3
345	Myo1e	398	Gm3096	451	Ube2e1
346	Oxr1	399	Gm33489	452	Zfp85os
347	Pkd2l2	400	Gm45080	453	4930597A21Rik
348	Pnisr	401	Gm5533	454	Arntl
349	Prkcb	402	Gnas	455	Bcl2l11
350	Rad21	403	Heg1	456	Cdc6

Rank	Gene Name	Rank	Gene Name	Rank	Gene Name
457	Celsr1	510	Gm31562	563	Ncoa2
458	Cmtm6	511	Gm34073	564	Otub2
459	Cpn1	512	Gm35154	565	Pdlim5
460	Dcps	513	Gm47918	566	Psma3
461	Dgkd	514	Gng12	567	Rad51b
462	Dock10	515	H6pd	568	Rbm47
463	Fnbp1	516	Hpf1	569	Rest
464	Frs2	517	Ice2	570	Rfc4
465	Gm30211	518	Klhdc1	571	Simc1
466	Gm34276	519	Masp2	572	Srsf3
467	Fbxw7	520	MYC	573	Tnfaip8
468	Gm8873	521	Nap1l1	574	Tnip1
469	Gm8973	522	Nedd4l	575	Ywhae
470	Gng7	523	Ppp2r5c	576	Ywhaz
471	Hdac7	524	Pum1	577	Zfp704
472	Itsn2	525	Reep3	578	A630001O12Rik
473	Kansl2	526	Sesn3	579	Akap12
474	Kmo	527	Setd3	580	Antxr1
475	Lsm12	528	Slc16a4	581	Chst3
476	Lsm14a	529	Syk	582	Ctnna1
477	Map3k1	530	Tmem243	583	Dcun1d1
478	Mecom	531	Tnrc6c	584	Dnm3
479	Metap2	532	Trim8	585	Eml1
480	Mllt3	533	Ttc7b	586	Fam149b
481	Parp8	534	Xpnpep2	587	Fcrl1
482	Prdm2	535	Zfp608	588	Gm28441
483	Rasgrf1	536	Znrf2	589	Gm38098
484	Rbbp6	537	9530018F02Rik	590	Tcf12
485	Scaf4	538	Akr1a1	591	Dpp8
486	Senp1	539	Apc	592	Gm47769
487	Slc25a51	540	Arhgap17	593	Gse1
488	Snx5	541	Atp11b	594	Kctd5
489	Spata13	542	BC035044	595	Leo1
490	Tbc1d14	543	Bcl11a	596	Lims1
491	Tnpo3	544	Ccnt2	597	Nav2
492	Traf3ip3	545	Dennd4b	598	Nr1h2
493	Trak1	546	Dgkg	599	Osbpl9
494	Vwa8	547	Dido1	600	Prdm1
495	Wdr82	548	Dnajc15	601	Prrc2c
496	Wwox	549	Gcnt1	602	Sec63
497	Zfp516	550	Gm20940	603	Slc44a4
498	1700092K14Rik	551	Gm24484	604	Snx2
499	2310047D07Rik	552	Smpd3	605	Sp2
500	A930005H10Rik	553	Gm2a	606	Spred2
501	AC139671.1	554	Gm40915	607	Stk10
502	Cacnb1	555	Gm45155	608	Stoml1
503	Capza1	556	Gm5436	609	Stx17
504	Ccm2	557	Gtf2a1	610	Tpm4
505	Eif4g2	558	Gtf3c6	611	Xpot
506	Fam134b	559	Hipk1	612	Zfp131
507	Foxm1	560	Hlcs	613	Adrb2
508	Fubp1	561	Maml3	614	Akt2
509	Gm28502	562	Myo1d	615	Arhgdib

Rank	Gene Name	Rank	Gene Name	Rank	Gene Name
616	Atp13a3	669	Erg	722	Gprc5c
617	Ctsk	670	Mcph1	723	Hmbs
618	Cuedc1	671	Gm24690	724	Jak3
619	Dopey2	672	Cmtr1	725	Jakmip1
620	Eif4b	673	Gm36211	726	Lmtk2
621	Etv6	674	Gm44064	727	Lncpint
622	Fgfr1op2	675	Gm47766	728	Mir7688
623	Fryl	676	Ier5	729	Ncbp1
624	Gm26834	677	Ighd4-1	730	Nup210
625	Gm31108	678	Jade1	731	P2ry10b
626	Gm32051	679	Map3k8	732	Pag1
627	Gm47241	680	Mtpn	733	Prkcd
628	Gm7160	681	Nfia	734	Ptbp2
629	Gnaq	682	Nod2	735	Ptpn12
630	Hfm1	683	Plpp3	736	Ptprv
631	Ildr1	684	Prdm16	737	Reck
632	Kcnmb3	685	Rab10	738	Ripor2
633	Kdm6a	686	Rhobtb2	739	Selenon
634	Kmt2c	687	Sdccag8	740	Srebf2
635	Lrmp	688	Sh3bp5	741	Tbc1d15
636	Mapre2	689	Socs2	742	Tqif1
637	Mast4	690	Sox5	743	Tnks
638	Mcoln3	691	Srrm2	744	Ubash3a
639	Mybl1	692	Ssbp3	745	Ube2n
640	Mylip	693	Tfap4	746	Uvrag
641	Nr2c2	694	Tg	747	Zeb1
642	Nudt3	695	Thrap3	748	Zfhx3
643	P2rx7	696	Tle3	749	2310008N11Rik
644	Pgap2	697	Tmcc3	750	Bfsp2
645	Pik3ap1	698	Ttc28	751	9330179D12Rik
646	Rpn1	699	Ube4b	752	9430041J12Rik
647	Rps6ka5	700	Wdr81	753	Bicra
648	Senp6	701	Zfp664	754	Brwd3
649	Sf1	702	Abcb1a	755	Crebrf
650	St3gal6	703	AC114585.2	756	Gimap4
651	St6gal1	704	Acvrl1	757	Gm10640
652	Tcte2	705	AL611986.1	758	Gm10709
653	Tmem131	706	Atrnl1	759	Gm12066
654	Zbtb1	707	Btk	760	Bcl2l12
655	Zdhhc19	708	Cdc37l1	761	Gm26887
656	Zfp407	709	Cdc42	762	Gm34424
657	Sept11	710	Cenpv	763	Gm37294
658	1600020E01Rik	711	Cfap43	764	Gm47697
659	1700013A02Rik	712	Dstyk	765	Gm47953
660	2900092O11Rik	713	E230029C05Rik	766	Gm48606
661	Aicda	714	Efna1	767	Ctcf
662	Atxn7l1	715	F12	768	Igf2bp3
663	Cacna1e	716	Fbxo11	769	Iqgap1
664	Capza2	717	Fgfr1	770	Kdm4a
665	Cdca2	718	Fkbp8	771	Lcp1
666	Cep164	719	Gm12156	772	Lta
667	Ctse	720	Gm14542	773	Map4k5
668	Dlk1	721	Gm37306	774	Mrvi1

Rank	Gene Name	Rank	Gene Name	Rank	Gene Name
775	Msra	828	Coro1c	881	Slc16a1
776	Nsmce1	829	Dock9	882	Sms
777	Nucks1	830	Edem1	883	Stk26
778	Osbpl3	831	Eif3d	884	Syne3
779	Parvb	832	Eno1	885	Tifa
780	Pdlim3	833	Foxn3	886	Tnni2
781	Plaur	834	Fyn	887	Zbtb7a
782	Rnf115	835	Gm15465	888	Aanat
783	Sec11c	836	Gm23905	889	Col4a2
784	Sgk3	837	Gm24922	890	E330011O21Rik
785	Slc25a19	838	Gm32235	891	Fem1c
786	Slc9a7	839	Gm4714	892	Zfpm1
787	Spin1	840	Gm595	893	Gm20465
788	Susd3	841	Lmo4	894	Myom1
789	Tnpo2	842	Lsm6	895	Cox5a
790	Tor1aip1	843	Mkl1	896	Gm37267
791	Ubxn11	844	Mppe1	897	Gm48199
792	Xxylt1	845	Nuak2	898	Gpm6b
793	Zfp36l2	846	Pdzd2	899	Hsdl1
794	Zfx	847	Ppp1ca	900	Il10ra
795	Znrf3	848	Ptpn2	901	Inq1
796	1700029J03Rik	849	Pwp2	902	Msn
797	Acap2	850	Rere	903	Mul1
798	Adgre5	851	Sesn1	904	Oard1
799	Ago2	852	Sox4	905	Ppp3cc
800	Akna	853	Tfrc	906	Renbp
801	AL590144.2	854	Xrcc6	907	Rin3
802	Cd180	855	Zfp984	908	Sf3a2
803	Ddx6	856	4930573C15Rik	909	Sipa1l2
804	Ftx	857	AC108416.3	910	Tmem163
805	Fxr1	858	Alg14	911	Wdfy4
806	Ankrd11	859	Baiap2	912	Arid3a
807	Gm25486	860	Ccdc6	913	Ccng2
808	Gm27008	861	Celf4	914	D230017M19Rik
809	Hnrnpr	862	Chd9	915	Flad1
810	Ksr1	863	Fam178b	916	Gm10293
811	Lrrc8c	864	Fam20b	917	Suv39h1
812	Nupl1	865	Fbxo42	918	Gm20337
813	Olfr372	866	Gja3	919	Itpr2
814	Plxnc1	867	Gm10556	920	Jpx
815	Rb1	868	Gm15889	921	Kctd2
816	Rmnd5b	869	Arid3b	922	Morn3
817	Rnaseh2b	870	Gm26561	923	Polr1c
818	Scn8a	871	Gm47283	924	Ptp4a3
819	Slc44a3	872	Hes6	925	Rasgrp3
820	Tnrc18	873	Itpkb	926	Sost
821	Zfp619	874	Ktn1	927	Srp68
822	AC142114.1	875	Msi2	928	Ssmem1
823	AI506816	876	Ramp1	929	Tmsb10
824	Armc9	877	Rcbtb2	930	Ubl7
825	Bod1l	878	Relt	931	Uck2
826	Calr	879	Rnf144a	932	Zmiz1
827	Cep97	880	Rrp1	933	AL611987.1

Rank	Gene Name	Rank	Gene Name	Rank	Gene Name
934	Erf				
935	Galnt14				
936	Gm15754				
937	Gm2788				
938	Mbp				
939	Mettl3				
940	Rcc2				
941	Rlim				
942	Rubcnl				
943	Scml4				
944	Tcf20				
945	Tulp2				
946	Agpat3				
947	Anks1				
948	Gm13648				
949	Gm20388				
950	Mid1				
951	Rab9				
952	Rps20				
953	Tmem255a				
954	Vmn1r-ps151				
955	2900026A02Rik				
956	Acacb				
957	Slc25a45				
958	Exoc3l				

7.2 Reactome pathway enrichment analysis

Rank	Name	*FDR P-value*
1	Antigen activates B-cell Receptor (BCR) leading to generation of second messengers	1.94e-10
2	Factors involved in megakaryocyte development and platelet production	1.13e-5
3	G alpha (12/13) signalling events	2.77e-5
4	VEGFA-VEGFR2 Pathway	2.81e-5
5	SUMOylation of DNA damage response and repair proteins	7.81e-5
6	Rho GTPase cycle	1.20e-4
7	PKMTs methylate histone lysines	2.18e-4
8	Effects of PIP2 hydrolysis	4.66e-4
9	Deadenylation of mRNA	5.39e-4
10	RAF/MAP kinase cascade	0.0010
11	FCERI mediated Ca+2 mobilization	0.0021
12	Translocation of GLUT4 to the plasma membrane	0.0029
13	CD28 dependent PI3K/Akt signaling	0.0055
13	Synthesis of PIPs at the plasma membrane	0.0055
15	CD209 (DC-SIGN) signaling	0.0061
16	Glucagon-like Peptide-1 (GLP1) regulates insulin secretion	0.0086
17	Deactivation of the beta-catenin transactivating complex	0.0092

18	Cohesin Loading onto Chromatin	0.0102
18	Interleukin receptor SHC signaling	0.0102
18	NRAGE signals death through JNK	0.0102
21	Notch-HLH transcription pathway	0.0121
22	PIP3 activates AKT signaling	0.0127
23	G beta:gamma signalling through PI3Kgamma	0.0166
23	GPVI-mediated activation cascade	0.0166
23	Interferon gamma signaling	0.0166
23	RHO GTPases activate IQGAPs	0.0166
23	Regulation of actin dynamics for phagocytic cup formation	0.0166
23	mRNA Splicing - Major Pathway	0.0166
29	DAP12 signaling	0.0187
30	Rap1 signalling	0.0223
30	Regulation of signaling by CBL	0.0223
32	O-linked glycosylation of mucins	0.0225
33	NOTCH2 intracellular domain regulates transcription	0.0256
33	Role of phospholipids in phagocytosis	0.0256
35	Beta-catenin phosphorylation cascade	0.0287
35	Processing of Capped Intron-Containing Pre-mRNA	0.0287
35	Regulation of lipid metabolism by Peroxisome proliferator-activated receptor alpha (PPARalpha)	0.0287
38	RHO GTPases activate PKNs	0.0333
39	Interleukin-3, 5 and GM-CSF signaling	0.0389
40	CDO in myogenesis	0.0446
40	Post-transcriptional silencing by small RNAs	0.0446

8 LITERATURE

Abbas, M., Shanmugam, I., Bsaili, M., Hromas, R., and Shaheen, M. (2014). The role of the human psoralen 4 (hPso4) protein complex in replication stress and homologous recombination. J Biol Chem *289*, 14009-14019.

Alegre, K. O., and Reverter, D. (2011). Swapping small ubiquitin-like modifier (SUMO) isoform specificity of SUMO proteases SENP6 and SENP7. J Biol Chem *286*, 36142-36151.

Alizadeh, A. A., Eisen, M. B., Davis, R. E., Ma, C., Lossos, I. S., Rosenwald, A., Boldrick, J. C., Sabet, H., Tran, T., Yu, X., Powell, J. I., Yang, L., Marti, G. E., Moore, T., Hudson, J., Jr., Lu, L., Lewis, D. B., Tibshirani, R., Sherlock, G., Chan, W. C., Greiner, T. C., Weisenburger, D. D., Armitage, J. O., Warnke, R., Levy, R., Wilson, W., Grever, M. R., Byrd, J. C., Botstein, D., Brown, P. O., and Staudt, L. M. (2000). Distinct types of diffuse large B-cell lymphoma identified by gene expression profiling. Nature *403*, 503-511.

Au, W. Y., Horsman, D. E., Viswanatha, D. S., Connors, J. M., Klasa, R. J., and Gascoyne, R. D. (2000). 8q24 translocations in blastic transformation of mantle cell lymphoma. Haematologica *85*, 1225-1227.

Bailey, M. L., O'Neil, N. J., van Pel, D. M., Solomon, D. A., Waldman, T., and Hieter, P. (2014). Glioblastoma cells containing mutations in the cohesin component STAG2 are sensitive to PARP inhibition. Mol Cancer Ther *13*, 724-732.

Baluapuri, A., Hofstetter, J., Dudvarski Stankovic, N., Endres, T., Bhandare, P., Vos, S. M., Adhikari, B., Schwarz, J. D., Narain, A., Vogt, M., Wang, S. Y., Duster, R., Jung, L. A., Vanselow, J. T., Wiegering, A., Geyer, M., Maric, H. M., Gallant, P., Walz, S., Schlosser, A., Cramer, P., Eilers, M., and Wolf, E. (2019). MYC Recruits SPT5 to RNA Polymerase II to Promote Processive Transcription Elongation. Mol Cell *74*, 674-687 e611.

Barber, T. D., McManus, K., Yuen, K. W., Reis, M., Parmigiani, G., Shen, D., Barrett, I., Nouhi, Y., Spencer, F., Markowitz, S., Velculescu, V. E., Kinzler, K. W., Vogelstein, B., Lengauer, C., and Hieter, P. (2008). Chromatid cohesion defects may underlie chromosome instability in human colorectal cancers. Proc Natl Acad Sci U S A *105*, 3443-3448.

Bergink, S., and Jentsch, S. (2009). Principles of ubiquitin and SUMO modifications in DNA repair. Nature *458*, 461-467.

Biederstadt, A., Hassan, Z., Schneeweis, C., Schick, M., Schneider, L., Muckenhuber, A., Hong, Y., Siegers, G., Nilsson, L., Wirth, M., Dantes, Z., Steiger, K., Schunck, K., Langston, S., Lenhof, H. P., Coluccio, A., Orben, F., Slawska, J., Scherger, A., Saur, D., Muller, S., Rad, R., Weichert, W., Nilsson, J., Reichert, M., Schneider, G., and Keller, U. (2020). SUMO pathway inhibition targets an aggressive pancreatic cancer subtype. Gut.

Bisso, A., Sabo, A., and Amati, B. (2019). MYC in Germinal Center-derived lymphomas: Mechanisms and therapeutic opportunities. Immunol Rev *288*, 178-197.

Bodrug, S. E., Warner, B. J., Bath, M. L., Lindeman, G. J., Harris, A. W., and Adams, J. M. (1994). Cyclin D1 transgene impedes lymphocyte maturation and collaborates in lymphomagenesis with the myc gene. EMBO J *13*, 2124-2130.

Boxer, L. M., and Dang, C. V. (2001). Translocations involving c-myc and c-myc function. Oncogene *20*, 5595-5610.

Bric, A., Miething, C., Bialucha, C. U., Scuoppo, C., Zender, L., Krasnitz, A., Xuan, Z., Zuber, J., Wigler, M., Hicks, J., McCombie, R. W., Hemann, M. T., Hannon, G. J., Powers, S., and Lowe, S. W. (2009). Functional identification of tumor-suppressor genes through an in vivo RNA interference screen in a mouse lymphoma model. Cancer Cell *16*, 324-335.

Campbell, K. J., Bath, M. L., Turner, M. L., Vandenberg, C. J., Bouillet, P., Metcalf, D., Scott, C. L., and Cory, S. (2010). Elevated Mcl-1 perturbs lymphopoiesis, promotes transformation of hematopoietic stem/progenitor cells, and enhances drug resistance. Blood *116*, 3197-3207.

Chapuy, B., Stewart, C., Dunford, A. J., Kim, J., Kamburov, A., Redd, R. A., Lawrence, M. S., Roemer, M. G. M., Li, A. J., Ziepert, M., Staiger, A. M., Wala, J. A., Ducar, M. D., Leshchiner, I., Rheinbay, E., Taylor-Weiner, A., Coughlin, C. A., Hess, J. M., Pedamallu, C. S., Livitz, D., Rosebrock, D., Rosenberg, M., Tracy, A. A., Horn, H., van Hummelen, P., Feldman, A. L., Link, B. K., Novak, A. J., Cerhan, J. R., Habermann, T. M., Siebert, R., Rosenwald, A., Thorner, A. R., Meyerson, M. L., Golub, T. R., Beroukhim, R., Wulf, G. G., Ott, G., Rodig, S. J., Monti, S., Neuberg, D. S., Loeffler, M., Pfreundschuh, M., Trumper, L., Getz, G., and Shipp, M. A. (2018). Molecular subtypes of diffuse large B cell lymphoma are associated with distinct pathogenic mechanisms and outcomes. Nat Med *24*, 679-690.

Compagno, M., Lim, W. K., Grunn, A., Nandula, S. V., Brahmachary, M., Shen, Q., Bertoni, F., Ponzoni, M., Scandurra, M., Califano, A., Bhagat, G., Chadburn, A., Dalla-Favera, R., and Pasqualucci, L. (2009). Mutations of multiple genes cause deregulation of NF-kappaB in diffuse large B-cell lymphoma. Nature *459*, 717-721.

Dalla-Favera, R., Bregni, M., Erikson, J., Patterson, D., Gallo, R. C., and Croce, C. M. (1982). Human c-myc onc gene is located on the region of chromosome 8 that is translocated in Burkitt lymphoma cells. Proc Natl Acad Sci U S A *79*, 7824-7827.

Dang, C. V. (2012). MYC on the path to cancer. Cell *149*, 22-35.

Davis, A. C., Wims, M., Spotts, G. D., Hann, S. R., and Bradley, A. (1993). A null c-myc mutation causes lethality before 10.5 days of gestation in homozygotes and reduced fertility in heterozygous female mice. Genes Dev *7*, 671-682.

de la Rosa, J., Weber, J., Friedrich, M. J., Li, Y., Rad, L., Ponstingl, H., Liang, Q., de Quiros, S. B., Noorani, I., Metzakopian, E., Strong, A., Li, M. A., Astudillo, A., Fernandez-Garcia, M. T., Fernandez-Garcia, M. S., Hoffman, G. J., Fuente, R., Vassiliou, G. S., Rad, R., Lopez-Otin, C., Bradley, A., and Cadinanos, J. (2017). A single-copy Sleeping Beauty transposon mutagenesis screen identifies new PTEN-cooperating tumor suppressor genes. Nat Genet *49*, 730-741.

De Silva, N. S., and Klein, U. (2015). Dynamics of B cells in germinal centres. Nat Rev Immunol *15*, 137-148.

Dominguez-Sola, D., and Gautier, J. (2014). MYC and the control of DNA replication. Cold Spring Harb Perspect Med *4*.

Dou, H., Huang, C., Singh, M., Carpenter, P. B., and Yeh, E. T. (2010). Regulation of DNA repair through deSUMOylation and SUMOylation of replication protein A complex. Mol Cell *39*, 333-345.

Durand-Panteix, S., Farhat, M., Youlyouz-Marfak, I., Rouaud, P., Ouk-Martin, C., David, A., Faumont, N., Feuillard, J., and Jayat-Vignoles, C. (2012). B7-H1, which represses EBV-immortalized B cell killing by autologous T and NK cells, is oppositely regulated by c-Myc and EBV latency III program at both mRNA and secretory lysosome levels. J Immunol *189*, 181-190.

Eilers, M., and Eisenman, R. N. (2008). Myc's broad reach. Genes & development *22*, 2755-2766.

Eischen, C. M., Weber, J. D., Roussel, M. F., Sherr, C. J., and Cleveland, J. L. (1999). Disruption of the ARF-Mdm2-p53 tumor suppressor pathway in Myc-induced lymphomagenesis. Genes Dev *13*, 2658-2669.

Flotho, A., and Melchior, F. (2013). Sumoylation: a regulatory protein modification in health and disease. Annu Rev Biochem *82*, 357-385.

Friedrich, M. J., Rad, L., Bronner, I. F., Strong, A., Wang, W., Weber, J., Mayho, M., Ponstingl, H., Engleitner, T., Grove, C., Pfaus, A., Saur, D., Cadinanos, J., Quail, M. A., Vassiliou, G. S., Liu, P., Bradley, A., and Rad, R. (2017). Genome-wide transposon screening and quantitative insertion site sequencing for cancer gene discovery in mice. Nat Protoc *12*, 289-309.

Garvin, A. J., and Morris, J. R. (2017). SUMO, a small, but powerful, regulator of double-strand break repair. Philos Trans R Soc Lond B Biol Sci *372*.

Garvin, A. J., Walker, A. K., Densham, R. M., Chauhan, A. S., Stone, H. R., Mackay, H. L., Jamshad, M., Starowicz, K., Daza-Martin, M., Ronson, G. E., Lanz, A. J., Beesley, J. F., and Morris, J. R. (2019). The deSUMOylase SENP2 coordinates homologous recombination and nonhomologous end joining by independent mechanisms. Genes Dev *33*, 333-347.

Gibbs-Seymour, I., Oka, Y., Rajendra, E., Weinert, B. T., Passmore, L. A., Patel, K. J., Olsen, J. V., Choudhary, C., Bekker-Jensen, S., and Mailand, N. (2015). Ubiquitin-SUMO circuitry controls activated fanconi anemia ID complex dosage in response to DNA damage. Mol Cell *57*, 150-164.

Gonzalez-Prieto, R., Cuijpers, S. A., Kumar, R., Hendriks, I. A., and Vertegaal, A. C. (2015). c-Myc is targeted to the proteasome for degradation in a SUMOylation-dependent manner, regulated by PIAS1, SENP7 and RNF4. Cell Cycle *14*, 1859-1872.

Guarente, L. (1993). Synthetic enhancement in gene interaction: a genetic tool come of age. Trends in genetics : TIG *9*, 362-366.

Halazonetis, T. D., Gorgoulis, V. G., and Bartek, J. (2008). An oncogene-induced DNA damage model for cancer development. Science *319*, 1352-1355.

Hanahan, D., and Weinberg, R. A. (2011). Hallmarks of cancer: the next generation. Cell *144*, 646-674.

Harris, A. W., Pinkert, C. A., Crawford, M., Langdon, W. Y., Brinster, R. L., and Adams, J. M. (1988). The E mu-myc transgenic mouse. A model for high-incidence spontaneous lymphoma and leukemia of early B cells. J Exp Med *167*, 353-371.

Hattersley, N., Shen, L., Jaffray, E. G., and Hay, R. T. (2011). The SUMO protease SENP6 is a direct regulator of PML nuclear bodies. Mol Biol Cell *22*, 78-90.

He, X., Riceberg, J., Soucy, T., Koenig, E., Minissale, J., Gallery, M., Bernard, H., Yang, X., Liao, H., Rabino, C., Shah, P., Xega, K., Yan, Z. H., Sintchak, M., Bradley, J., Xu, H., Duffey, M., England, D., Mizutani, H., Hu, Z., Guo, J., Chau, R., Dick, L. R., Brownell, J. E., Newcomb, J., Langston, S., Lightcap, E. S., Bence, N., and Pulukuri, S. M. (2017). Probing the roles of SUMOylation in cancer cell biology by using a selective SAE inhibitor. Nat Chem Biol *13*, 1164-1171.

Hemann, M. T., Fridman, J. S., Zilfou, J. T., Hernando, E., Paddison, P. J., Cordon-Cardo, C., Hannon, G. J., and Lowe, S. W. (2003). An epi-allelic series of p53 hypomorphs created by stable RNAi produces distinct tumor phenotypes in vivo. Nat Genet *33*, 396-400.

Hoeijmakers, J. H. (2009). DNA damage, aging, and cancer. N Engl J Med *361*, 1475-1485.

Hoellein, A., Fallahi, M., Schoeffmann, S., Steidle, S., Schaub, F. X., Rudelius, M., Laitinen, I., Nilsson, L., Goga, A., Peschel, C., Nilsson, J. A., Cleveland, J. L., and Keller, U. (2014). Myc-induced SUMOylation is a therapeutic vulnerability for B-cell lymphoma. Blood *124*, 2081-2090.

Hoelzer, D., Walewski, J., Dohner, H., Viardot, A., Hiddemann, W., Spiekermann, K., Serve, H., Duhrsen, U., Huttmann, A., Thiel, E., Dengler, J., Kneba, M., Schaich, M., Schmidt-Wolf, I. G., Beck, J., Hertenstein, B., Reichle, A., Domanska-Czyz, K., Fietkau, R., Horst, H. A., Rieder, H., Schwartz, S., Burmeister, T., Gokbuget, N., and German Multicenter Study Group for Adult Acute Lymphoblastic, L. (2014). Improved outcome of adult Burkitt lymphoma/leukemia with rituximab and chemotherapy: report of a large prospective multicenter trial. Blood *124*, 3870-3879.

Horn, H., Schmelter, C., Leich, E., Salaverria, I., Katzenberger, T., Ott, M. M., Kalla, J., Romero, M., Siebert, R., Rosenwald, A., and Ott, G. (2011). Follicular lymphoma grade 3B is a distinct neoplasm according to cytogenetic and immunohistochemical profiles. Haematologica *96*, 1327-1334.

Hu, S., Xu-Monette, Z. Y., Tzankov, A., Green, T., Wu, L., Balasubramanyam, A., Liu, W. M., Visco, C., Li, Y., Miranda, R. N., Montes-Moreno, S., Dybkaer, K., Chiu, A., Orazi, A., Zu, Y., Bhagat, G., Richards, K. L., Hsi, E. D., Choi, W. W., Zhao, X., van Krieken, J. H., Huang, Q., Huh, J., Ai, W., Ponzoni, M., Ferreri, A. J., Zhou, F., Slack, G. W., Gascoyne, R. D., Tu, M., Variakojis, D., Chen, W., Go, R. S., Piris, M. A., Moller, M. B., Medeiros, L. J., and Young, K. H. (2013). MYC/BCL2 protein coexpression contributes to the inferior survival of activated B-cell subtype of diffuse large B-cell lymphoma and demonstrates high-risk gene expression signatures: a report from The International DLBCL Rituximab-CHOP Consortium Program. Blood *121*, 4021-4031; quiz 4250.

Huang, J., Huen, M. S., Kim, H., Leung, C. C., Glover, J. N., Yu, X., and Chen, J. (2009). RAD18 transmits DNA damage signalling to elicit homologous recombination repair. Nat Cell Biol *11*, 592-603.

Huh, Y. O., Lin, K. I., Vega, F., Schlette, E., Yin, C. C., Keating, M. J., Luthra, R., Medeiros, L. J., and Abruzzo, L. V. (2008). MYC translocation in chronic lymphocytic leukaemia is associated with increased prolymphocytes and a poor prognosis. Br J Haematol *142*, 36-44.

Hurlin, P. J., Zhou, Z. Q., Toyo-Oka, K., Ota, S., Walker, W. L., Hirotsune, S., and Wynshaw-Boris, A. (2003). Deletion of Mnt leads to disrupted cell cycle control and tumorigenesis. Embo J *22*, 4584-4596.

Ivics, Z., Hackett, P. B., Plasterk, R. H., and Izsvak, Z. (1997). Molecular reconstruction of Sleeping Beauty, a Tc1-like transposon from fish, and its transposition in human cells. Cell *91*, 501-510.

Jacobs, J. J., Scheijen, B., Voncken, J. W., Kieboom, K., Berns, A., and van Lohuizen, M. (1999). Bmi-1 collaborates with c-Myc in tumorigenesis by inhibiting c-Myc-induced apoptosis via INK4a/ARF. Genes Dev *13*, 2678-2690.

Ji, H., Wu, G., Zhan, X., Nolan, A., Koh, C., De Marzo, A., Doan, H. M., Fan, J., Cheadle, C., Fallahi, M., Cleveland, J. L., Dang, C. V., and Zeller, K. I. (2011). Cell-type independent MYC

target genes reveal a primordial signature involved in biomass accumulation. PLoS One *6*, e26057.

Jitschin, R., Braun, M., Qorraj, M., Saul, D., Le Blanc, K., Zenz, T., and Mougiakakos, D. (2015). Stromal cell-mediated glycolytic switch in CLL cells involves Notch-c-Myc signaling. Blood *125*, 3432-3436.

Johnson, N. A., Slack, G. W., Savage, K. J., Connors, J. M., Ben-Neriah, S., Rogic, S., Scott, D. W., Tan, K. L., Steidl, C., Sehn, L. H., Chan, W. C., Iqbal, J., Meyer, P. N., Lenz, G., Wright, G., Rimsza, L. M., Valentino, C., Brunhoeber, P., Grogan, T. M., Braziel, R. M., Cook, J. R., Tubbs, R. R., Weisenburger, D. D., Campo, E., Rosenwald, A., Ott, G., Delabie, J., Holcroft, C., Jaffe, E. S., Staudt, L. M., and Gascoyne, R. D. (2012). Concurrent expression of MYC and BCL2 in diffuse large B-cell lymphoma treated with rituximab plus cyclophosphamide, doxorubicin, vincristine, and prednisone. J Clin Oncol *30*, 3452-3459.

Kaelin, W. G., Jr. (2005). The concept of synthetic lethality in the context of anticancer therapy. Nature reviews Cancer *5*, 689-698.

Kaiser, C., Laux, G., Eick, D., Jochner, N., Bornkamm, G. W., and Kempkes, B. (1999). The proto-oncogene c-myc is a direct target gene of Epstein-Barr virus nuclear antigen 2. J Virol *73*, 4481-4484.

Keiten-Schmitz, J., Schunck, K., and Muller, S. (2019). SUMO Chains Rule on Chromatin Occupancy. Front Cell Dev Biol *7*, 343.

Kessler, J. D., Kahle, K. T., Sun, T., Meerbrey, K. L., Schlabach, M. R., Schmitt, E. M., Skinner, S. O., Xu, Q., Li, M. Z., Hartman, Z. C., Rao, M., Yu, P., Dominguez-Vidana, R., Liang, A. C., Solimini, N. L., Bernardi, R. J., Yu, B., Hsu, T., Golding, I., Luo, J., Osborne, C. K., Creighton, C. J., Hilsenbeck, S. G., Schiff, R., Shaw, C. A., Elledge, S. J., and Westbrook, T. F. (2012). A SUMOylation-dependent transcriptional subprogram is required for Myc-driven tumorigenesis. Science *335*, 348-353.

Koch, K., Hoster, E., Ziepert, M., Unterhalt, M., Ott, G., Rosenwald, A., Hansmann, M. L., Bernd, W., Stein, H., Poschel, V., Dreyling, M., Trumper, L., Loffler, M., Schmitz, N., Hiddemann, W., Pfreundschuh, M., and Klapper, W. (2016). Clinical, pathological and genetic features of follicular lymphoma grade 3A: a joint analysis of the German low-grade and high-grade lymphoma study groups GLSG and DSHNHL. Ann Oncol *27*, 1323-1329.

Kridel, R., Meissner, B., Rogic, S., Boyle, M., Telenius, A., Woolcock, B., Gunawardana, J., Jenkins, C., Cochrane, C., Ben-Neriah, S., Tan, K., Morin, R. D., Opat, S., Sehn, L. H., Connors, J. M., Marra, M. A., Weng, A. P., Steidl, C., and Gascoyne, R. D. (2012). Whole transcriptome sequencing reveals recurrent NOTCH1 mutations in mantle cell lymphoma. Blood *119*, 1963-1971.

Kunz, K., Piller, T., and Muller, S. (2018). SUMO-specific proteases and isopeptidases of the SENP family at a glance. J Cell Sci *131*.

Kuppers, R. (2005). Mechanisms of B-cell lymphoma pathogenesis. Nat Rev Cancer *5*, 251-262.

Landau, D. A., Tausch, E., Taylor-Weiner, A. N., Stewart, C., Reiter, J. G., Bahlo, J., Kluth, S., Bozic, I., Lawrence, M., Bottcher, S., Carter, S. L., Cibulskis, K., Mertens, D., Sougnez, C. L., Rosenberg, M., Hess, J. M., Edelmann, J., Kless, S., Kneba, M., Ritgen, M., Fink, A., Fischer, K., Gabriel, S., Lander, E. S., Nowak, M. A., Dohner, H., Hallek, M., Neuberg, D., Getz, G., Stilgenbauer, S., and Wu, C. J. (2015). Mutations driving CLL and their evolution in progression and relapse. Nature *526*, 525-530.

Lange, S., Engleitner, T., Mueller, S., Maresch, R., Zwiebel, M., Gonzaléz-Silva, L., Schneider, G., Banerjee, R., Yang, F., Vassiliou, G., Friedrich, M., Saur, D., Varela, I., and Rad, R. (2019). Analysis pipelines for cancer genome sequencing in mice. Nature Protocols.

Lefebure, M., Tothill, R. W., Kruse, E., Hawkins, E. D., Shortt, J., Matthews, G. M., Gregory, G. P., Martin, B. P., Kelly, M. J., Todorovski, I., Doyle, M. A., Lupat, R., Li, J., Schroeder, J., Wall, M., Craig, S., Poortinga, G., Cameron, D., Bywater, M., Kats, L., Gearhart, M. D., Bardwell, V. J., Dickins, R. A., Hannan, R. D., Papenfuss, A. T., and Johnstone, R. W. (2017). Genomic characterisation of Emu-Myc mouse lymphomas identifies Bcor as a Myc co-operative tumour-suppressor gene. Nat Commun *8*, 14581.

Leich, E., Hoster, E., Wartenberg, M., Unterhalt, M., Siebert, R., Koch, K., Klapper, W., Engelhard, M., Puppe, B., Horn, H., Staiger, A. M., Stuhlmann-Laeisz, C., Bernd, H. W., Feller, A. C., Hummel, M., Lenze, D., Stein, H., Hartmann, S., Hansmann, M. L., Moller, P., Hiddemann, W., Dreyling, M., Ott, G., Rosenwald, A., and German Low Grade Lymphoma Study, G. (2016). Similar clinical features in follicular lymphomas with and without breaks in the BCL2 locus. Leukemia *30*, 854-860.

Li, J., Lu, D., Dou, H., Liu, H., Weaver, K., Wang, W., Li, J., Yeh, E. T. H., Williams, B. O., Zheng, L., and Yang, T. (2018). Desumoylase SENP6 maintains osteochondroprogenitor homeostasis by suppressing the p53 pathway. Nat Commun *9*, 143.

Liebelt, F., Jansen, N. S., Kumar, S., Gracheva, E., Claessens, L. A., Verlaan-de Vries, M., Willemstein, E., and Vertegaal, A. C. O. (2019). The poly-SUMO2/3 protease SENP6 enables assembly of the constitutive centromere-associated network by group deSUMOylation. Nat Commun *10*, 3987.

Lin, C. Y., Loven, J., Rahl, P. B., Paranal, R. M., Burge, C. B., Bradner, J. E., Lee, T. I., and Young, R. A. (2012). Transcriptional amplification in tumor cells with elevated c-Myc. Cell *151*, 56-67.

Litwin, I., Pilarczyk, E., and Wysocki, R. (2018). The Emerging Role of Cohesin in the DNA Damage Response. Genes (Basel) *9*.

Lord, C. J., and Ashworth, A. (2012). The DNA damage response and cancer therapy. Nature *481*, 287-294.

Loven, J., Orlando, D. A., Sigova, A. A., Lin, C. Y., Rahl, P. B., Burge, C. B., Levens, D. L., Lee, T. I., and Young, R. A. (2012). Revisiting global gene expression analysis. Cell *151*, 476-482.

Mahajan, K. (2016). hPso4/hPrp19: a critical component of DNA repair and DNA damage checkpoint complexes. Oncogene *35*, 2279-2286.

McKeown, M. R., and Bradner, J. E. (2014). Therapeutic strategies to inhibit MYC. Cold Spring Harb Perspect Med *4*.

Meyer, N., and Penn, L. Z. (2008). Reflecting on 25 years with MYC. Nature reviews Cancer *8*, 976-990.

Mikkers, H., Allen, J., Knipscheer, P., Romeijn, L., Hart, A., Vink, E., and Berns, A. (2002). High-throughput retroviral tagging to identify components of specific signaling pathways in cancer. Nat Genet *32*, 153-159.

Mondal, G., Stevers, M., Goode, B., Ashworth, A., and Solomon, D. A. (2019). A requirement for STAG2 in replication fork progression creates a targetable synthetic lethality in cohesin-mutant cancers. Nat Commun *10*, 1686.

Mori, S., Rempel, R. E., Chang, J. T., Yao, G., Lagoo, A. S., Potti, A., Bild, A., and Nevins, J. R. (2008). Utilization of pathway signatures to reveal distinct types of B lymphoma in the Emicro-myc model and human diffuse large B-cell lymphoma. Cancer Res *68*, 8525-8534.

Moyo, T. K., Wilson, C. S., Moore, D. J., and Eischen, C. M. (2017). Myc enhances B-cell receptor signaling in precancerous B cells and confers resistance to Btk inhibition. Oncogene.

Mukhopadhyay, D., and Dasso, M. (2010). The fate of metaphase kinetochores is weighed in the balance of SUMOylation during S phase. Cell Cycle *9*, 3194-3201.

Nagy, B., Lundan, T., Larramendy, M. L., Aalto, Y., Zhu, Y., Niini, T., Edgren, H., Ferrer, A., Vilpo, J., Elonen, E., Vettenranta, K., Franssila, K., and Knuutila, S. (2003). Abnormal expression of apoptosis-related genes in haematological malignancies: overexpression of MYC is poor prognostic sign in mantle cell lymphoma. Br J Haematol *120*, 434-441.

Nayak, A., and Muller, S. (2014). SUMO-specific proteases/isopeptidases: SENPs and beyond. Genome Biol *15*, 422.

Nie, Z., Hu, G., Wei, G., Cui, K., Yamane, A., Resch, W., Wang, R., Green, D. R., Tessarollo, L., Casellas, R., Zhao, K., and Levens, D. (2012). c-Myc is a universal amplifier of expressed genes in lymphocytes and embryonic stem cells. Cell *151*, 68-79.

Nilsson, J. A., and Cleveland, J. L. (2003). Myc pathways provoking cell suicide and cancer. Oncogene *22*, 9007-9021.

Nilsson, J. A., Maclean, K. H., Keller, U. B., Pendeville, H., Baudino, T. A., and Cleveland, J. L. (2004). Mnt loss triggers Myc transcription targets, proliferation, apoptosis, and transformation. Mol Cell Biol *24*, 1560-1569.

Pasqualucci, L., and Dalla-Favera, R. (2018). Genetics of diffuse large B-cell lymphoma. Blood *131*, 2307-2319.

Pasqualucci, L., Khiabanian, H., Fangazio, M., Vasishtha, M., Messina, M., Holmes, A. B., Ouillette, P., Trifonov, V., Rossi, D., Tabbo, F., Ponzoni, M., Chadburn, A., Murty, V. V., Bhagat, G., Gaidano, G., Inghirami, G., Malek, S. N., Rabadan, R., and Dalla-Favera, R. (2014). Genetics of follicular lymphoma transformation. Cell Rep *6*, 130-140.

Pasqualucci, L., Trifonov, V., Fabbri, G., Ma, J., Rossi, D., Chiarenza, A., Wells, V. A., Grunn, A., Messina, M., Elliot, O., Chan, J., Bhagat, G., Chadburn, A., Gaidano, G., Mullighan, C. G., Rabadan, R., and Dalla-Favera, R. (2011). Analysis of the coding genome of diffuse large B-cell lymphoma. Nat Genet *43*, 830-837.

Peukert, K., Staller, P., Schneider, A., Carmichael, G., Hanel, F., and Eilers, M. (1997). An alternative pathway for gene regulation by Myc. Embo J *16*, 5672-5686.

Pomeranz Krummel, D. A., Oubridge, C., Leung, A. K., Li, J., and Nagai, K. (2009). Crystal structure of human spliceosomal U1 snRNP at 5.5 A resolution. Nature *458*, 475-480.

Pozzo, F., Bittolo, T., Vendramini, E., Bomben, R., Bulian, P., Rossi, F. M., Zucchetto, A., Tissino, E., Degan, M., D'Arena, G., Di Raimondo, F., Zaja, F., Pozzato, G., Rossi, D., Gaidano, G., Del Poeta, G., Gattei, V., and Dal Bo, M. (2017). NOTCH1-mutated chronic

lymphocytic leukemia cells are characterized by a MYC-related overexpression of nucleophosmin 1 and ribosome-associated components. Leukemia.

Psakhye, I., Castellucci, F., and Branzei, D. (2019). SUMO-Chain-Regulated Proteasomal Degradation Timing Exemplified in DNA Replication Initiation. Mol Cell *76*, 632-645 e636.

Rad, R., Rad, L., Wang, W., Cadinanos, J., Vassiliou, G., Rice, S., Campos, L. S., Yusa, K., Banerjee, R., Li, M. A., de la Rosa, J., Strong, A., Lu, D., Ellis, P., Conte, N., Yang, F. T., Liu, P., and Bradley, A. (2010). PiggyBac transposon mutagenesis: a tool for cancer gene discovery in mice. Science *330*, 1104-1107.

Rad, R., Rad, L., Wang, W., Strong, A., Ponstingl, H., Bronner, I. F., Mayho, M., Steiger, K., Weber, J., Hieber, M., Veltkamp, C., Eser, S., Geumann, U., Ollinger, R., Zukowska, M., Barenboim, M., Maresch, R., Cadinanos, J., Friedrich, M., Varela, I., Constantino-Casas, F., Sarver, A., Ten Hoeve, J., Prosser, H., Seidler, B., Bauer, J., Heikenwalder, M., Metzakopian, E., Krug, A., Ehmer, U., Schneider, G., Knosel, T., Rummele, P., Aust, D., Grutzmann, R., Pilarsky, C., Ning, Z., Wessels, L., Schmid, R. M., Quail, M. A., Vassiliou, G., Esposito, I., Liu, P., Saur, D., and Bradley, A. (2015). A conditional piggyBac transposition system for genetic screening in mice identifies oncogenic networks in pancreatic cancer. Nat Genet *47*, 47-56.

Rappsilber, J., Mann, M., and Ishihama, Y. (2007). Protocol for micro-purification, enrichment, pre-fractionation and storage of peptides for proteomics using StageTips. Nat Protoc *2*, 1896-1906.

Raschle, M., Smeenk, G., Hansen, R. K., Temu, T., Oka, Y., Hein, M. Y., Nagaraj, N., Long, D. T., Walter, J. C., Hofmann, K., Storchova, Z., Cox, J., Bekker-Jensen, S., Mailand, N., and Mann, M. (2015). DNA repair. Proteomics reveals dynamic assembly of repair complexes during bypass of DNA cross-links. Science *348*, 1253671.

Reddy, A., Zhang, J., Davis, N. S., Moffitt, A. B., Love, C. L., Waldrop, A., Leppa, S., Pasanen, A., Meriranta, L., Karjalainen-Lindsberg, M. L., Norgaard, P., Pedersen, M., Gang, A. O., Hogdall, E., Heavican, T. B., Lone, W., Iqbal, J., Qin, Q., Li, G., Kim, S. Y., Healy, J., Richards, K. L., Fedoriw, Y., Bernal-Mizrachi, L., Koff, J. L., Staton, A. D., Flowers, C. R., Paltiel, O., Goldschmidt, N., Calaminici, M., Clear, A., Gribben, J., Nguyen, E., Czader, M. B., Ondrejka, S. L., Collie, A., Hsi, E. D., Tse, E., Au-Yeung, R. K. H., Kwong, Y. L., Srivastava, G., Choi, W. W. L., Evens, A. M., Pilichowska, M., Sengar, M., Reddy, N., Li, S., Chadburn, A., Gordon, L. I., Jaffe, E. S., Levy, S., Rempel, R., Tzeng, T., Happ, L. E., Dave, T., Rajagopalan, D., Datta, J., Dunson, D. B., and Dave, S. S. (2017). Genetic and Functional Drivers of Diffuse Large B Cell Lymphoma. Cell *171*, 481-494 e415.

Redecke, V., Wu, R., Zhou, J., Finkelstein, D., Chaturvedi, V., High, A. A., and Hacker, H. (2013). Hematopoietic progenitor cell lines with myeloid and lymphoid potential. Nat Methods *10*, 795-803.

Riley, T., Sontag, E., Chen, P., and Levine, A. (2008). Transcriptional control of human p53-regulated genes. Nat Rev Mol Cell Biol *9*, 402-412.

Ritchie, M. E., Phipson, B., Wu, D., Hu, Y., Law, C. W., Shi, W., and Smyth, G. K. (2015). limma powers differential expression analyses for RNA-sequencing and microarray studies. Nucleic Acids Res *43*, e47.

Rojas-Fernandez, A., Plechanovova, A., Hattersley, N., Jaffray, E., Tatham, M. H., and Hay, R. T. (2014). SUMO chain-induced dimerization activates RNF4. Mol Cell *53*, 880-892.

Rosenwald, A., Wright, G., Chan, W. C., Connors, J. M., Campo, E., Fisher, R. I., Gascoyne, R. D., Muller-Hermelink, H. K., Smeland, E. B., Giltnane, J. M., Hurt, E. M., Zhao, H., Averett,

L., Yang, L., Wilson, W. H., Jaffe, E. S., Simon, R., Klausner, R. D., Powell, J., Duffey, P. L., Longo, D. L., Greiner, T. C., Weisenburger, D. D., Sanger, W. G., Dave, B. J., Lynch, J. C., Vose, J., Armitage, J. O., Montserrat, E., Lopez-Guillermo, A., Grogan, T. M., Miller, T. P., LeBlanc, M., Ott, G., Kvaloy, S., Delabie, J., Holte, H., Krajci, P., Stokke, T., Staudt, L. M., and Lymphoma/Leukemia Molecular Profiling, P. (2002). The use of molecular profiling to predict survival after chemotherapy for diffuse large-B-cell lymphoma. N Engl J Med *346*, 1937-1947.

Ryu, H. Y., Lopez-Giraldez, F., Knight, J., Hwang, S. S., Renner, C., Kreft, S. G., and Hochstrasser, M. (2018). Distinct adaptive mechanisms drive recovery from aneuploidy caused by loss of the Ulp2 SUMO protease. Nat Commun *9*, 5417.

Sabo, A., Kress, T. R., Pelizzola, M., de Pretis, S., Gorski, M. M., Tesi, A., Morelli, M. J., Bora, P., Doni, M., Verrecchia, A., Tonelli, C., Faga, G., Bianchi, V., Ronchi, A., Low, D., Muller, H., Guccione, E., Campaner, S., and Amati, B. (2014). Selective transcriptional regulation by Myc in cellular growth control and lymphomagenesis. Nature *511*, 488-492.

Savage, K. J., Johnson, N. A., Ben-Neriah, S., Connors, J. M., Sehn, L. H., Farinha, P., Horsman, D. E., and Gascoyne, R. D. (2009). MYC gene rearrangements are associated with a poor prognosis in diffuse large B-cell lymphoma patients treated with R-CHOP chemotherapy. Blood *114*, 3533-3537.

Schmitt, C. A., and Lowe, S. W. (2002). Apoptosis and chemoresistance in transgenic cancer models. J Mol Med (Berl) *80*, 137-146.

Seeler, J. S., and Dejean, A. (2017). SUMO and the robustness of cancer. Nat Rev Cancer *17*, 184-197.

Sheiness, D., and Bishop, J. M. (1979). DNA and RNA from uninfected vertebrate cells contain nucleotide sequences related to the putative transforming gene of avian myelocytomatosis virus. J Virol *31*, 514-521.

Solomon, D. A., Kim, T., Diaz-Martinez, L. A., Fair, J., Elkahloun, A. G., Harris, B. T., Toretsky, J. A., Rosenberg, S. A., Shukla, N., Ladanyi, M., Samuels, Y., James, C. D., Yu, H., Kim, J. S., and Waldman, T. (2011). Mutational inactivation of STAG2 causes aneuploidy in human cancer. Science *333*, 1039-1043.

Sondka, Z., Bamford, S., Cole, C. G., Ward, S. A., Dunham, I., and Forbes, S. A. (2018). The COSMIC Cancer Gene Census: describing genetic dysfunction across all human cancers. Nat Rev Cancer *18*, 696-705.

Soucek, L., Whitfield, J., Martins, C. P., Finch, A. J., Murphy, D. J., Sodir, N. M., Karnezis, A. N., Swigart, L. B., Nasi, S., and Evan, G. I. (2008). Modelling Myc inhibition as a cancer therapy. Nature *455*, 679-683.

Soumerai, J. D., Zelenetz, A. D., Moskowitz, C. H., Palomba, M. L., Hamlin, P. A., Jr., Noy, A., Straus, D. J., Moskowitz, A. J., Younes, A., Matasar, M. J., Horwitz, S. M., Portlock, C. S., Konner, J. A., Gounder, M. M., Hyman, D. M., Voss, M. H., Fury, M. G., Gajria, D., Carvajal, R. D., Ho, A. L., Beumer, J. H., Kiesel, B., Zhang, Z., Chen, A., Little, R. F., Jarjies, C., Dang, T. O., France, F., Mishra, N., and Gerecitano, J. F. (2017). The PARP Inhibitor Veliparib Can Be Safely Added to Bendamustine and Rituximab and Has Preliminary Evidence of Activity in B-Cell Lymphoma. Clin Cancer Res *23*, 4119-4126.

Stockel, D., Kehl, T., Trampert, P., Schneider, L., Backes, C., Ludwig, N., Gerasch, A., Kaufmann, M., Gessler, M., Graf, N., Meese, E., Keller, A., and Lenhof, H. P. (2016). Multi-omics enrichment analysis using the GeneTrail2 web service. Bioinformatics *32*, 1502-1508.

Strasser, A., Harris, A. W., Bath, M. L., and Cory, S. (1990). Novel primitive lymphoid tumours induced in transgenic mice by cooperation between myc and bcl-2. Nature *348*, 331-333.

Swerdlow, S. H., Campo, E., Pileri, S. A., Harris, N. L., Stein, H., Siebert, R., Advani, R., Ghielmini, M., Salles, G. A., Zelenetz, A. D., and Jaffe, E. S. (2016). The 2016 revision of the World Health Organization classification of lymphoid neoplasms. Blood *127*, 2375-2390.

Taub, R., Kirsch, I., Morton, C., Lenoir, G., Swan, D., Tronick, S., Aaronson, S., and Leder, P. (1982). Translocation of the c-myc gene into the immunoglobulin heavy chain locus in human Burkitt lymphoma and murine plasmacytoma cells. Proc Natl Acad Sci U S A *79*, 7837-7841.

Uhlen, M., Fagerberg, L., Hallstrom, B. M., Lindskog, C., Oksvold, P., Mardinoglu, A., Sivertsson, A., Kampf, C., Sjostedt, E., Asplund, A., Olsson, I., Edlund, K., Lundberg, E., Navani, S., Szigyarto, C. A., Odeberg, J., Djureinovic, D., Takanen, J. O., Hober, S., Alm, T., Edqvist, P. H., Berling, H., Tegel, H., Mulder, J., Rockberg, J., Nilsson, P., Schwenk, J. M., Hamsten, M., von Feilitzen, K., Forsberg, M., Persson, L., Johansson, F., Zwahlen, M., von Heijne, G., Nielsen, J., and Ponten, F. (2015). Proteomics. Tissue-based map of the human proteome. Science *347*, 1260419.

Ulrich, H. D. (2008). The fast-growing business of SUMO chains. Mol Cell *32*, 301-305.

Uren, A. G., Kool, J., Berns, A., and van Lohuizen, M. (2005). Retroviral insertional mutagenesis: past, present and future. Oncogene *24*, 7656-7672.

Vertegaal, A. C. (2010). SUMO chains: polymeric signals. Biochem Soc Trans *38*, 46-49.

Wagner, K., Kunz, K., Piller, T., Tascher, G., Holper, S., Stehmeier, P., Keiten-Schmitz, J., Schick, M., Keller, U., and Muller, S. (2019). The SUMO Isopeptidase SENP6 Functions as a Rheostat of Chromatin Residency in Genome Maintenance and Chromosome Dynamics. Cell Rep *29*, 480-494 e485.

Walz, S., Lorenzin, F., Morton, J., Wiese, K. E., von Eyss, B., Herold, S., Rycak, L., Dumay-Odelot, H., Karim, S., Bartkuhn, M., Roels, F., Wustefeld, T., Fischer, M., Teichmann, M., Zender, L., Wei, C. L., Sansom, O., Wolf, E., and Eilers, M. (2014). Activation and repression by oncogenic MYC shape tumour-specific gene expression profiles. Nature *511*, 483-487.

Weber, J., de la Rosa, J., Grove, C. S., Schick, M., Rad, L., Baranov, O., Strong, A., Pfaus, A., Friedrich, M. J., Engleitner, T., Lersch, R., Ollinger, R., Grau, M., Menendez, I. G., Martella, M., Kohlhofer, U., Banerjee, R., Turchaninova, M. A., Scherger, A., Hoffman, G. J., Hess, J., Kuhn, L. B., Ammon, T., Kim, J., Schneider, G., Unger, K., Zimber-Strobl, U., Heikenwalder, M., Schmidt-Supprian, M., Yang, F., Saur, D., Liu, P., Steiger, K., Chudakov, D. M., Lenz, G., Quintanilla-Martinez, L., Keller, U., Vassiliou, G. S., Cadinanos, J., Bradley, A., and Rad, R. (2019). PiggyBac transposon tools for recessive screening identify B-cell lymphoma drivers in mice. Nat Commun *10*, 1415.

Witt, A. E., Hines, L. M., Collins, N. L., Hu, Y., Gunawardane, R. N., Moreira, D., Raphael, J., Jepson, D., Koundinya, M., Rolfs, A., Taron, B., Isakoff, S. J., Brugge, J. S., and LaBaer, J. (2006). Functional proteomics approach to investigate the biological activities of cDNAs implicated in breast cancer. J Proteome Res *5*, 599-610.

Wolf, E., Lin, C. Y., Eilers, M., and Levens, D. L. (2015). Taming of the beast: shaping Myc-dependent amplification. Trends Cell Biol *25*, 241-248.

9 PUBLICATIONS IN PEER-REVIEWED JOURNALS

Schick M, Maurer S, Zhang L, Isaakidis K, Schneider L, Schunck K, Rohleder E, Maurer C, Hofstetter J, Baluapuri A, Zhang L, Scherger AK, Slotta-Huspenina J, Weber J, Engleitner T, Maresch R, Slawska J, Isaakaidis K, Lewis R, Istvanffy R, Habringer S, Steiger K, Baiker A, Oostendorp R, Miething C, Lenhof HP, Bassermann F, Chapuy B, Wolf E, Rad R, Müller S, and Keller U. Actionable genetic alterations of the SUMO isopeptidase SENP6 drive lymphomagenesis and genetic instability in diffuse large B-cell lymphoma. Manuscript submitted.

Hassan Z*, Schneeweis C*, **Schick M**, Keller U, Schneider G. The SUMO pathway in pancreatic cancer: Insights and inhibition. Manuscript in revision.

Biederstädt A*, Hassan Z*, Schneeweis C*, **Schick M***, SchneiderL, Muckenhuber A, Hong Y, Siegers G, Nilsson L, Wirth M, Dantes Z, Steiger K, Schunck K, Langston S, Lenhof HP, Coluccio A, Orben F, Slawska J, Scherger AK, Saur D, Müller S, Rad R, Weichert W, Nilsson J, Reichert M ,Schneider G , Keller U. SUMO pathway inhibition targets an aggressive pancreatic cancer subtype. **Gut.** 2020. doi:10.1136/gutjnl-2018-317856. ***contributed equally**

Wagner K, Kunz K, Piller T, Tascher G, Hölper S, Stehmeier P, Keiten-Schmitz J, **Schick M**, Keller U, Müller S. The SUMO Isopeptidase SENP6 Functions as a Rheostat of Chromatin Residency in Genome Maintenance and Chromosome Dynamics. **Cell Rep. 2019** Oct 8;29(2):480-494.e5.

O'Connor T, Zhou X, Kosla J, Adili A, Garcia Beccaria M, Kotsiliti E, Pfister D, Johlke AL, Sinha A, Sankowski R, **Schick M**, Lewis R, Dokalis N, Seubert B, Höchst B, Inverso D, Heide D, Zhang W, Weihrich P, Manske K, Wohlleber D, Anton M, Hoellein A, Seleznik G, Bremer J, Bleul S, Augustin HG, Scherer F, Koedel U, Weber A, Protzer U, Förster R, Wirth T, Aguzzi A, Meissner F, Prinz M, Baumann B, Höpken UE, Knolle PA, von Baumgarten L, Keller U, Heikenwalder M. Age-Related Gliosis Promotes Central Nervous System Lymphoma through CCL19-Mediated Tumor Cell Retention. **Cancer Cell. 2019** Sep 16;36(3):250-267.e9.

Scherger AK, Al-Maarri M, Maurer HC, **Schick M**, Maurer S, Öllinger R, Gonzalez-Menendez I, Martella M, Thaler M, Pechloff K, Steiger K, Sander S, Ruland J, Rad R, Quintanilla-Martinez L, Wunderlich FT, Rose-John S, Keller U. Activated gp130 signaling selectively targets B-cell differentiation to induce mature lymphoma and plasmacytoma. **JCI Insight.** 2019 Aug 8;4(15). pii: 128435.

Weber J, de la Rosa J, Grove CS, **Schick M**, Rad L, Baranov O, Strong A, Pfaus A, Friedrich MJ, Engleitner T, Lersch R, Öllinger R, Grau M, Menendez IG, Martella M, Kohlhofer U, Banerjee R, Turchaninova MA, Scherger A, Hoffman GJ, Hess J, Kuhn LB, Ammon T, Kim J, Schneider G, Unger K, Zimber-Strobl U, Heikenwälder M, Schmidt-Supprian M, Yang F, Saur

D, Liu P, Steiger K, Chudakov DM, Lenz G, Quintanilla-Martinez L, Keller U, Vassiliou GS, Cadiñanos J, Bradley A, Rad R. PiggyBac transposon tools for recessive screening identify B-cell lymphoma drivers in mice. **Nat Commun. 2019** Mar 29;10(1):1415.

Stellberger T, Stockmar I, Draxler J, Dhar P, Pavlovic M, Anton M, Koehler N, Dinkelmeier A, Haase M, **Schick M**, Keller U, Busch U, Baiker A. Characterization of retroviral vector derived DNA-isoforms by PCR and sequencing. **J Consum Prot Food Saf.** 2019 Feb. doi:10.1007/s00003-019-01215-7.

Kehl T, Schneider L, Kattler K, Stöckel D, Wegert J, Gerstner N, Ludwig N, Distler U, **Schick M**, Keller U, Tenzer S, Gessler M, Walter J, Keller A, Graf N, Meese E, Lenhof HP. REGGAE: a novel approach for the identification of key transcriptional regulators. **Bioinformatics**. 2018 Oct 15;34(20):3503-3510.

Schick M*, Habringer S*, Nilsson JA, Keller U. Pathogenesis and therapeutic targeting of aberrant MYC expression in haematological cancers. **Br J Haematol**. 2017 Dec;179(5):724-738. ***contributed equally**

Herhaus P, Habringer S, Philipp-Abbrederis K, Vag T, Gerngross C, Schottelius M, Slotta-Huspenina J, Steiger K, Altmann T, Weißer T, Steidle S, **Schick M**, Jacobs L, Slawska J, Müller-Thomas C, Verbeek M, Subklewe M, Peschel C, Wester HJ, Schwaiger M, Götze K, Keller U. Targeted positron emission tomography imaging of CXCR4 expression in patients with acute myeloid leukemia. **Haematologica**. 2016 Aug;101(8):932-40.

Voth W, **Schick M**, Gates S, Li S, Vilardi F, Gostimskaya I, Southworth DR, Schwappach B, Jakob U. The protein targeting factor Get3 functions as ATP-independent chaperone under oxidative stress conditions. **Mol Cell.** 2014 Oct 2;56(1):116-27.

10 ACKNOWLEDGEMENTS

First and foremost I want to express my sincere gratitude to my doctoral adviser Ulrich Keller for the opportunity to join his dynamic research group. I want to thank Ulrich Keller for his continuous support during my time in his laboratory and for the right balance between supervision and scientific freedom, which enabled me to develop and pursue my own ideas. I highly appreciate his constant feedback, guidance and motivation for all projects.

I particularly thank Stefan Müller for superb collaborations and discussions from the very beginning of the SUMO projects on. His expertise in the field of SUMO biology was substantial for the success of the projects.

I thank my second assessor Michael Groll for valuable scientific discussions. Although our meetings were only few, he had great impact on the progress and success of my projects.

I thank my mentor Roland Rad for valuable scientific discussions, his guidance and support in exciting collaborations.

I thank all members of the Keller, Götze and Oostendorp laboratories for creating a dynamic atmosphere and for making it a pleasure to perform research in the lab at Trogerstraße.

I am deeply grateful to my family, foremost to my parents Monika and Anton Schick for their unconditional support. I owe them everything.